

PDF hosted at the Radboud Repository of the Radboud University Nijmegen

The following full text is a publisher's version.

For additional information about this publication click this link.

<http://hdl.handle.net/2066/87201>

Please be advised that this information was generated on 2017-12-06 and may be subject to change.

Ultrafast Path for Magnetization Reversal in Ferrimagnetic GdFeCo Films

Kadir Vahaplar

Printed by PrintPartners Ipskamp, Enschede, The Netherlands

ISBN/EAN: 978-94-91211-78-2

Copyright © 2011, by Kadir Vahaplar

Illustrated with references.

Cover design by K. Vahaplar.

Cover background image courtesy of: <http://www.psdgraphics.com>

An electronic version of this thesis can be found at: <http://www.kadirvahaplar.com>

Ultrafast Path for Magnetization Reversal in Ferrimagnetic GdFeCo Films

Een wetenschappelijke proeve op het gebied van de
Natuurwetenschappen, Wiskunde & Informatica

Proefschrift

ter verkrijging van de graad van doctor
aan de Radboud Universiteit Nijmegen
op gezag van de rector magnificus prof. mr. S.C.J.J. Kortmann,
volgens besluit van het College van Decanen
in het openbaar te verdedigen op donderdag 1 september 2011
om 10.30 uur precies

door

Kadir Vahaplar

geboren op 28 juli 1981
te Izmir, Turkije

Promotor : Prof. dr. Th. Rasing

Copromotores : Dr. A. V. Kimel

: Dr. A. Kirilyuk

Manuscriptcommissie:

Prof. dr. M. I. Katsnelson

Prof. dr. F. Nolting Paul Scherrer Institute,
Swiss Light Source,
Villigen PSI, Switzerland.

Prof. dr. H. Munekata Imaging Science & Engineering Laboratory,
Tokyo Institute of Technology,
Yokohama, Japan.

Ultrafast Path for Magnetization Reversal in Ferrimagnetic GdFeCo Films

An academic essay in the
Natural Sciences, Mathematics and Computer Science

Doctoral thesis

to obtain the degree of doctor
from Radboud University Nijmegen
on the authority of the Rector Magnificus prof. dr. S.C.J.J. Kortmann,
according to the decision of the Council of Deans
to be defended in public on Thursday, 1 September 2011
at precisely 10:30 hours

by

Kadir Vahaplar

born on 28 July 1981
in Izmir, Turkey

Doctoral supervisor : Prof. dr. Th. Rasing

Co-supervisors : Dr. A. V. Kimel

: Dr. A. Kirilyuk

Doctoral Thesis Committee:

Prof. dr. M. I. Katsnelson

Prof. dr. F. Nolting Paul Scherrer Institute,
Swiss Light Source,
Villigen PSI, Switzerland.

Prof. dr. H. Munekata Imaging Science & Engineering Laboratory,
Tokyo Institute of Technology,
Yokohama, Japan.

The work described in this thesis was financially supported by de Nederlandse Organisatie voor Wetenschappelijk Onderzoek (NWO), de Stichting voor Fundamenteel Onderzoek der Materie (FOM), the Dutch Nanotechnology Initiative NanoNed, European Commission (EC) 7th Framework Programme (FP7) under grants No. NMP3-SL-2008-214469 (UltraMagnetron) and No. 214810 (FANTOMAS), as well as the European Research Council (ERC) grant agreement No. N257280 (Femtomagnetism).

to my whole family and to my fiancée, Pınar

Preface

Finally I finished up writing my thesis, concluding one of the most important chapters in my life! However, writing this short preface seems much more difficult than I had expected. After everything else has been finished, I would like to thank all the people who helped me out in many ways during my PhD and made my stay in Nijmegen an unforgettable experience. Now it is time to say thank you!

First and foremost, I want to thank my promotor Prof. Theo Rasing for giving me the opportunity to work in such a great group. His valuable comments, insightful suggestions and constructive criticisms on my manuscripts and presentations always encouraged me in all the time of my research. It has been a privilege working in his group and he has been invaluable on both an academic and a personal level, for which I am extremely grateful.

I am very grateful to my supervisor Dr. Alexey Kimel for the continuous support of my PhD study and research. Although my background in magneto-optics was not strong, he never hesitated to offer me the position for this project in 2007. I owe a special thanks to him for his trust, patience, motivation, and enthusiasm during these four years, and for his immense knowledge. His guidance helped me throughout my research and in writing this thesis. I could not have imagined having a better advisor and mentor for my PhD study.

I am also indebted to my other supervisor Dr. Andrei Kirilyuk for his precious teachings, extremely important comments and suggestions, as well as for his support and guidance. I would like to thank again Theo and both my supervisors for giving me the privilege of working with the best scientists in the field of magnetization dynamics and for giving me the possibility to attend various conferences and workshops on magnetism all around the world.

For this dissertation I would like to thank my thesis committee members: Prof. Frithjof Nolting, Prof. Hiro Munekata, and Prof. Mikhail Katsnelson for their time, interest, and helpful comments.

Words fail to express my appreciation to Marilou for her kindness, support, and generous care during my stay in Nijmegen. I am thankful to Marilou, Riki and Marie-Louise for their patience in helping me with all administrative issues. It was always a pleasure to drop by and find a smiling and helpful person in your office.

Special thanks go to my colleagues Sasha and Ilie, i.e. my co-supervisors! What makes them special is that they have not only been very good friends, but also taught me almost everything about magnetization dynamics during these four years. Dear Sasha, you taught me how good experimental physics is done, from aligning lasers to interpreting the results. I truly appreciate all your great contributions, ideas, and guidance adding to the quality of this thesis. And Ilie, it was a great pleasure to work and achieve “awesome” results with you at BESSY II in Berlin. I learned many things about lasers, X-rays, synchrotrons, and magnetism from you. Thank you guys!

For the technical support during my PhD, for all the laser equipment in our laboratories and any other help I needed I want to thank Albert van Etteger, Tonnie Toonen, and Andre van Roij. I appreciate their kind help and time spent teaching me about optics and lasers.

All the results presented in this thesis would not have been possible without a close collaboration with few groups. I owe a great deal of appreciation and gratitude to Dr. Arata Tsukamoto and Prof. Akiyoshi Itoh from Nihon University for providing us with the best quality GdFeCo samples and sharing their extended experience.

During my PhD research, I had the good fortune to work a couple of months (in total) with the group of Prof. Hermann Dürr¹ at BESSY II in Berlin. I learned a lot about synchrotrons and X-rays with the help of some great scientists: Christian Stamm, Torsten Kachel, Niko Pontius, Andrea Eschenlohr, Florin Radu, and Radu Abrudan, who I would like to thank for the scientific discussions, collaborations and for their help especially during the tough night shifts.

I would also like to express my gratitude to our other collaborators, the group of Prof. Roy Chantrell from the University of York and the group of Prof. Ulrich Nowak from the University of Konstanz for their innovative contributions to our work.

My time in Nijmegen was made enjoyable and unforgettable due to the many friends that became a part of my life. These incredible people, who have always been there for me, made me feel at home no matter where I was. First of all, I am grateful for the time spent with my roommates Loïc, Lucian, Marina, Johan M., Addis, Alex, Matteo, Thomas, Ilie, and Diana. It has been always fun and pleasant to discuss everything and share the office with you.

Many people have joined and left our group during my stay in Nijmegen. Their friendships together with the many fun activities have been unforgettable memories for me during these four years. I really enjoyed gluhwein parties, especially those prepared by Oleg; summer barbeques organized by Theo and Maria; the pizza party at Marilou's place by the master chef Matteo; days-out organized by Marilou and other colleagues; raki parties (I hope we can arrange the third one before I leave!); the joint SSI-dynamics meeting at Andrei's place and wine tasting trips with him in California; *Absolute Zero* nights; Matteo's *Don Pablo* dinner nights; *Cafe Jos* whisky nights; "unforgettable!" *In de Blauwe Hand* nights; the waterskiing experience (10 meters max. for me!) with the professional Roman; karting races; playing paintball, football, volleyball, bowling, and especially table-soccer everyday; being a private driver for the shopping days of Sasha and Jelena; swimming days with Fred and Alex; going out and coffee breaks with all the members of our group; and many more events which I cannot remember at the moment. Additionally, I would like thank Matteo and his parents for their wonderful hospitality and giving us a taste of their delicious traditional Italian cuisine in Maggiora. *Piacere di conoscervi!..* Here I want to thank again Matteo for teaching us how to express emotional feelings about people in Italian!

¹Now at SLAC National Accelerator Laboratory, Menlo Park, USA.

I take this opportunity to say heartfelt thanks to my dear colleagues: Sasha, Fred (mysterious b.....d!), Daniel, Chris, Loïc (yeah, no, maybe!), Jelena, Sam (kick ass time!), Matteo (fanculo!), Laura, Johan de J. (cookie monster!), Johan M., Addis (Adu!), Alex, Raja M. (lovely!), Jeroen, Davide (that's the way!), Ilie (awesome!), Jan, Mathieu, Dmitry, Tahoor, Benny, Ilya, Boldizar, Dennis, Lars, Siebe, Sergey, Koen, Raja G., Steven, Roman, Jing, Lucian, Minko, Michiel, Thomas, Duncan, Monique, Natascha, Serhiy, and Weizhe for their precious friendship, help, support and creating a pleasant atmosphere for me here. I am sure that our friendship will continue throughout our lives.

I would especially like to thank Johan M. for his help in translating the summary section of this thesis into Dutch. My special thanks to Sam and Matteo for accepting to be my paranymphs at my thesis defence (I can hear you saying: "What goes around comes around!").

I would also like to extend my gratitude to all of my Turkish friends here: Serap and her family, Saliha, Haki, Maside, and Deniz for their kind help and sharing a nice atmosphere here in the Netherlands. I hope we will keep in touch and that our paths will often cross in the future.

I am grateful to my former supervisor, Dr. Süleyman Tarı, who supported me during my master study and encouraged me to undertake a PhD degree abroad. I would also like to thank Dr. Lütfi Özyüzer and Dr. Yusuf Selamet for their support and helping me in the very beginning of my research career.

And last but not least, I would like to warmly thank my whole family in Turkey! Thank you for your unconditional love, care and never ending support as always in every moment of my life. You know how much I love you all. I would also like to express my gratitude to my best friends in Turkey: Cemal, Cihan, Uğur, Serkan, Şükrü and Tarık, who have never forgotten me and have always made me feel close to home. Thanks for their phone calls, messages, emails and visits to Nijmegen.

Finally, I would like to express my special thanks to my lovely fiancée, Pınar, who has been patiently waiting for me with her faithful love, always ready to sacrifice her time to see me via Skype everyday! Your continuous encouragement made these days pass quickly. Despite being so far away from you for such a long time, I would not have finished this thesis without you and your love. *Seni çok seviyorum aşkım!..*

To all of you, thank you very much!

Kadir Vahaplar
Radboud University Nijmegen
Nijmegen, June 2011.

Contents

1	Introduction	1
1.1	Magnetism and magnetic recording	1
1.2	Control of magnetization	3
1.2.1	Landau-Lifshitz-Gilbert equation	3
1.2.2	Magnetization reversal: state of the art and challenges	5
1.3	Laser-induced magnetization dynamics	7
1.3.1	Historical review and ultrafast demagnetization	7
1.3.2	Three-temperature model (3TM)	8
1.3.3	Laser control of magnetization	10
1.4	All-optical magnetization reversal	12
1.5	Scope of this thesis	14
	References	15
2	Amorphous rare earth – transition metal alloys	21
2.1	Introduction	21
2.2	Magnetic and magneto-optical properties	22
2.3	Gadolinium-iron-cobalt (GdFeCo)	27
2.3.1	Growth	28
2.3.2	Samples studied in this work	28
2.4	Summary	29
	References	30

3	Experimental techniques	33
3.1	Linear magneto-optical effects	33
3.2	Static Faraday effect measurements	37
3.2.1	Magneto-optical polarimetry	37
3.2.2	Magneto-optical imaging	38
3.3	Time-resolved pump-probe spectroscopy	39
3.3.1	The femtosecond laser system	40
3.3.2	Pump-probe experimental setup	42
3.4	Single-shot time-resolved magneto-optical imaging technique	44
3.5	Time-resolved X-ray spectroscopy	46
	References	51
4	All-optical magnetization reversal triggered by circularly-polarized laser pulses	55
4.1	Introduction	55
4.2	Samples	57
4.3	Methods	60
4.3.1	Experimental technique	60
4.3.2	Theoretical methods	60
4.4	Results and discussion	65
4.4.1	Determination of the laser pulse fluence dependence for the helicity dependent reversal	65
4.4.2	Dynamics of the all-optical helicity-dependent reversal	70
4.4.3	Helicity-dependent all-optical reversal as a function of the laser pulse parameters	75
4.4.4	Helicity-dependent all-optical reversal in various ferrimagnetic alloys of GdFeCo	81
4.5	Conclusions	84
	References	87
5	Element-specific studies of ultrafast magnetization reversal in ferrimagnetic GdFeCo alloys	91
5.1	Introduction	91
5.2	Switching over the compensation point	93
5.3	Nonequilibrium spin dynamics of magnetic sublattices in ferrimagnetic GdFeCo alloy	97
5.3.1	X-ray magnetic circular dichroism (XMCD)	97
5.3.2	Experimental details	100
5.3.3	Theoretical methods	104
5.4	Results and discussion	106
5.5	Conclusions	111

References	112
Summary and outlook	117
Samenvatting en vooruitblik	119
List of Publications	123
Curriculum Vitae	125

CHAPTER 1

Introduction

1.1 Magnetism and magnetic recording

Magnetism has been known for thousands of years. However, the underlying principles and mechanisms that explain magnetic phenomena are complex and their understanding has eluded scientists until relatively recent times. Many of our modern technological devices are based on magnetism and magnetic materials; these include hard disks, read/write heads, magnetic sensors and components of sound and video systems.

In order to keep pace with the ever increasing demands for higher data storage capacities and higher data rates, the recording industry faces the challenge of growth in information storage density. The storage capacity has doubled almost every year because the size of the region used to store each '1' or '0' of binary data has continued to decrease deep into the nano-scale regime. The current bit width is approximately 20 nm and further reductions will bring us closer to the atomic limit. Since we expect the stored information to be almost instantly available, reduced bit sizes have been accompanied by reduced read and write times. These developments have triggered current research on two correlated areas: the quest for *smaller* magnetic bits and *faster* writing and reading of its content.

As the system approaches to a few nanometers (tens of atomic dimensions), thermal fluctuations reduce the signal strength and make the bits unstable causing the magnetization to fluctuate between different orientations. This effect is explained

in terms of the *super-paramagnetic limit* [1]. In ferromagnets, the stable magnetic moment of a single-domain particle is usually aligned along a specific axis, called the *easy axis*. These particles possess a strong uniaxial anisotropy, so that the magnetization occupies one of the two stable states and the orientation (parallel or antiparallel) along the easy axis defines the information stored, either “up” (‘1’) or “down” (‘0’). For magnetization reversal via a coherent spin rotation in a very small magnetic particle, with volume V and anisotropy constant K_u , the relaxation time τ , is given by the Néel-Brown law:

$$\tau = \frac{1}{f_0} \exp(K_u V / k_B T). \quad (1.1)$$

where f_0 is a frequency factor with a value of about 10^{10} sec^{-1} , k_B is Boltzmann’s constant and T is the absolute temperature. The value of τ depends on the competition between magnetic anisotropy energy and thermal energy. It is a measure of the probability that a grain will have sufficient thermal energy to overcome the anisotropy energy and switch its moment.

Thermal stability of magnetized particles for over 10 years, requires $K_u V / k_B T > 50$. This means that for present values of $K_u = 1 - 2 \times 10^6 \text{ erg/cm}^3$ in particles with volume V smaller than 10^4 nm^3 , the stability is not preserved for a long time [2]. FePt and CoPt have large values of K_u ($\sim 5 - 7 \times 10^7 \text{ erg/cm}^3$), and thus have the potential to serve as building blocks for thermally stable high-density recording media [3]. As the domain size is pushed down to $\sim 10 \text{ nm}$, the anisotropy must be stronger and the magnetization must be controlled directly through spin degrees of freedom; so called *spintronics*¹. Moreover, an increase in K_u is equivalent to an increase in the anisotropy field of the medium, given by $H_a = 2K_u / M_s$ with M_s – the saturation magnetization value. This also leads to an increase of the coercivity of the medium and thus requires larger magnetic fields to be applied during writing. Today’s hard disk technology faces a major difficulty because this limits the writing speed to low GHz rates. In other words, the writing process of each bit, i.e. the magnetization reversal time in a bit, is not faster than $\sim 1 \text{ ns}$ [4]. These requirements constitute a well known “*magnetic recording trilemma*”, as shown in Figure 1.1 [1, 5–7]. Therefore, today researchers are actively working on new fundamental and practical solutions to increase the speed of manipulating magnetic bits, which is an issue of vital importance for modern storage technology.

¹Spintronics, or spin electronics, refers to the study of the role played by electron spin in solid state physics, and possible devices that specifically exploit spin properties instead of or in addition to charge degrees of freedom.

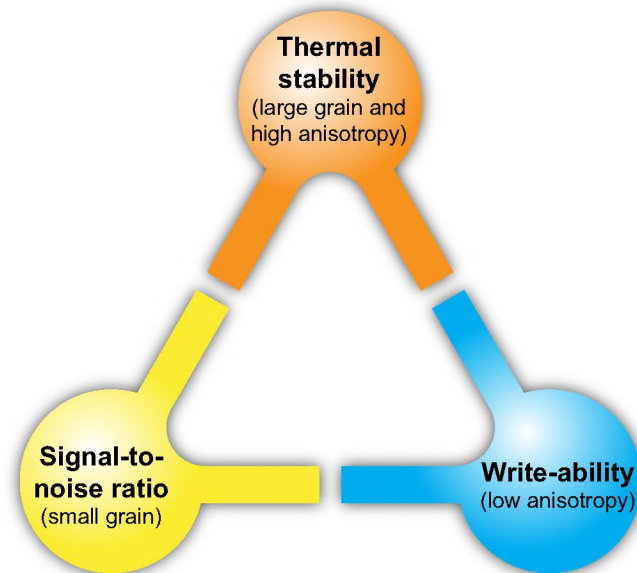


Figure 1.1: The primary problem for ultra-high density magnetic recording system is the so-called “thermal stability – grain size – write-ability trilemma”.

1.2 Control of magnetization

The principle of magnetic recording and storing a logical bit in magnetic memory devices is setting the magnetization vector of individual magnetic domains either “up” or “down”. Hence, recording of one bit corresponds to magnetization reversal. Since the speed of magnetic recording devices is defined by the reversal of the magnetization direction in each bit, a crucial question about the ultimate speed of the magnetization reversal arises. It is known that the spins are responsible for forming the magnetization. Thus, in order to answer this question one has to focus first on the spin motion in an external magnetic field and possible mechanisms of magnetization reversal.

1.2.1 Landau-Lifshitz-Gilbert equation

The interaction of a magnetic moment with a magnetic field is the essence of all magnetic phenomena. The dynamical process of magnetization is governed by the angular momentum accompanying the magnetic moment. According to quantum mechanics, there is a proportionality relationship between magnetic moment \mathbf{m} and

angular momentum \mathbf{L} . This relationship can be expressed as $\mathbf{m} = \gamma\mathbf{L}$, where γ is the *gyromagnetic ratio*. The sign of γ depends on the charge of the particle. The torque on the magnetic moment \mathbf{m} exerted by a magnetic field \mathbf{H} is:

$$\mathbf{T} = \mathbf{m} \times \mathbf{H}. \quad (1.2)$$

By applying the momentum theorem, the significance of angular momentum \mathbf{L} arises from its derivative with respect to time:

$$\frac{d\mathbf{L}}{dt} = \mathbf{T} = \mathbf{m} \times \mathbf{H}. \quad (1.3)$$

By substituting $\mathbf{m} = \gamma\mathbf{L}$, one ends up with a model which describes the precession of the spin magnetic moment \mathbf{m} around the magnetic field \mathbf{H} :

$$\frac{d\mathbf{m}}{dt} = \gamma(\mathbf{m} \times \mathbf{H}), \quad (1.4)$$

The frequency of this precession is a linear function of the external magnetic field ($\omega = |\gamma|\mathbf{H}$). At equilibrium, the change in angular momentum with time is zero, and thus the torque is zero.

Since the spins experience not only the action of the external magnetic field, but is also affected by the magneto-crystalline anisotropy, shape anisotropy, etc., the contribution of all these interactions can be considered as an effective magnetic field \mathbf{H}_{eff} . This expression is also known as the Landau-Lifshitz equation in the nondissipative approximation [8, 9].

In order to describe the motion of a precessing magnetic moment toward equilibrium (\mathbf{H}_{eff}), a dissipative (damping) term must be included to Eq. 1.4. This damping term slows down the motion of the magnetic moment and eventually aligns \mathbf{m} to \mathbf{H}_{eff} , as shown in Figure 1.2. This damped precessional dynamics can be described by the Landau-Lifshitz-Gilbert (LLG) equation of motion [10]:

$$\frac{d\mathbf{m}}{dt} = \gamma(\mathbf{m} \times \mathbf{H}_{\text{eff}}) + \frac{\alpha}{m} \left(\mathbf{m} \times \frac{d\mathbf{m}}{dt} \right), \quad (1.5)$$

where α is the dimensionless phenomenological Gilbert damping constant. The LLG equation describing the magnetization motion indicates that a suddenly applied magnetic field exerts a torque on the magnetization vector that may result in a precession taking place on picosecond time scales. In other words, for an applied magnetic field of 1 T, an electron spin makes one full precession in 36 ps. This precession is one of the fastest known ways of changing the magnetization direction [4].

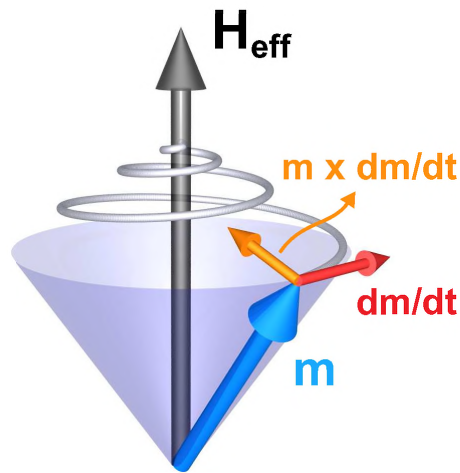


Figure 1.2: Schematic illustration of the magnetization precession according to Eq. 1.5. The magnetization precesses around \mathbf{H}_{eff} . The damping term slows down the motion of the magnetic moment and eventually aligns \mathbf{M} to \mathbf{H}_{eff} .

1.2.2 Magnetization reversal: state of the art and challenges

The conventional way of writing a magnetic bit, in particular, switching the magnetization \mathbf{M} , is to apply a pulse of magnetic field \mathbf{H} antiparallel to \mathbf{M} [9]. In this configuration shown in Figure 1.3(a), the magnetic field induces a precession of the magnetic moment around the field axis. This precession is accompanied by damping of the motion with transfer of energy and angular momentum to the underlying lattice and finally the magnetization stabilizes in the new direction (the second term on the right-hand side of Eq. 1.5). The overall process is, however, relatively slow, taking place on a few nanoseconds, due to the required angular momentum transfer between the lattice and spins [4, 11].

One of the alternative high-speed writing methods is *precessional magnetization switching* (or *ballistic switching*) [9, 12–17]. In precessional switching shown in Figure 1.3(b), the magnetic field is applied orthogonal to the equilibrium direction of magnetization ($\mathbf{M} \perp \mathbf{H}$) during half of the precessional period (typically 10–1000 ps). The first term on the right-hand side of Eq. 1.5 describes the torque on the magnetization that causes a precessional motion of \mathbf{M} (see also Figure 1.2). It is seen that after half a period of such a precession, the magnetization reverses. Since the speed of precessional switching is defined by the rate of precession, the switching in this geometry is expected to be very fast and limited only by the strength and the duration of the magnetic field pulse. If the pulse lasts too long in the medium, \mathbf{M} might switch back to its initial state. Therefore, in order to achieve fast and deterministic magnetization switching, one needs short and strong magnetic field pulses [15, 17]. Recent experiments on magnetization reversal using uniquely short (picosecond-long) and strong (several teslas) magnetic field pulses generated by relativistic electrons from

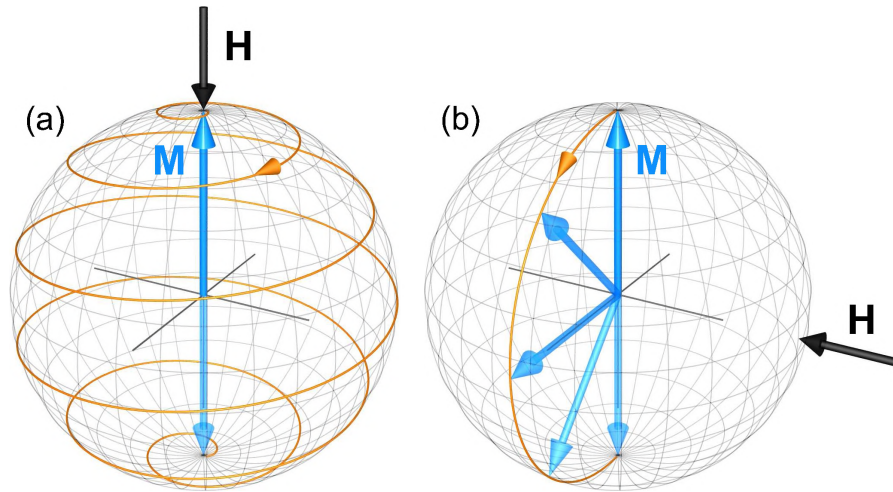


Figure 1.3: (a) Conventional magnetization switching process. An external magnetic field \mathbf{H} is applied in the direction opposite to \mathbf{M} . Then \mathbf{M} changes its direction via precession and aligns along the opposite direction. (b) High-speed precessional switching occurs if the pulse of external magnetic field \mathbf{H} is applied perpendicular to \mathbf{M} during half of the precessional period.

the Stanford Linear Accelerator (SLAC) suggest that there is a speed limit on such a switching. It has been shown that deterministic magnetization reversal does not take place if the magnetic field pulse is shorter than 2.3 ps [18, 19]. However, using such magnetic field generators, there is no possibility to study dynamics of magnetization reversal since the generation of such magnetic field pulses (with picosecond durations and an amplitude of a few Tesla) in a laboratory is technically challenging.

Besides the switching techniques mentioned above there have been also a number of new alternatives suggested, such as those based on vortices. It was recently demonstrated using micromagnetic simulations that an efficient and faster method for magnetization reversal is to nucleate a vortex-antivortex pair, promoting an annihilation processes [20]. This switching is driven by the exchange field and thus occurs in a few tens of picoseconds.

At all events mentioned up to now, there are still disadvantages which restrict us to achieve subpicosecond reversal times. This brings us to a key device, which is able to generate subpicosecond events – the laser. An ultrashort laser pulse (in the femtosecond regime) can indeed be exploited to control the magnetization in a magnetic system; employing so called *opto-magnetism* [21]. This exciting new research area on the interaction of intense femtosecond laser pulses with materials leads to

ultrafast magnetization dynamics, sometimes referred to as *femtomagnetism*. In the following section, the laser-induced magnetization dynamics and recent developments are discussed in more details.

1.3 Laser-induced magnetization dynamics

1.3.1 Historical review and ultrafast demagnetization

The pioneering experimental study of changing the magnetic state in a magnetic system by an intense short laser pulses was performed by Agranat *et al.* in 1984 [22]. Using 10 ps and 40 ns laser pulses they showed that the characteristic time scale of demagnetization in a ferromagnetic Ni film was in the nanosecond regime. This observation was subsequently followed by Vaterlaus *et al.*, who reported that the spin-lattice relaxation occurs on the time scale of 100 ps for Gd, whereas it takes from 30 ps to 20 ns for Fe [23–25]. Since the duration of the laser pulses was the same or even longer than the observed time scales, the system was always in equilibrium with such long excitations. In order to enter and study non-equilibrium regimes of faster time scales, much shorter stimuli are required.

A surprising discovery of ultrafast demagnetization of a Ni film by a 60 fs optical laser pulses was published by Beaurepaire *et al.* in 1996 [26]. Using a time-resolved pump-probe setup² the Strasbourg group demonstrated for the first time that a femtosecond laser pulse leads to a rapid demagnetization on a subpicosecond time scale, i.e. much faster than previously reported [see Figure 1.4(a)]. It was estimated from the transient MOKE signal that the electron thermalization time was ~ 260 fs and the electron temperature decay constant 1 ps. Soon after, employing second-harmonic generation technique, an ultrafast demagnetization (≈ 150 fs) of Ni was observed by Hohlfeld *et al.* [27]. These interesting results motivated intense experimental as well as theoretical investigations.

Subsequent research not only confirmed these findings [28–34] but also demonstrated the possibility to optically generate magnetic precession [35, 36], laser-induced spin reorientation [37], or even modification of the magnetic structure [38, 39] and that all these events occurred on a time scale of 1 ps or less [21]. Recent promising experiments using 100 fs X-ray pulses to probe magnetization yielded that demagnetization occurred within 120 ± 70 fs [40]. The authors were also able to separate the orbital and spin momentum contribution to the demagnetization process.

²Magneto-optical effects and femtosecond pump-probe experimental setup are explained in more details in Chapter 3.

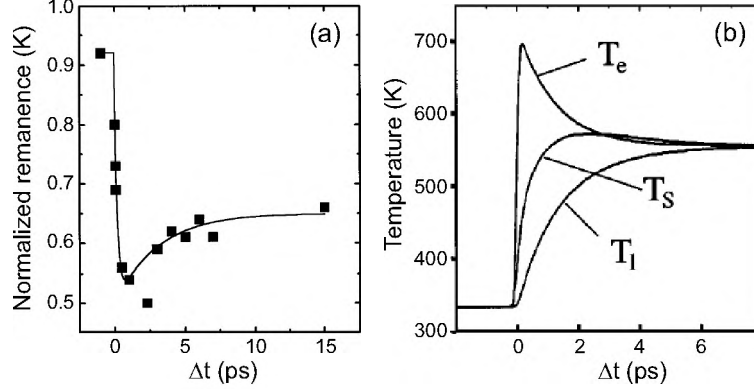


Figure 1.4: Results of time-resolved pump-probe measurements by Beaurepaire *et al.* on a nickel film using 60 fs laser pulses. (a) Transient reflectivity indicates ultrafast loss of magnetic order of the ferromagnetic material within a picosecond after laser excitation. (b) Evolution of calculated spin (T_s), electron (T_e), and lattice (T_l) temperatures according to three-temperature model (from [26]).

1.3.2 Three-temperature model (3TM)

Many laser-induced magnetization dynamics experiments already confirmed that the resulting demagnetization is a complicated process, where various components of such a system are participating that involve different relaxation processes. The characteristic interaction and energy transfer between these channels were described by a model that contains three separate but correlated reservoirs: the electrons, lattice, and spins. In order to explain the experimental findings, a *three-temperature model* (3TM) was adopted [26, 41]. A particular effective temperature can be assigned to each of these reservoirs: the electron temperature T_e , the spin temperature T_s , and the lattice temperature T_l . The process of the equilibration between the different reservoirs following the excitation with a femtosecond laser pulse is schematically shown in Figure 1.4(b). According to the three-temperature model, the temporal evolution of these baths can be described by three coupled heat diffusion equations:

$$C_e \frac{dT_e}{dt} = -G_{el}(T_e - T_l) - G_{es}(T_e - T_s) + P(t), \quad (1.6a)$$

$$C_l \frac{dT_l}{dt} = -G_{el}(T_l - T_e) - G_{sl}(T_l - T_s), \quad (1.6b)$$

$$C_s \frac{dT_s}{dt} = -G_{es}(T_s - T_e) - G_{sl}(T_s - T_l), \quad (1.6c)$$

where $P(t)$ is the initial excitation from the laser, C describes the heat capacity of each system and G represents the coupling constants between them. Depending on the heat capacities C , the differences between the effective temperatures of three reservoirs can be very large. Due to its small heat capacity, T_e may reach several thousand Kelvin within the first tens of femtoseconds after excitation, while T_l remains relatively low even after the equilibration process [see Figure 1.4(b)].

A typical sequence of steps for the process leading to a laser-induced demagnetization is as follows. Upon absorption of a laser pulse, energy is initially deposited only in the electron subsystem because only electrons are able to respond to an electromagnetic excitation instantaneously at optical frequencies³. This process leads to a rapid raising of the electron temperature T_e (< 100 fs) and then heat is subsequently redistributed among the electron, spin and lattice by increasing T_s and T_l until the systems are in thermal equilibrium with each other. At that point, $T_e = T_l = T_s$ at an elevated temperature (within 100 fs – 1 ps for metals). A schematic representation of all the steps mentioned above is given in Figure 1.5.

In this model the magnetization $M(T_s)$ is defined by the spin temperature T_s , an increase of which implies a reduction of the magnetization. In the process of demagnetization, transfer of energy and angular momentum occurs among the reservoirs and the magnetization reduces along the quantization axis. This reduction was believed to be due to the spin-lattice interaction. However, after the experiments by Beaurepaire *et al.* it was found that there is a much stronger coupling between the spins and electrons. The main mechanisms of an effective electron-spin or spin-lattice coupling leading to a laser-induced ultrafast demagnetization are only partly understood and still under discussion.

Previously, Zhang and Hübner theoretically suggested that ultrafast demagnetization is mediated by direct coupling of spin and angular momentum [43, 44]. On the other hand, Stamm *et al.* recently demonstrated by separating spin and orbital contribution that the electron orbitals were not responsible for the ultrafast demagnetization, i.e. the lattice was the only possible reservoir of angular momentum (spin-lattice interaction) [40]. They argued that the dissipation of the angular momentum to the lattice could be via light-induced virtual states, enhancing the spin-lattice interaction. A model has been recently proposed by Koopmans *et al.* in which the speed of the demagnetization is defined by the speed of spin-flip processes via Elliot-Yafet type of scattering [45]. Although this model can describe the macroscopic demagnetization process, Bigot *et al.* claimed that the laser-induced ultrafast demagnetization could be related to a direct coupling between photons and spins, i.e. a novel quantum mechanical mechanism could be responsible for the demagnetization [42].

In conclusion, many ultrafast demagnetization studies using ultrashort duration of laser pulses triggered a wealth of experimental and theoretical research. Nevertheless,

³Spins are conserved in optical transitions. Thus, in the electric dipole approximation spin-flip transitions are forbidden.

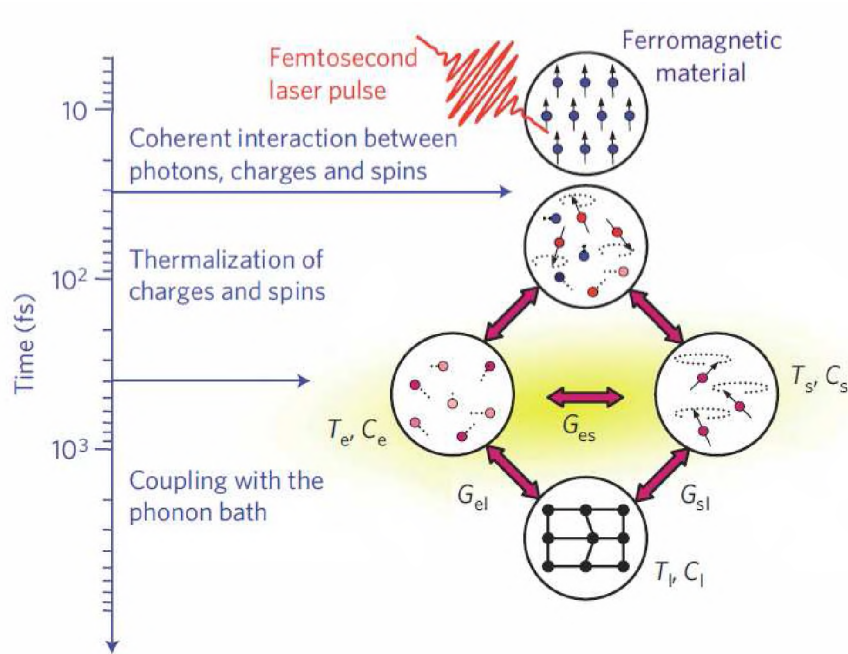


Figure 1.5: A pictorial representation of ultrafast demagnetization. A femtosecond laser pulse interacts coherently with charges and spins of electrons, which subsequently thermalize and interact together with the lattice (from [42]).

many fundamental questions are still unanswered. The response of the spins on subpicosecond time scales and the characteristic times of interactions among different reservoirs of angular momentum are the main questions to be answered on the way to ultrafast control of magnetism.

1.3.3 Laser control of magnetization

Since femtosecond laser pulses offer the intriguing possibility to probe a magnetic system on a time scale of the exchange interaction, responsible for the existence of magnetic order, a laser could be a solution to unveil the fundamental issues of conservation of angular momentum, which is intimately connected to the magnetization.

Currently there is a proposed technology using lasers to manipulate magnetization and extend magnetic recording beyond the super-paramagnetic limit: *heat-assisted magnetic recording* (HAMR) [46–48]. The idea of HAMR is to use a medium with a

large magnetic anisotropy and to locally reduce the magnitude of the magnetic field required to write a bit by applying a very short and localized heat pulse with a laser, as illustrated in Figure 1.6(a). Challenges associated with this idea include the cost of the laser and the technology required to deliver the heat pulses on the required small bit areas, as well as problems associated with keeping the heat localized in the metallic storage medium, which is a good heat conductor.

In all the magnetization switching processes described above, the reversal can be obtained using an external magnetic field. This, however, introduces a difficulty of having magnetic fields varied rapidly in time. A similar problem is experienced by the emerging field of spintronics as in, for example, magnetic random access memory (MRAM) devices. The observed laser-induced magnetic changes mentioned above were of *thermal* origin. It means that the magnetic changes were a result of optical absorption followed by a rapid temperature increase. This thermal origin of spin excitation considerably limits potential applications because the repetition frequency is limited by the cooling time, during which no further writing may occur [49]. Moreover, because of this thermal excitation mechanism, the recording density and the stability of the recording device will also suffer from heat diffusion, the removal of

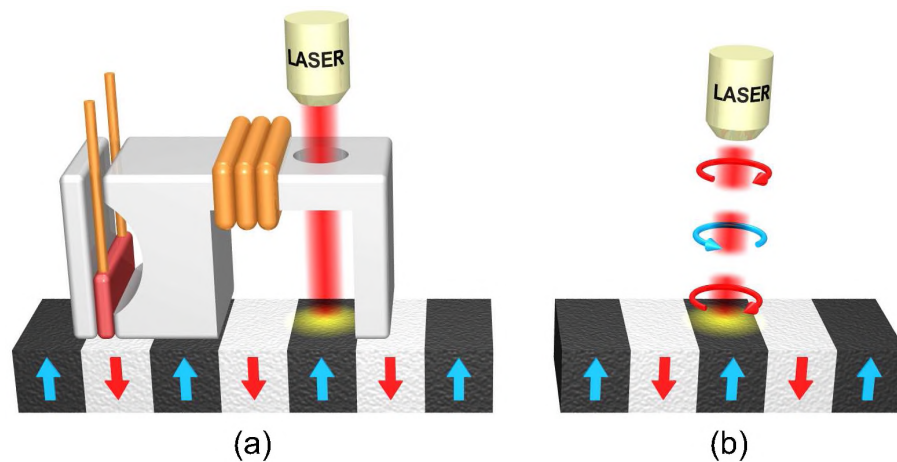


Figure 1.6: (a) HAMR works by adding a laser to the write-head assembly which heats the media at the exact spot where data needs to be written. The heat enables the media to become easier to write at higher densities with small magnitude of magnetic fields. Upon completion of the switching, the laser turns off, the media cools, and the media and bit at that spot will remain stable. (b) In all-optical switching, the magnetization of a magnetic bit can be controlled only by the helicity of circularly polarized laser pulses without the aid of an external magnetic field.

which is not a trivial process. The solution to these problems could be a *nonthermal* optical method of manipulating the magnetization, a method controlling the electron spins without relying on absorption of the light, as pictured in Figure 1.6(b).

Is it possible that photons affect magnetization? The magneto-optical Faraday effect is the rotation of the polarization vector of linearly polarized light as it propagates through a transparent sample in a magnetic field [50, 51]; it is discussed in detail in Chapter 3. This effect clearly demonstrates that a magnetically ordered medium can indeed affect photons and change the polarization of light [52]. Is the inverse phenomenon feasible?

In 2005, a remarkable experimental result was reported by Kimel *et al.*: circularly polarized laser pulses were shown to non-thermally excite coherent spin precession in the dielectric antiferromagnet DyFeO_3 [53]. They proposed that a circularly polarized laser pulse acts on the magnetic system as an effective magnetic field pulse \mathbf{H}_F , the direction of which is defined by the wavevector and the helicity of the light. This opto-magnetic effect was described as the *inverse Faraday effect* (IFE) [54–56]:

$$\mathbf{H}_F = \alpha [\mathbf{E}(\omega) \times \mathbf{E}^*(\omega)] \quad (1.7)$$

where $\mathbf{E}(\omega)$ and $\mathbf{E}^*(\omega)$ are respectively the electric field of the light wave and its complex conjugate at the frequency ω ; α is the magneto-optical susceptibility. Recently, many experiments have been performed and proved the existence of this effect in ferromagnetic garnet films [57, 58], another type of rare-earth orthoferrite [59], metallic GdFeCo alloy [60], and antiferromagnetic NiO [61]. Additionally, nonthermal opto-magnetic effects with both linearly⁴ and circularly polarized pulses were also measured in antiferromagnetic iron borate (FeBO_3) that possesses a strong magneto-optical response [62, 63]. All these results, which inspired the studies in this thesis, showed that circularly polarized light can be an effective tool to control spins in magnetically ordered materials and on a femtosecond time scale. The suggested mechanism for laser control of spins does not require annihilation of photons and the light-induced spin-flip does not require the loss of the angular momentum of the photons [21, 64].

1.4 All-optical magnetization reversal

As was discussed above, using femtosecond laser pulses one may trigger spin oscillations and have a control over the spin motion at ultrafast time scales. More interestingly, circularly polarized ultrashort laser pulses can even act as equally short magnetic field pulses via inverse Faraday effect. The observation of this effect leads to a fundamentally important and technologically challenging issue: is it possible to reverse the magnetization by a subpicosecond stimulus?

⁴The effective fields induced by linearly polarized light can be referred to as an ultrafast inverse Cotton-Mouton or inverse Voigt effect.



Figure 1.7: The effect of single 40 fs left- and right-handed circularly polarized laser pulses on the magnetic domains in GdFeCo ferrimagnetic metal (from [66, 67]). These experiments showed the possibility of magnetization reversal with a femtosecond stimulus. However, the actual time scales of such a reversal are unclear.

This challenge was considered by estimating the number of photons that are absorbed and the dichroism of the magnetic medium. Koopmans *et al.* reported that the photon angular momentum is irrelevant for the direct transfer of angular momentum from the light to the magnetic system [31]. Additionally, using circularly polarized light they showed that after the excitation, the magnetic system is left in the same state regardless the polarization [65]. In contrast to these results, Stanciu *et al.* demonstrated that a single 40 fs circularly polarized laser pulse can cause well controlled permanent magnetization reversal (180° switching) in materials typically used for data storage [66]. As it can be seen from Figure 1.7, the reversed magnetic domains are defined by the helicity of the circularly polarized laser pulses, which are swept at high speeds across the sample so that each pulse landed at a different spot. Initially, the optical excitation of the laser pulses leads to an ultrafast heating of the magnetic system. This heating makes the magnetic system highly susceptible to the magnetic field simultaneously generated by the circularly polarized light pulses. The combination of these two effect allows one to reverse the magnetization in a reproducible way. These experiments unambiguously demonstrate that (i) all-optical magnetization reversal can be achieved by single 40 fs circularly polarized laser pulses without the aid of an external magnetic field, and (ii) the information about the angular momentum of photons is transferred to the magnetic system during the presence of the laser pulse.

Although these experiments showed the intriguing possibility of magnetization reversal with a femtosecond stimulus, the actual time scales and the microscopical mechanism of such an optically induced magnetization reversal are unclear. A precessional magnetic switching within such a short duration would require enormous effec-

tive magnetic fields, and an unrealistically strong damping. Since the time needed for magnetic recording is an important parameter for present storage systems, the actual speed and the mechanism of all-optical magnetization reversal are very crucial for the future of the magnetic storage technologies. Therefore, the main goal of this thesis concentrated on these two key issues to provide more insights into the fundamental speed of the magnetic switching.

1.5 Scope of this thesis

Among the above-mentioned key issues in laser-induced magnetization dynamics, the ultrafast magnetization switching is the most challenging topic in modern magnetism with a potentially high impact for future spintronics, data storage and manipulation, and quantum computation. Therefore, the study of the fundamental and practical limits on the speed of manipulation of the magnetization is obviously of great importance for magnetic recording. Understanding the underlying mechanisms of this reversal process implies understanding the interaction of photons with charges, spins, and lattice, and the angular momentum transfer between them. Hence, the present thesis describes an experimental study of ultrafast laser-induced magnetization dynamics in amorphous ferrimagnetic alloys. The study is supported theoretically by the groups of Prof. Roy Chantrell (University of York) and Prof. Ulrich Nowak (University of Konstanz).

Starting with this introduction chapter, the interaction of light with magnetically ordered matter and the challenges of possible magnetization switching are discussed. Chapter 2 describes the materials which are used in this study. The fundamental magnetic and magneto-optical properties of amorphous rare earth – transition metal (RE–TM) alloys, which are the most favorable magneto-optical recording media, are explained. In Chapter 3, we outline the experimental apparatus and three different techniques that allow us to study ultrafast magnetization dynamics. In particular, we describe (i) an all-optical pump-probe technique which is used to study laser-induced magnetization dynamics, (ii) a single-shot time-resolved magneto-optical imaging technique which is used to reveal the evolution and speed of the magnetization reversal, and (iii) time-resolved X-ray spectroscopy, which was employed to investigate the magnetization dynamics in an element-specific way.

The experimental results are presented in Chapters 4 and 5. Chapter 4, in particular, focuses on all-optical magnetization reversal by single circularly polarized laser pulses in RE–TM alloys. Using single-shot time-resolved magneto-optical microscopy we identify the speed of magnetization reversal and describe the unconventional path followed by the magnetization during the reversal process. Moreover, we also experimentally investigate the optimal conditions for all-optical magnetization switching in terms of alloy composition, and duration and polarization of the laser pulse.

In Chapter 5 we study the spin reversal in a RE–TM alloy, which is optically

excited on a time scale pertinent to the characteristic time of the exchange interaction between the sublattice spins. Based on the X-ray magnetic circular dichroism (XMCD) effect, the behavior of each magnetic sublattice is investigated by using a laser pump – X-ray probe technique. We find that following the optical excitation, the magnetizations of the sublattices switch their direction at different time scales. These surprising observations, which are supported by atomistic simulations, show that the ultimately fast magnetization reversal occurs on a time scale of the exchange interaction, which is an unexplored territory in magnetism. Finally, we end with a summary of the results presented in this thesis and give an overview of future directions in the field of ultrafast magnetization dynamics.

References

- [1] D. Weller and A. Moser, *IEEE Trans. Magn.* **35**, 4423 (1999).
- [2] G. C. Hadjipanayis, *Magnetic Storage Systems Beyond 2000* (Springer, 2001).
- [3] D. Sellmyer, M. Yan, Y. Xu, and R. Skomski, *IEEE Trans. Magn.* **41**, 560 (2005).
- [4] J. Stöhr and H. C. Siegmann, *Magnetism: From Fundamentals to Nanoscale Dynamics* (Springer-Verlag, Berlin, 2006).
- [5] F. G. Sánchez, Ph.D. thesis, Universidad Autónoma de Madrid (2007).
- [6] K. Z. Gao, O. Heinonen, and Y. Chen, *J. of Magn. Magn. Mater.* **321**, 495 (2009).
- [7] Z. Lu, Ph.D. thesis, University of Alabama (2009).
- [8] L. Landau and E. Lifshitz, *Phys. Z. Sowjetunion.* **8**, 153 (1935).
- [9] B. Hillebrands and K. Ounadjela, *Spin Dynamics in Confined Magnetic Structures I*, Topics in Applied Physics (Springer-Verlag, Berlin, 2002).
- [10] T. Gilbert, *IEEE Trans. Magn.* **40**, 3443 (2004).
- [11] J. Pommier, P. Meyer, G. Pénissard, J. Ferré, P. Bruno, and D. Renard, *Phys. Rev. Lett.* **65**, 2054 (1990).
- [12] C. H. Back, D. Weller, J. Heidmann, D. Mauri, D. Guarisco, E. L. Garwin, and H. C. Siegmann, *Phys. Rev. Lett.* **81**, 3251 (1998).
- [13] C. H. Back, R. Allenspach, W. Weber, S. S. P. Parkin, D. Weller, E. L. Garwin, and H. C. Siegmann, *Science* **285**, 864 (1999).
- [14] S. Kaka and S. E. Russek, *Appl. Phys. Lett.* **80**, 2958 (2002).

-
- [15] T. Gerrits, H. A. M. van den Berg, J. Hohlfeld, L. Bar, and T. Rasing, *Nature* **418**, 509 (2002).
 - [16] H. W. Schumacher, C. Chappert, P. Crozat, R. C. Sousa, P. P. Freitas, J. Miltat, and J. Ferre, *IEEE Trans. Magn.* **38**, 2480 (2002).
 - [17] H. W. Schumacher, C. Chappert, P. Crozat, R. C. Sousa, P. P. Freitas, J. Miltat, J. Fassbender, and B. Hillebrands, *Phys. Rev. Lett.* **90**, 017201 (2003).
 - [18] I. Tudosa, C. Stamm, A. B. Kashuba, F. King, H. C. Siegmann, J. Stöhr, G. Ju, B. Lu, and D. Weller, *Nature* **428**, 831 (2004).
 - [19] I. Tudosa, Ph.D. thesis, Stanford University (2005).
 - [20] R. Hertel, S. Gliga, M. Fähnle, and C. M. Schneider, *Phys. Rev. Lett.* **98**, 117201 (2007).
 - [21] A. Kirilyuk, A. V. Kimel, and T. Rasing, *Rev. Mod. Phys.* **82**, 2731 (2010).
 - [22] M. B. Agranat, S. Ashitkov, A. Granovsky, and G. Rukman, *Zh. Eksp. Teor. Fiz.* **86**, 1376 (1984).
 - [23] A. Vaterlaus, D. Guarisco, M. Lutz, M. Aeschlimann, M. Stampanoni, and F. Meier, *J. Appl. Phys.* **67**, 5661 (1990).
 - [24] A. Vaterlaus, T. Beutler, and F. Meier, *Phys. Rev. Lett.* **67**, 3314 (1991).
 - [25] A. Vaterlaus, T. Beutler, D. Guarisco, M. Lutz, and F. Meier, *Phys. Rev. B* **46**, 5280 (1992).
 - [26] E. Beaurepaire, J.-C. Merle, A. Daunois, and J.-Y. Bigot, *Phys. Rev. Lett.* **76**, 4250 (1996).
 - [27] J. Hohlfeld, E. Matthias, R. Knorren, and K. H. Bennemann, *Phys. Rev. Lett.* **78**, 4861 (1997).
 - [28] A. Scholl, L. Baumgarten, R. Jacquemin, and W. Eberhardt, *Phys. Rev. Lett.* **79**, 5146 (1997).
 - [29] J. Güdde, U. Conrad, V. Jähnke, J. Hohlfeld, and E. Matthias, *Phys. Rev. B* **59**, R6608 (1999).
 - [30] G. Ju, A. V. Nurmikko, R. F. C. Farrow, R. F. Marks, M. J. Carey, and B. A. Gurney, *Phys. Rev. Lett.* **82**, 3705 (1999).
 - [31] B. Koopmans, M. van Kampen, J. T. Kohlhepp, and W. J. M. de Jonge, *Phys. Rev. Lett.* **85**, 844 (2000).

-
- [32] H.-S. Rhie, H. A. Dürr, and W. Eberhardt, *Phys. Rev. Lett.* **90**, 247201 (2003).
- [33] J.-Y. Bigot, L. Guidoni, E. Beaurepaire, and P. N. Saeta, *Phys. Rev. Lett.* **93**, 077401 (2004).
- [34] T. Ogasawara, K. Ohgushi, Y. Tomioka, K. S. Takahashi, H. Okamoto, M. Kawasaki, and Y. Tokura, *Phys. Rev. Lett.* **94**, 087202 (2005).
- [35] G. Ju, A. V. Nurmikko, R. F. C. Farrow, R. F. Marks, M. J. Carey, and B. A. Gurney, *Phys. Rev. B* **58**, R11857 (1998).
- [36] M. van Kampen, C. Jozsa, J. T. Kohlhepp, P. LeClair, L. Lagae, W. J. M. de Jonge, and B. Koopmans, *Phys. Rev. Lett.* **88**, 227201 (2002).
- [37] A. V. Kimel, A. Kirilyuk, A. Tsvetkov, R. V. Pisarev, and T. Rasing, *Nature* **429**, 850 (2004).
- [38] G. Ju, J. Hohlfeld, B. Bergman, R. J. M. van de Veerdonk, O. N. Mryasov, J.-Y. Kim, X. Wu, D. Weller, and B. Koopmans, *Phys. Rev. Lett.* **93**, 197403 (2004).
- [39] J.-U. Thiele, M. Buess, and C. H. Back, *Appl. Phys. Lett.* **85**, 2857 (2004).
- [40] C. Stamm, T. Kachel, N. Pontius, R. Mitzner, T. Quast, K. Holldack, S. Khan, C. Lupulescu, E. F. Aziz, M. Wietstruk, et al., *Nature Materials* **6**, 740 (2007).
- [41] G. Zhang, W. Hübner, E. Beaurepaire, and J.-Y. Bigot, *Spin Dynamics in Confined Magnetic Structures I, Topics in Applied Physics*, vol. 83 (Springer, New York, 2002).
- [42] J.-Y. Bigot, M. Vomir, and E. Beaurepaire, *Nature Physics* **5**, 515 (2009).
- [43] W. Hübner and G. P. Zhang, *Phys. Rev. B* **58**, R5920 (1998).
- [44] G. P. Zhang and W. Hübner, *Phys. Rev. Lett.* **85**, 3025 (2000).
- [45] B. Koopmans, G. Malinowski, F. Dalla Longa, D. Steiauf, M. Fahnle, T. Roth, M. Cinchetti, and M. Aeschlimann, *Nature Materials* **9**, 259 (2010).
- [46] <http://spectrum.ieee.org/computing/hardware/laserheated-hard-drives-could-break-data-density-barrier/>.
- [47] M. A. Seigler, W. A. Challener, E. Gage, N. Gokemeijer, G. Ju, B. Lu, K. Pelhos, C. Peng, R. E. Rottmayer, X. Yang, et al., *IEEE Trans. Magn.* **44**, 119 (2008).
- [48] W. A. Challener, C. Peng, A. V. Itagi, D. Karns, W. Peng, Y. Peng, X. Yang, X. Zhu, N. J. Gokemeijer, Y.-T. Hsia, et al., *Nature Photonics* **3**, 220 (2009).

-
- [49] J. Hohlfeld, T. Gerrits, M. Bilderbeek, T. Rasing, H. Awano, and N. Ohta, *Phys. Rev. B* **65**, 012413 (2001).
- [50] M. Faraday, *Philos. Trans. R. Soc. London* **136**, 1 (1845).
- [51] M. Faraday, *Philos. Mag.* **28**, 294 (1846).
- [52] A. K. Zvezdin and V. A. Kotov, *Modern Magneto-optics and Magneto-optical Materials* (Institute of Physics Publishing, London, 1997).
- [53] A. V. Kimel, A. Kirilyuk, P. A. Usachev, R. V. Pisarev, A. M. Balbashov, and T. Rasing, *Nature* **435**, 655 (2005).
- [54] L. P. Pitaevskii, *Sov. Phys. JETP* **12**, 1008 (1961).
- [55] J. P. van der Ziel, P. S. Pershan, and L. D. Malmstrom, *Phys. Rev. Lett.* **15**, 190 (1965).
- [56] P. S. Pershan, J. P. van der Ziel, and L. D. Malmstrom, *Phys. Rev.* **143**, 574 (1966).
- [57] F. Hansteen, A. Kimel, A. Kirilyuk, and T. Rasing, *Phys. Rev. Lett.* **95**, 047402 (2005).
- [58] F. Hansteen, A. Kimel, A. Kirilyuk, and T. Rasing, *Phys. Rev. B* **73**, 014421 (2006).
- [59] A. V. Kimel, C. D. Stanciu, P. A. Usachev, R. V. Pisarev, V. N. Gridnev, A. Kirilyuk, and T. Rasing, *Phys. Rev. B* **74**, 060403 (2006).
- [60] C. D. Stanciu, F. Hansteen, A. V. Kimel, A. Tsukamoto, A. Itoh, A. Kirilyuk, and T. Rasing, *Phys. Rev. Lett.* **98**, 207401 (2007).
- [61] T. Satoh, S.-J. Cho, R. Iida, T. Shimura, K. Kuroda, H. Ueda, Y. Ueda, B. A. Ivanov, F. Nori, and M. Fiebig, *Phys. Rev. Lett.* **105**, 077402 (2010).
- [62] A. M. Kalashnikova, A. V. Kimel, R. V. Pisarev, V. N. Gridnev, A. Kirilyuk, and T. Rasing, *Phys. Rev. Lett.* **99**, 167205 (2007).
- [63] A. M. Kalashnikova, A. V. Kimel, R. V. Pisarev, V. N. Gridnev, P. A. Usachev, A. Kirilyuk, and T. Rasing, *Phys. Rev. B* **78**, 104301 (2008).
- [64] A. Kimel, A. Kirilyuk, and T. Rasing, *Laser & Photon. Rev.* **1**, 275 (2007).
- [65] F. Dalla Longa, J. T. Kohlhepp, W. J. M. de Jonge, and B. Koopmans, *Phys. Rev. B* **75**, 224431 (2007).

-
- [66] C. D. Stanciu, F. Hansteen, A. V. Kimel, A. Kirilyuk, A. Tsukamoto, A. Itoh, and T. Rasing, *Phys. Rev. Lett.* **99**, 047601 (2007).
- [67] C. D. Stanciu, Ph.D. thesis, Radboud University Nijmegen (2008).

Amorphous rare earth – transition metal alloys

2.1 Introduction

Beginning with the first commercial hard-disk drive¹ (HDD) in 1955, magnetic disk drive technology has integrated many science and engineering disciplines [1]. The demands for faster information storage and larger bit areal density triggered the improvements in materials which are used for magnetic recording. Although it had been believed that magnetic ordering could only occur in crystalline materials, in 1973 it was discovered that rare earth – transition metal (RE–TM) amorphous alloys possessed magnetic order [2]. The first investigations showed that RE–TM alloys exhibited a number of unique properties [2–39]. By now these properties have been used in numerous commercial products.

Among the magnetic recording systems, optical recording has great potential as an erasable/rewritable storage technology. Combination of optical data storage techniques and magnetic storage media, so-called *magneto-optical recording* (MO), has been used in magnetic drives to improve data density. In this emerging technology, the understanding of the fundamental magnetic and magneto-optical properties of the storage media is essential. The magnetic properties of these materials can be continuously tuned over a large range making them more versatile than other MO recording materials. This chapter provides an overview of these properties and the structure of RE–TM alloys studied in this work.

¹The first HDD was the 2-ton IBM 305 with 4.4 Mbytes of storage space.

2.2 Magnetic and magneto-optical properties

The RE–TM alloys have attracted considerable attention in the past decades in both technology and fundamental research. Since they are commonly used as the storage layer in magneto-optical storage media, over the years, a large variety of RE–TM combinations have been extensively investigated. By changing the compositions and deposition conditions, different magnetic properties can be achieved with these alloys. In order to discuss the magnetic properties of RE–TM amorphous alloys, it is convenient to classify them into the following two categories [27, 29, 40]:

1. Light RE–TM amorphous alloys:

In these alloys, the spins of light RE atoms (La, Ce, Pr, Nd, Pm, Sm and Eu) with a less than half-filled f -shell couple antiferromagnetically with the spins of the TM (Fe, Co, Ni) atoms. However, according to Hund’s rule, the spin-orbit coupling for such RE atoms is positive. The orbital moment of the atoms is larger than the spin moment and since it is aligned antiparallel to the spin moment, the magnetic moment of the RE is parallel (and randomly canted) to the net TM moment. In other words, these RE–TM alloys are effectively *ferromagnetic*;

2. Heavy RE–TM amorphous alloys:

In RE–TM alloys containing heavy RE atoms (Gd, Tb, Dy, Ho, Er, Tm, Yb and Lu) with a more than half-filled f -shell, the coupling of the RE spins with those of the TM (Fe, Co, Ni) atoms is also antiferromagnetic. However, for these RE atoms, according to Hund’s rule, the spin-orbit coupling is negative. Thus, the net RE moments align antiparallel (and randomly canted) to the TM moments and these alloys show *ferrimagnetism*.

The amorphous RE–TM alloys consist of heavy RE and TM atoms, which means that they show *ferrimagnetic* behavior. Among the heavy RE atoms, Gd is an S-state ion and shows a zero local anisotropy. Thus, the coupling between Gd and strong ferromagnetic TMs exhibits a unique collinear ferrimagnetic behavior. In other cases, the random anisotropy at the non-S-state RE (light or heavy RE) site competes with the exchange interaction to determine the orientation of the RE moment, leading to speromagnetic, asperomagnetic, or sperimagnetic order [20, 41].

In a ferrimagnet, the magnetizations of the sublattices are antiparallel but not identical and thus they do not cancel each other. The magnetizations of two sublattices generally exhibit different temperature dependencies, but they both have the same Curie temperature T_C . Figure 2.1 shows the typical temperature dependence of RE and TM magnetic moments with saturation magnetization (M_s) of the material. At low temperatures, the RE magnetization (M_{RE}) dominates, and the net magnetization points in the same direction as the M_{RE} . Due to different exchange interactions

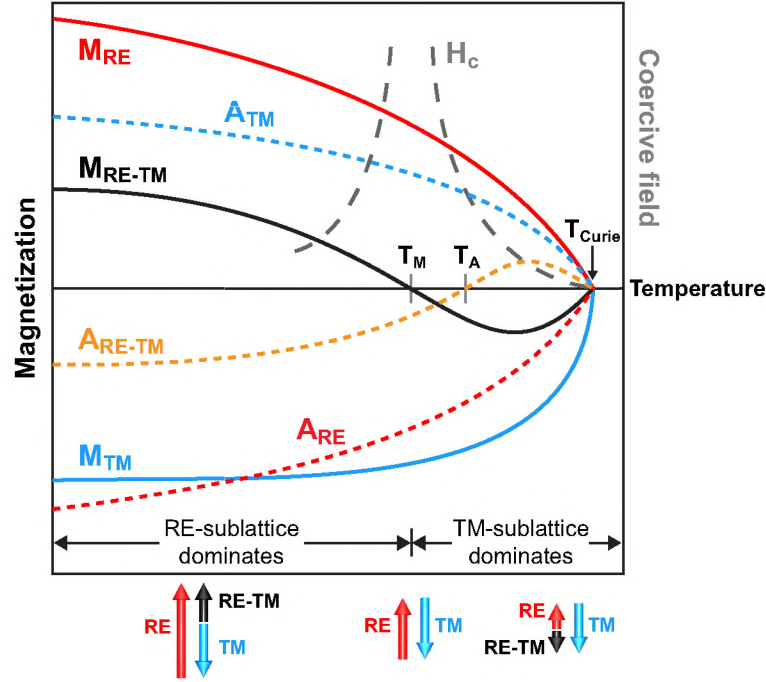


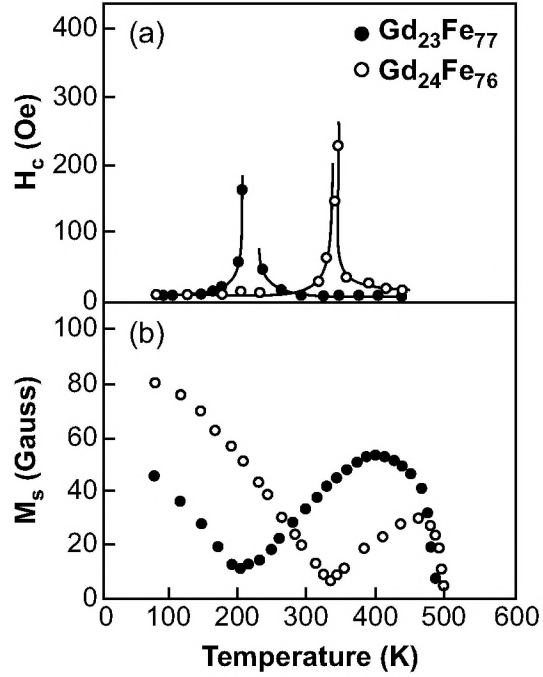
Figure 2.1: The temperature dependencies of sublattice magnetizations (M), angular momentum (A) and the coercive field (H_c) for a ferrimagnetic RE–TM alloy. The net magnetization and the angular momentum of each sublattices are opposite and decreases in a different way. This causes certain points, called the magnetization compensation temperature T_M , and angular momentum compensation temperature T_A . The coercivity H_c diverges around T_M .

within each sublattice, the decrease of the RE magnetization M_{RE} with increasing temperature is faster than that of the TM magnetization M_{TM} . At an intermediate temperature, called the *magnetization compensation temperature*, T_M , where:

$$M_T = \sum M_i = M_{RE} + M_{TM} = 0, \quad (2.1)$$

the two sublattice magnetizations are equal and opposite in direction, which causes the net magnetization to go to zero (see Figure 2.1). Above T_M , the M_{TM} becomes dominant and the net magnetization M_s points in the direction of the M_{TM} . At sufficiently high temperatures, thermal energy overcomes the exchange coupling and the ferrimagnetic behavior vanishes at the Curie temperature, T_C [23]. Furthermore, ferrimagnets may also exhibit an *angular momentum compensation point*, T_A , at which

Figure 2.2: (a) Coercive field H_c and (b) spontaneous saturation magnetization M_s versus temperature for ferrimagnetic GdFe films with variation of composition (from [6]).



the angular momentum of the magnetic sublattices is compensated due to the difference between the gyromagnetic ratios ($\gamma = \mathbf{m}/\mathbf{L}$) of the RE and TM sublattices. As can be seen in Figure 2.1, the angular momentum is coupled antiparallel with the magnetization due to the negative charge of the electron.

Such a behavior of these alloys leads to a strong temperature dependent coercivity H_c . As the temperature of the sample approaches T_M , a larger external magnetic field must be applied to overcome the energy barrier to switch the magnetization and the coercivity tends towards infinity at T_M (see Figure 2.1). This behavior is due to the fact that $H_c \sim 2K_u/M$, where K_u is the uniaxial anisotropy constant. Since M goes to zero at T_M , H_c diverges. Conversely, towards T_C , where the ferrimagnetic phase undergoes a transition to a paramagnetic one, the coercivity vanishes since K_u has a stronger temperature dependence than M .

The reduction of the coercivity with increasing temperature was used in MO recording. The writing and re-writing of data on MO media rely on the heat generated by a focused laser beam to raise the material's temperature and bring it in the vicinity of the Curie point T_C . A small externally applied magnetic field (~ 100 Oe) can then define the direction of the magnetization of the heated spot after the laser has been turned off and the material has cooled down. Such a writing can be achieved

by a continuous-wave (CW) laser beam and modulated magnetic field [29]. Since the coercive field value, which is the required applied magnetic field to reverse the magnetization, diverges at the compensation point T_M of the medium, for typical MO media T_M is usually placed in the vicinity of room temperature, making the disk resistant to possible erasure by stray fields. Figure 2.2 shows the variation of the compensation points, T_M , by simply changing the composition of the RE and TM components.

The anisotropy energy E_a of RE-TM films strongly depends on the RE content of the film and the deposition conditions, such as sputtering gas pressures, etc. The highly energetic sputtered atoms can cause a local atomic rearrangement in the film such that they can induce perpendicular magnetic anisotropy. Thus, the magnetization prefers to lie perpendicular to the film plane. The anisotropy energy may be described by the equation:

$$E_a = K_u \sin^2 \theta. \quad (2.2)$$

where θ is the angle of the magnetization with respect to the film normal. In ferromagnetic light RE-TM alloys, the saturation magnetization with perpendicular anisotropy is large, therefore due to the large demagnetizing field it is very difficult to obtain completely square hysteresis loops. Conversely, in the heavy RE-TM alloys, perpendicular magnetization with a remanence ratio of one ($M_s/M_r \approx 1$, where M_r is the remanence magnetization) can be acquired even when the perpendicular anisotropy energy is relatively small. This means that once the magnetization of the medium has been saturated in the direction of the applied field, changing or removing

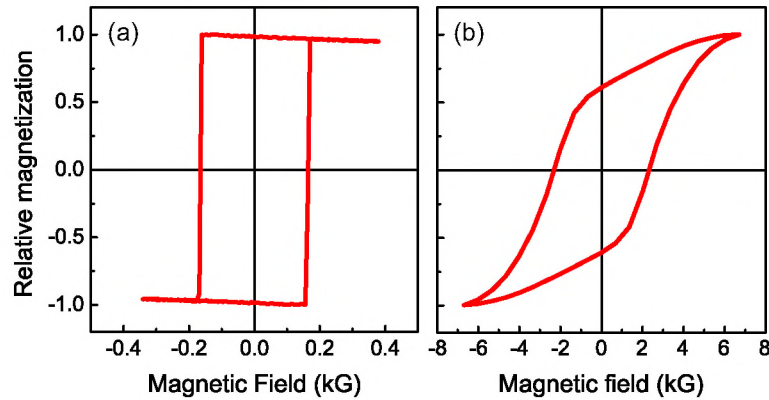


Figure 2.3: (a) A square magnetic hysteresis loop for an ideal heavy RE-TM alloy. (b) In light RE-TM alloys the loop is typically skewed by the aggregated perpendicular demagnetizing field.

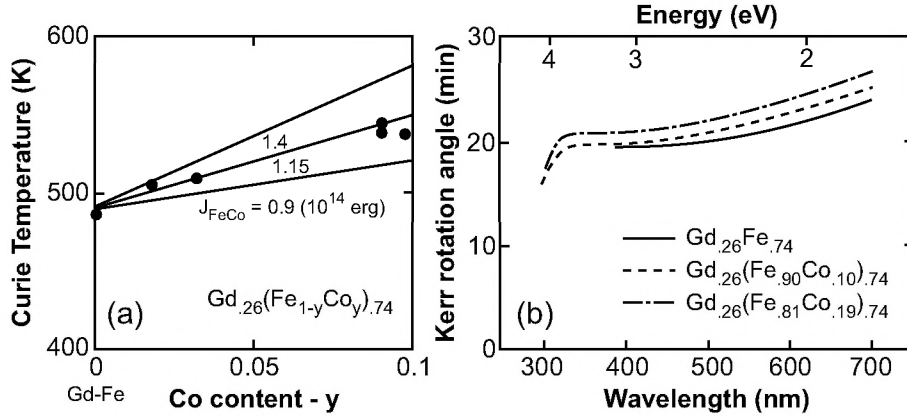


Figure 2.4: (a) The Curie temperature T_C as a function of Co content and (b) the Kerr rotation spectra for GdFe and GdFeCo amorphous alloys (from [8]).

the applied magnetic field does not cause a reduction of the magnetization. In addition, when the applied magnetic field reaches the coercive field value H_c , the reversal and saturation of the magnetization occur abruptly. A comparison of hysteresis loops regarding the RE class is shown in Figure 2.3.

An enhancement of the magneto-optical effects in RE–TM alloys is also crucial to make these materials more favorable for magneto-optical recording. It is well known that the Faraday (or Kerr) rotation correlates with the atomic magnetic moment or spin, due to spin-orbit interaction. Through this interaction the light interacts mainly with the TM magnetic sublattice in the near infrared or visible range, while the RE magnetic sublattice becomes dominant in the ultraviolet region (below $\lambda = 300$ nm) [10, 13, 15, 19, 23, 29, 33, 37]. The magnetic electrons of 3d transition metal, like Fe and Co, are located in the 3d electronic shell, which forms the outer layer of the ion once the 4s electrons escape into the sea of conduction electrons [29, 40]. Unlike in the 3d TMs, the Fermi level of the 4f electrons responsible for the magnetic moment in the REs lies too deep for the 4f electrons to be excited by visible or near infrared wavelengths of light. For shorter wavelengths, some of the RE 4f states can be excited so that they can contribute to the Faraday rotation from RE 4f – 5d transitions [27].

Since the MO effect originates from the polarization of RE and TM atoms in these alloys, the maximum effect can be achieved through the control of RE and TM concentrations and deposition conditions. For instance, in a RE–FeCo amorphous alloy it was shown that replacing some Fe atoms with Co enhances the Kerr rotation and the Curie temperature T_C becomes higher with increasing Co content [8, 22]. Figures 2.4(a,b) respectively show the effect of Co substitution on T_C and the wavelength

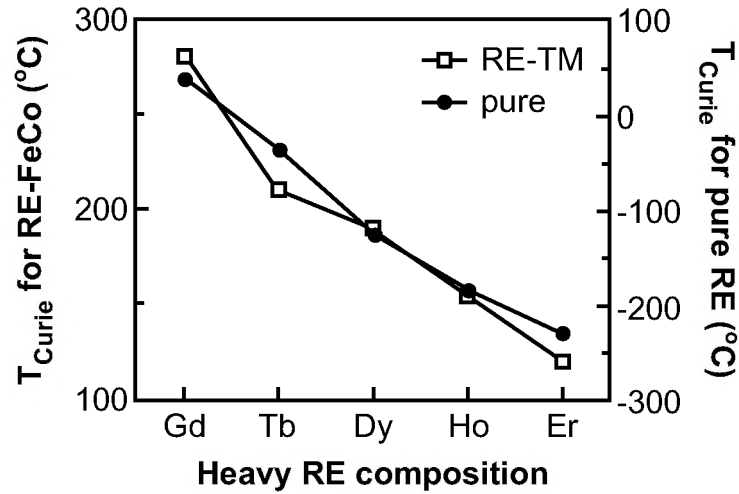


Figure 2.5: The Curie temperature T_C dependence upon composition for pure RE metals and RE-FeCo alloys (from [17]).

dependence of the Kerr rotation spectra. Additionally, it can be seen from Figure 2.5 that as the RE gets heavier, T_C decreases [17]. Once the M_{TM} is effectively reduced, the Faraday rotation, which in the visible spectral range depends upon the interaction of the light with $3d$ valance electrons, is also reduced.

A comparison of the above described dependencies for various RE-TM combinations indicates that the most suitable properties can be obtained in GdFeCo amorphous alloys.

2.3 Gadolinium-iron-cobalt (GdFeCo)

In the earlier discussion it was mentioned that some of the most important features in MO media can be controlled over a wide range by choosing the elements that form the RE and TM components of the film, and adjusting the stoichiometry. The effects of various RE metals on the properties of RE-TM films were studied by Hairston and Kryder [17]. It was shown that in a multilayer structure, films where Gd dominated the rare earth composition can be used as MO layer to provide a higher Kerr (or Faraday) effect. Therefore, in this section we will focus on ferrimagnetic amorphous gadolinium-iron-cobalt (GdFeCo) alloys studied in this thesis.

2.3.1 Growth

Amorphous RE–TM films can be prepared in a wide compositional range by electron beam evaporation or magnetron sputtering. The structure and the magnetic properties depend sensitively on the preparation method and parameters. Among the methods, d.c. magnetron sputtering is the most favored because it gives much higher deposition rates and does not require substrate cooling [18]. Some of the more important parameters include target power, working gas, working gas pressure, type of substrate and substrate to target distance. Furthermore, these variables may be used directly to influence the parameters θ_F and K_u .

The design of MO disks not only has to improve the write-read efficiency by dielectric and metal layers but also to protect the MO layer in between. Therefore, a practical form of MO disks consists of a thin RE–TM film sandwiched between two dielectric layers on a highly reflecting aluminum layer. In this multilayer structure, the dielectric protection layers act as diffusion barriers for oxygen. Dielectric layers such as Si_3N_4 and AlN , and metallic layers such as Al and Cr have the proper optical and thermal properties [18].

The substrate of the multilayer structure is also another key issue. In general, a transparent plastic substrate is used for MO recording to allow optical access to the recording layer. There is an emerging trend to use glass to replace the plastic substrate. The glass, being rigid and smoother, provides a substantial improvement in minimal optical distortion and birefringence [16].

2.3.2 Samples studied in this work

The Gd-TM alloys studied in this work are ferrimagnetic amorphous GdFeCo^2 alloys, which have received great deal of attention in recent years. As discussed earlier, GdFeCo alloys that contain a small amount of Co exhibit an enhanced MO effect and addition of Co increases the T_C and their magneto-optical susceptibility [42, 43].

As shown in Figure 2.6(a), the films, prepared by magnetron sputtering, have the following multilayer structure: glass | AlTi (10 nm) | SiN (5 nm) | GdFeCo (20 nm) | SiN (60 nm). The AlTi layer serves as a reflector and heat sink and the dielectric layer SiN as buffer and capping layer respectively. These alloys are members of a very successful material class for MO recording because of their high perpendicular anisotropy, square hysteresis loops and high values of signal-to-noise ratio.

Gadolinium (Gd) is a member of the lanthanide series with the ground-state electronic configuration of $4f^7(5d6s)^3$ [35, 40]. According to Hund's rule, Gd with half-filled $4f$ shell possesses the maximum spin moment of $S = 7/2$ and no orbital moment, $L = 0$ [44]. The coupling between Gd and TM spins is antiferromagnetic and thus Gd–TM alloys have a ferrimagnetic structure.

²The samples were grown by Dr. A. Tsukamoto and Prof. A. Itoh at the College of Science and Technology, Nihon University, Chiba, Japan.

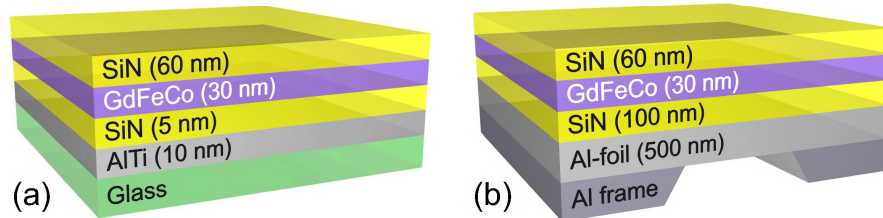


Figure 2.6: (a) Overview of the sample structure for the experiments with visible range of light. (b) For element specific X-ray experiments, 500 nm thick Al-foil layer is replaced instead AlTi heat sink layer.

As mentioned earlier, in the near infrared and visible range of light, the magneto-optical effect is mainly attributed to the polarization of $3d$ TM electrons (FeCo). Therefore, in order to investigate the magnetization of the RE atoms (Gd), one should be able to excite $4f$ electrons. This is possible by using shorter wavelengths, for instance X-rays. For the absorption geometry in the soft X-ray range from 0.12 to 12 keV (10 nm to 0.10 nm), the multilayer structure is deposited on a 500 nm thick free-standing Al-foil (Lebow Company), which is fixed on an Al frame. The structure of Al frame | Al-foil | SiN(100 nm) | GdFeCo(30 nm) | SiN(60 nm) is prepared by using magnetron sputtering. A side-view of the sample structure is shown in Figure 2.6(b). The Al-foil is nearly transparent (67% for Fe and 90% for Gd transmission) to X-rays, and structurally strong enough to support the multilayer structure. The transmission of a 500 nm thick Al film as a function of photon energy is plotted in Figure 2.7.

2.4 Summary

To summarize the above described properties of ferrimagnetic amorphous RE–TM alloys, we can list the most important issues which make these alloys an attractive model system for our study:

- the alloys possess a *ferrimagnetic structure* with a *magnetization compensation point*. This ferrimagnetic behavior can be used to tune both T_C and T_M over fairly wide temperature range by varying the composition;
- large *magneto-optical effects* and a pronounced *perpendicular magnetic anisotropy* in the alloys make readout of the magnetic state easy;
- the alloys have an *amorphous structure* and their reflectivity is uniform. Due to this fact, when the beam is moved across the sample, the fluctuations of the read signal are minimal.

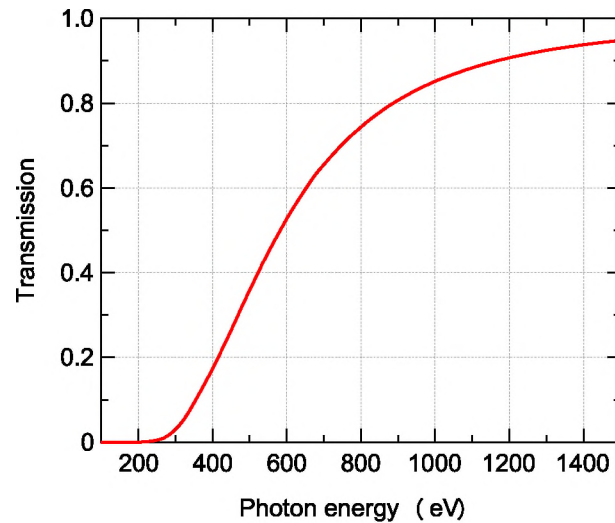


Figure 2.7: The transmission curve for a 500 nm thick Al film [45].

These advantages enhances the usability of RE–TM alloys and allow one to optimize the magnetic and magneto-optical parameters of these alloys nearly independently from one another. Therefore, these materials offer a rather rich ground to search for novel mechanism of magnetization reversal in magnetic and magneto-optical materials.

References

- [1] Z. Bandic and R. H. Victora, *Proceedings of the IEEE* **96**, 1749 (2008).
- [2] P. Chaudhari, J. Cuomo, and R. Gambino, *Appl. Phys. Lett.* **22**, 337 (1973).
- [3] J. M. D. Coey, J. Chappert, J. P. Rebouillat, and T. S. Wang, *Phys. Rev. Lett.* **36**, 1061 (1976).
- [4] R. C. Taylor and A. Gangulee, *J. Appl. Phys.* **47**, 4666 (1976).
- [5] R. C. Taylor and A. Gangulee, *J. Appl. Phys.* **48**, 358 (1977).
- [6] Y. Mimura, N. Imamura, T. Kobayashi, A. Okada, and Y. Kushiro, *J. Appl. Phys.* **49**, 1208 (1978).
- [7] J. M. D. Coey, *J. Appl. Phys.* **49**, 1646 (1978).

-
- [8] S. Tsunashima, S. Masui, T. Kobayashi, and S. Uchiyama, *J. Appl. Phys.* **53**, 8175 (1982).
- [9] T. Kobayashi, F. Takahashi, K. Aratani, S. Tsunashima, and S. Uchiyama, *IEEE Trans. J. on Magn. in Japan* **1**, 684 (1985).
- [10] M. H. Kryder, *J. Appl. Phys.* **57**, 3913 (1985).
- [11] H.-P. D. Shieh and M. H. Kryder, *Appl. Phys. Lett.* **49**, 473 (1986).
- [12] W. Meiklejohn, *Proceedings of the IEEE* **74**, 1570 (1986).
- [13] G. Connell, *J. of Magn. Magn. Mater.* **54-57**, 1561 (1986).
- [14] M. Kryder, H.-P. Shieh, and D. Hairston, *IEEE Trans. Magn.* **23**, 165 (1987).
- [15] P. Hansen, C. Clausen, G. Much, M. Rosenkranz, and K. Witter, *J. Appl. Phys.* **66**, 756 (1989).
- [16] J.-S. Gau, *Mater. Sci. Eng. B* **3**, 371 (1989).
- [17] D. Hairston and M. Kryder, *IEEE Trans. Magn.* **25**, 3746 (1989).
- [18] S. Klahn, P. Hansen, and F. Greidanus, *Vacuum* **41**, 1160 (1990).
- [19] P. Hansen, *J. of Magn. Magn. Mater.* **83**, 6 (1990).
- [20] P. Hansen, S. Klahn, C. Clausen, G. Much, and K. Witter, *J. Appl. Phys.* **69**, 3194 (1991).
- [21] S. Defang, Y. Xiangyou, D. Tengda, J. Lina, J. Qi, and T. Jiuyao, *J. of Magn. Magn. Mater.* **115**, 35 (1992).
- [22] Z. Lee, X. Miao, P. Zhu, Y. Hu, D. Wan, D. Dai, S. Chen, and G. Lin, *J. of Magn. Magn. Mater.* **115**, 44 (1992).
- [23] M. H. Kryder, *Annu. Rev. Mater. Sci.* **23**, 411 (1993).
- [24] T. ho Wu, H. Fu, R. A. Hajjar, T. Suzuki, and M. Mansuripur, *J. Appl. Phys.* **73**, 1368 (1993).
- [25] J. Daval and B. Bechevet, *J. of Magn. Magn. Mater.* **129**, 98 (1994).
- [26] P. Hansen, D. Raasch, and D. Mergel, *J. Appl. Phys.* **75**, 5267 (1994).
- [27] J. Fernandez-Baca and W.-Y. Ching, *The magnetism of amorphous metals and alloys* (World Scientific, 1995).

-
- [28] R. Carey, D. M. Newman, and B. W. J. Thomas, *J. of Phys. D: Appl. Phys.* **28**, 2207 (1995).
- [29] M. Mansuripur, *The Physical Principles of Magneto-Optical Recording* (Cambridge University Press, Cambridge, 1995).
- [30] S. Uchiyama, X. Y. Yu, and S. Tsunashima, *J. Phys. Chem. Solids* **56**, 1557 (1995).
- [31] A. S. Andreenko and S. A. Nikitin, *Physics-Uspekhi* **40**, 581 (1997).
- [32] H. L. Gall, R. Sbiaa, and S. Pogossian, *J. Alloys Compd.* **275-277**, 677 (1998).
- [33] S. Tsunashima, *J. of Phys. D: Appl. Phys.* **34**, R87 (2001).
- [34] W. R. Hendren, R. Atkinson, R. J. Pollard, I. W. Salter, C. D. Wright, W. W. Clegg, and D. F. L. Jenkins, *J. Phys.: Condens. Matter* **15**, 1461 (2003).
- [35] O. S. Anilturk and A. R. Koymen, *Phys. Rev. B* **68**, 024430 (2003).
- [36] D. Jenkins, W. Clegg, J. Windmill, S. Edmund, P. Davey, D. Newman, C. D. Wright, M. Loze, M. Armand, R. Atkinson, et al., *Microsyst. Technol.* **10**, 66 (2003).
- [37] J. Y. Rhee, *J. Korean Phys. Soc.* **43**, 792 (2003).
- [38] T. Kobayashi, H. Hayashi, Y. Fujiwara, and S. Shiomi, *IEEE Trans. Magn.* **41**, 2848 (2005).
- [39] W. Rodewald, *Handbook of Magnetism and Advanced Magnetic Materials* (John Wiley & Sons, Ltd, 2007), chap. Rare-earth Transition-metal Magnets.
- [40] C. D. Stanciu, Ph.D. thesis, Radboud University Nijmegen (2008).
- [41] C. D. Mee and E. D. Daniel, *Magnetic Recording Technology* (The McGraw-Hill Companies, Inc., USA, 1990).
- [42] H. Tsujimoto, M. Shouji, A. Saito, S. Matsushita, and Y. Sakurai, *J. Magn. Soc. Jpn.* **7**, 119 (1983).
- [43] N. Endo, S. Masui, T. Kobayashi, S. Tsunashima, and S. Uchiyama, *J. Magn. Soc. Jpn.* **8**, 101 (1984).
- [44] I. E. Radu, Ph.D. thesis, Freie Universität Berlin (2006).
- [45] <http://www.cxro.lbl.gov/>.

CHAPTER 3

Experimental techniques

This chapter presents details of the experimental techniques that have been used to obtain the results described in this thesis. The basic characteristics of the techniques and technical details of the experimental setups are discussed. In the first section of this chapter the basic magneto-optical phenomena, that is, the Faraday effect and magnetic circular dichroism, are explained. Since our experiments were carried out in transmission we will mainly focus on the Faraday effect, which we used to investigate the magnetic and magneto-optical properties of the samples as a function of temperature. Next, the all-optical pump-probe approach will be introduced as a tool to study the ultrafast spin dynamics in magnetic systems. In addition to the conventional pump-probe technique, we modified the stroboscopic experimental setup in order to study the dynamics of all-optical magnetization reversal. Thereafter, a new technique, single-shot magneto-optical imaging, will be presented, and its advantages discussed that enable observation of all-optical magnetization switching. The final remarks in this chapter regard element-specific time-resolved X-ray magnetic circular dichroism (XMCD) experiments.

3.1 Linear magneto-optical effects

After the discovery of the magneto-optical (MO) effect in 1845 by M. Faraday, magneto-optical phenomena are extensively used for characterizing magnetic properties of solids including in-situ characterization of ultra-thin film structures under the con-

dition of ultra-high vacuum [1–4]. The first observation of a magneto-optical effect was performed studying an isotropic diamagnetic material, where $M_z = \chi H_z$ (M_z is the magnetization, χ is the magnetic susceptibility and H_z is the magnetic field strength). It was soon realized that the Faraday effect can be observed even without any magnetic field applied, in case the measurements are performed on a ferromagnetic material. Therefore, it is more correct to claim that the effect is proportional to M_z , not to H_z . In other words, an applied magnetic field has no influence on the electromagnetic wave; the Faraday effect is due to the interaction of light with the induced magnetization \mathbf{M} of the medium.

The Faraday effect, which is essential for most of the experiments presented in this thesis, takes place in most optically transparent materials (including liquids). In such materials the magnetic field breaks degeneracy between two circularly polarized states of electromagnetic radiation so that the materials possess two different refraction indices, n_L and n_R for left- and right-handed circularly polarized light, respectively. Linearly polarized light can be decomposed into the sum of two circularly polarized light waves rotating in opposite directions (left and right). The difference between n_L and n_R , Δn , induces a difference in the propagation velocity of the two light components. This difference in the propagation speeds creates a rotation θ_F of the polarization direction of the incident light:

$$\theta_F = \frac{\omega d_M}{2} \Delta n, \quad (3.1)$$

where ω is the frequency of the light beam, d_M is the thickness of the material and $\Delta n = n_L - n_R$.

For magnetic fields applied parallel to the z -axis, Δn is proportional to the z -component of the magnetic moment of the material M_z . Therefore, relation 3.1 can be approximated to:

$$\theta_F = V(\omega) d_M M_z, \quad (3.2)$$

where V is the Verdet constant, which is a function of the light frequency. Circular birefringence induced by a magnetic field is the origin of the Faraday effect, or Faraday rotation, which is schematically represented in Figure 3.1. This effect is a powerful technique to probe the magnetization M_z .

In order to understand the origin of the magneto-optical Faraday effect, we consider an interaction of light with a non-dissipative medium. The dielectric permittivity ($\hat{\epsilon}$) of such a (non-magnetic) medium without magnetic field can be described by a tensor:

$$\hat{\epsilon}(\omega) = \begin{pmatrix} \epsilon_{xx} & 0 & 0 \\ 0 & \epsilon_{yy} & 0 \\ 0 & 0 & \epsilon_{zz} \end{pmatrix}. \quad (3.3)$$

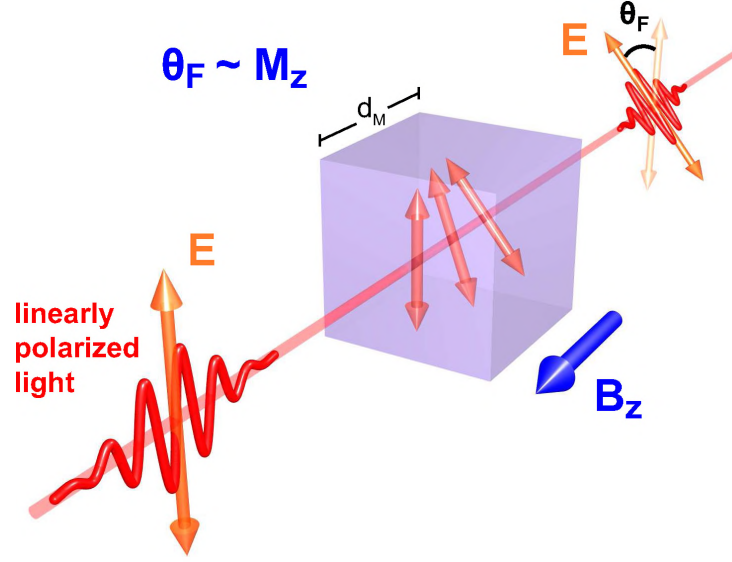


Figure 3.1: The Faraday effect: The polarization of a linearly polarized light beam rotates by an angle θ_F when it passes through matter in the direction of an applied magnetic field.

If the magnetization of the medium is non-zero, off-diagonal elements will appear. For an isotropic and non-absorbing medium without dissipations, the tensor $\hat{\epsilon}$ is Hermitian and its components satisfy:

$$\epsilon_{ij} = \epsilon_{ji}^*. \quad (3.4)$$

Regarding the generalized principle of symmetry of ϵ_{ij} , Eq.3.4 implies that the real and imaginary parts of the tensor in the absence of an applied magnetic field must be symmetrical [5]:

$$\epsilon_{ij} = \epsilon_{ji}, \quad (3.5)$$

and in the presence of a magnetic field ϵ_{ij} is no longer symmetrical and must obey the following relations:

$$\epsilon_{ij}(H) = \epsilon_{ji}(-H) = -\epsilon_{ji}(H), \quad (3.6)$$

which are the optical equivalent of the Onsager relations in thermodynamics. These relations show that the symmetric part of the tensor ϵ_{ij} is real and the antisymmetric

part is imaginary. Moreover, in an isotropic medium $\varepsilon_{xx} = \varepsilon_{yy} = \varepsilon_{zz}$ and considering the case where magnetization is parallel to the z -axis:

$$\hat{\varepsilon}(\omega) = \begin{pmatrix} \varepsilon_{xx} & i\varepsilon_{xy} & 0 \\ -i\varepsilon_{xy} & \varepsilon_{xx} & 0 \\ 0 & 0 & \varepsilon_{xx} \end{pmatrix}. \quad (3.7)$$

As can be seen, the Faraday rotation is dependent upon the relative direction of the light propagation to the magnetization direction. As a result of the time-reversal breaking, the direction of the Faraday angle depends on whether the light propagation is parallel or anti-parallel to the magnetization [6]. If the light propagates along the z -axis in an isotropic medium magnetized along the z -axis, two circularly polarized waves with opposite helicities will be the eigenwaves for the light in the medium. The refraction indices for these eigenwaves can be written as

$$n_R = \sqrt{\varepsilon_{xx} + \varepsilon_{xy}} \quad \text{and} \quad n_L = \sqrt{\varepsilon_{xx} - \varepsilon_{xy}}. \quad (3.8)$$

An expression due to Onsager relates the off-diagonal elements of the dielectric tensor and the magnetization:

$$\varepsilon_{ij} = \alpha M + \beta M^3 + \dots \quad (3.9)$$

Since ε_{xy} depends on \mathbf{M} , this will cause a magnetization-dependent polarization change. As discussed above, we consider the incident linearly polarized light beam as a superposition of two circularly polarized waves with opposite rotation direction but equal amplitude. These two superposing waves experience different refractive indices and thus different velocities within the medium. This effect, called *magnetic circular birefringence*, results in a phase shift between the two constituents and finally in rotation of the linear polarization plane. This rotation is proportional to the magnetization M , which is proportional to the ratio of the components of the dielectric tensor and to the distance d_M traveled by light in the medium:

$$\theta_F = \frac{\pi d_M}{\lambda} \Delta n = \frac{\pi d_M}{\lambda} \frac{\varepsilon_{xy}}{\sqrt{\varepsilon_{xx}}}, \quad (3.10)$$

where $\lambda = 2\pi c/\omega$ is the wavelength and $\Delta n = n_L - n_R$. If one considers a real medium where dissipations are present and the absorption coefficient k is not zero, due to the Kramers-Kronig relations [7] magnetic circular birefringence, Δn , should be accompanied by a *magnetic circular dichroism* (MCD), $\Delta k = k_L - k_R$, where k_L and k_R are the absorption coefficients for the left- and right-handed circularly polarized light, respectively.

For a system described by Eq. 3.7, the refraction index depends on the polarization of the absorbed radiation because of Eq. 3.5, which enhances the magnetic dichroism. In Chapter 5, X-Ray magnetic circular dichroism (XMCD), which we used

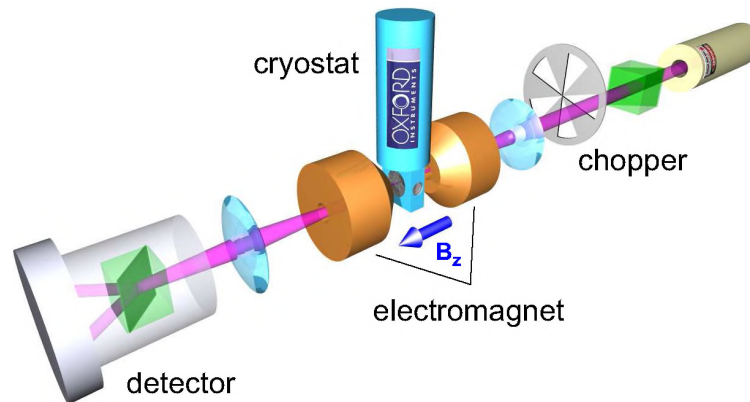


Figure 3.2: The experimental scheme used for measurements of the Faraday rotation θ_F . An optical cryostat is used for measurements in a broad temperature range.

for element-specific studies of ultrafast magnetization dynamics in complex alloys, will be introduced in more details.

3.2 Static Faraday effect measurements

3.2.1 Magneto-optical polarimetry

In optical experiments the light probes the magnetization over the optical penetration depth, typically 30 to 50 nm in metals, because absorption is generally high. The absorption coefficient of metals is usually between 10^5 and 10^6 cm^{-1} . For most of the ferromagnetic transition metals (Fe, Ni, Co), at saturation and for the visible spectral range, Faraday rotation angles are in the range of 10^5 deg/cm. For typical samples with a thickness of 10 nm, this yields a $\theta_F = 10^{-1}$ deg. In order to detect such angles, modulating techniques are required. In these techniques one may employ a modulation of the intensity or the polarization of light and record the signal at the frequency of the modulation with a lock-in amplifier. Using such techniques we were able to investigate the magnetic and magneto-optical properties of our samples.

The schematic drawing of the setup for Faraday rotation measurements is shown in Figure 3.2. In the scheme, the linearly polarized laser light with intensity I_0 passes through the magnetic medium along the magnetization direction. Afterwards, the light propagates through a Wollaston prism where it is split into two orthogonally-polarized beams. Both beams are detected by two photodiodes. The signal-to-noise ratio is increased by using lock-in detection which is accomplished by gating the beam

using an optical chopper. The chopper frequency serves as the reference for the phase sensitive detection scheme of the lock-in amplifier *SR830* (Stanford Research Systems Inc.). Using this setup the Faraday rotation as a function of applied magnetic field was measured with an accuracy of about 1 mdeg. To study the temperature dependence of the Faraday rotation, the samples were mounted in an optical cold-finger cryostat *Microstate^{He}* (Oxford Instruments) where the temperature could be stabilized in the range of 10 – 400 K with a precision better than 0.5 K.

3.2.2 Magneto-optical imaging

The interaction between light and magnetization of a material leads to a large variety of very useful magneto-optical techniques, such as domain imaging. Using the advantage of the Faraday effect, one can directly image the magnetic domain structures in a material. The relative geometry between the magnetization \mathbf{M} , and the polarization \mathbf{E} , determines which component of the magnetization will be visible in a particular magneto-optical image. Figure 3.3 shows a scheme of the Faraday effect application for magnetic domain imaging. Unpolarized light from a lamp is sent through a linear polarizer. The polarized light is then incident on a magnetic film with two types of domains with opposite directions of magnetization, \mathbf{M} .

From the image formed by the transmitted light, one can obtain information about the domain structure of the medium. This information is present in the intensity distribution of the light in the final image, because the intensity is dependent on the magnetization direction in the medium and the angle (ϕ) between the polarizer and analyzer. As shown in Figure 3.3, in the two opposite domains the Faraday rotation angle is $+\theta_F$ and $-\theta_F$ [8]. According to Malus law, the light, after passing the polarizer, magnetic film and the analyzer, has an intensity which obeys

$$I = \frac{1}{2}I_0 \cos^2(\phi + \theta_F), \quad \text{for one domain,}$$

$$I = \frac{1}{2}I_0 \cos^2(\phi - \theta_F), \quad \text{for the other domain.}$$

where I_0 is the intensity of the incident light. Thus, the light intensities from these two domains are different. The difference is used to obtain domain contrast in the image. Figure 3.3 also shows images of the same domain structure registered for different angles of the analyzer (ϕ).

Magneto-optical imaging can also yield a great deal of information about magnetization dynamics in a magnetic material. Pulsed laser illumination can reveal domain wall motion as well as the evolution of magnetization reversal over timescales as short as a few picosecond [9–11]. Transient changes can be captured by a single pulse or stroboscopically by a set of pulses. This technique, which we used in this thesis, is described in more details in Section 3.4.

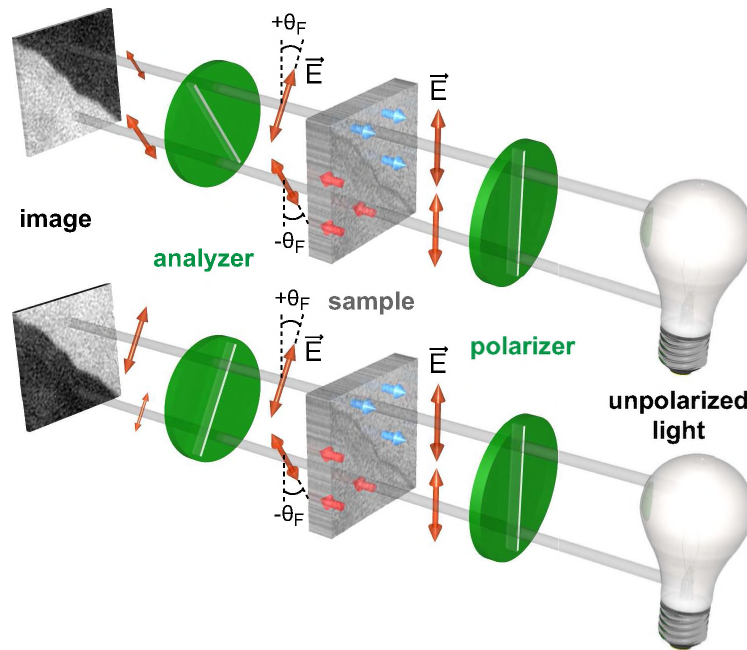


Figure 3.3: Schematic drawing of experimental setup for magnetic domain imaging using the Faraday effect. The two images correspond to two opposite signs of angles between analyzer and polarizer.

3.3 Time-resolved pump-probe spectroscopy

We have concluded in the previous section that the Faraday effect is a very powerful tool to locally probe the magnetic properties of thin films and multilayers. However, depending on the properties to be investigated, there are various techniques to probe the magnetic state as a function of given external parameters such as the applied magnetic field. Most of these techniques measure a stable or equilibrium state and require several milliseconds to accumulate information about the magnetic state. Therefore, these techniques cannot be used to monitor a fast transition between different states (such as domain wall propagation or magnetization oscillations) [12].

In order to access these transient states, time-resolved measurements with sub-nanosecond time resolution are required. Laser pulses are the fastest among the man-made events. In commercial systems pulse duration can achieve femtoseconds. One of the powerful techniques, which allows detection of changes in the magnetization with subpicosecond temporal resolution, is the stroboscopic pump-probe technique

where the delay between the pump and the probe pulses is adjusted depending on the time scale of the event to capture. Typically, an intense laser pulse (pump) is used to trigger magnetization dynamics, and the resulting changes are measured by a much weaker pulse (probe) to determine the effect of the excitation on the magnetic state of the medium via the changes in the magneto-optical effect [13]. The probe pulse, the duration of which determines the temporal resolution in the time-resolved measurements, can be selected in a wide spectral range. Since magneto-optical methods in the far-infrared, optical, ultraviolet or X-ray spectral ranges have different sensitivity to spin and orbital degrees of freedom, the measurements in these ranges allow us to obtain the most complete information about magnetization dynamics of the medium. Here we are interested in investigating the magnetization evolution in magnetic materials on a subnanosecond time scale. In this section, we describe the femtosecond laser system and the pump-probe technique used in Nijmegen to study the magnetization dynamics.

3.3.1 The femtosecond laser system

The laser system employed in our experiments is a *mode-locked* femtosecond laser system. Unlike a conventional continuous wave (CW) laser whose output is nominally constant over an interval of seconds or longer, the femtosecond lasers generate single pulses or series of pulses at regular intervals. The amplified femtosecond laser system from Spectra-Physics used in this work consists of the following units:

- a *Millennia* diode-pumped continuous wave Nd:YVO₄ laser;
- a *Tsunami* mode-locked Titanium-doped sapphire (Ti³⁺: Al₂O₃) laser;
- an *Empower* Q-switched intra cavity frequency doubled Nd:YLF laser;
- a *Spitfire Pro* pulsed Ti:sapphire regenerative amplifier;
- an *Ultrafast Optical Parametric Amplifier* (OPA-800C).

The configuration of the laser system is schematically shown in Figure 3.4. The train of femtosecond laser pulses (tunable over a broad band of emission wavelengths between ~ 700 nm and ~ 1000 nm) with wavelength centered at 800 nm and repetition rate of 82 MHz, is first generated by a mode-locked *Tsunami* seed laser, which is pumped by a 5 Watt continuous wave solid-state diode-pumped Nd:YVO₄ laser *Millennia*, at a 532 nm wavelength [14]. These laser pulses are then amplified by a 1 kHz Ti:sapphire Spectra-Physics *Spitfire Pro* regenerative amplifier, which is pumped by the *Empower* Q-switched intra cavity frequency doubled Nd:YLF laser at a 527 nm wavelength. The *Spitfire Pro* can amplify an input pulse with an energy of only a few nanojoules to an energy exceeding 1 millijoule [15].

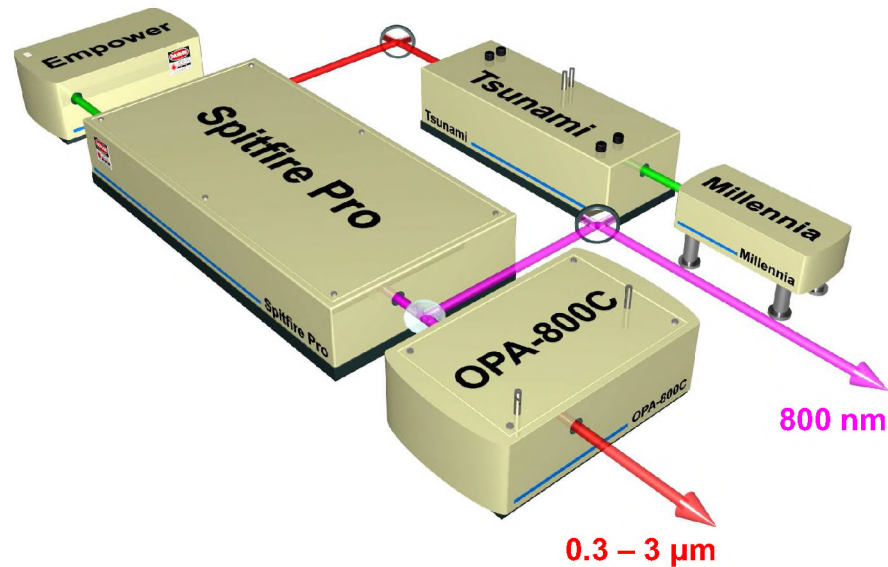


Figure 3.4: The femtosecond laser system: the Tsunami Ti:sapphire cavity pumped by a *Millennia* diode pumped Nd:YVO₄ laser, the regenerative amplifier *Spitfire Pro* pumped by a *Empower* Nd:YLF laser while seeded by the 60 fs pulses from the *Tsunami*. The output from the amplifier can be used to pump the *Ultrafast Optical Parametric Amplifier* (OPA-800C) which helps to vary the wavelength of the laser pulses between 300 nm and 3 μm .

The average output power of this *Empower* pump laser is 10 W with 1 kHz repetition rate of 100 ns wide pulses (30 mJ). The incoming seeding pulses from the *Tsunami* are temporally stretched in the *Spitfire Pro* using a multi-pass grating and mirror combination to avoid destructions to the amplifier oscillator. The timing and delay generator (TDG) provides the synchronization and control needed to select individual pulses from the train of stretched seed pulses and capture them in the regenerative amplifier by Pockels cells. The input Pockels cell allows the injection pulse from the *Tsunami* to arrive in the Ti:sapphire active laser crystal at the same time with the pump pulse from the *Empower*. The selected and stretched pulses then make multiple passes through the regenerative amplifier, increasing in energy. The output Pockels cell works in the amplifier cavity to release an amplified pulse at a time determined by the TDG [15]. After the pulse achieves its maximum level of amplification, the beam is then ejected to the compressor where the pulse can be compressed by multiple reflections on grating mirrors. The *Spitfire Pro* yields an output pulse energy of

2.2mJ with adjustable pulse durations from ~ 50 fs to several picoseconds at 1 kHz repetition rate, assuming a Gaussian pulse profile. The output fs laser pulses from the *Spitfire Pro* amplifier are monitored by a Spectra-Physics PulseScout autocorrelator.

The *Ultrafast Optical Parametric Amplifier* (OPA-800C) is an accessory of the femtosecond laser system that converts the output laser pulses from the amplifier to tunable pulses of wavelength of 300 nm - 3 μm with duration of ~ 100 fs. A small fraction of the laser beam from the amplifier is focused into a nonlinear optical medium to generate a spectrum of white light. The remainder of the beam is then split, focused and recombined with the white light at the β -Barium Borate (BBO) crystal. Different output wavelengths can be obtained by varying the crystal angle [16].

3.3.2 Pump-probe experimental setup

In order to investigate the magnetization dynamics induced by ultrashort laser pulses, a time-resolved all-optical pump-probe setup was employed; the corresponding experimental setup is shown in Figure 3.5. The output beam of the *Spitfire Pro* travels first through a beamsplitter which is used to separate the single beam into pump and probe parts. About 90% of the laser power is used as the pump beam to excite the magnetization dynamics, while the remaining reflected power is used as the probe to monitor the magnetic changes. Neutral-density optical filters are used in both pump and probe paths to adjust the intensities of the beams.

Introducing an optical delay between the pump and the probe pulses allows one to record the response of a medium to the pump pulses as a function of time. This is the reason why this technique is referred to as time-resolved spectroscopy. To achieve the necessary time delay between the pump and the probe pulses, the path length of the probe beam is changed by sending the probe beam via a retro-reflector mounted on a motorized mechanical stage (delay-line). The delay-line (Newport MM4006) has a 600 mm travel range corresponding to a maximum delay time up to 4 ns.

After aligning the probe beam with respect to the delay-line, the pump and probe beams are focused to a $\sim 200 \mu\text{m}$ and $\sim 100 \mu\text{m}$ spots on the sample, respectively. The probe beam is focused to a smaller spot than the pump to ensure that the probe beam only measures a part of the area uniformly excited by the pump beam. The pump beam is incident on the sample at normal incidence, while the probe beam makes a small angle with respect to the normal. As shown in Figure 3.5, a quarter wave plate ($\lambda/4$) is used to change the polarization of the pump pulses from linear to circular. The probe beam was linearly polarized. A half wave plate mounted on a motorized rotational stage is used in combination with a polarizer to tune the intensity of the pump pulses.

The thin magneto-optical layer in our samples allows us to detect magnetic changes via the Faraday effect in the transmission geometry. The measurements were performed in the following way. As the delay time between pump and probe pulses is

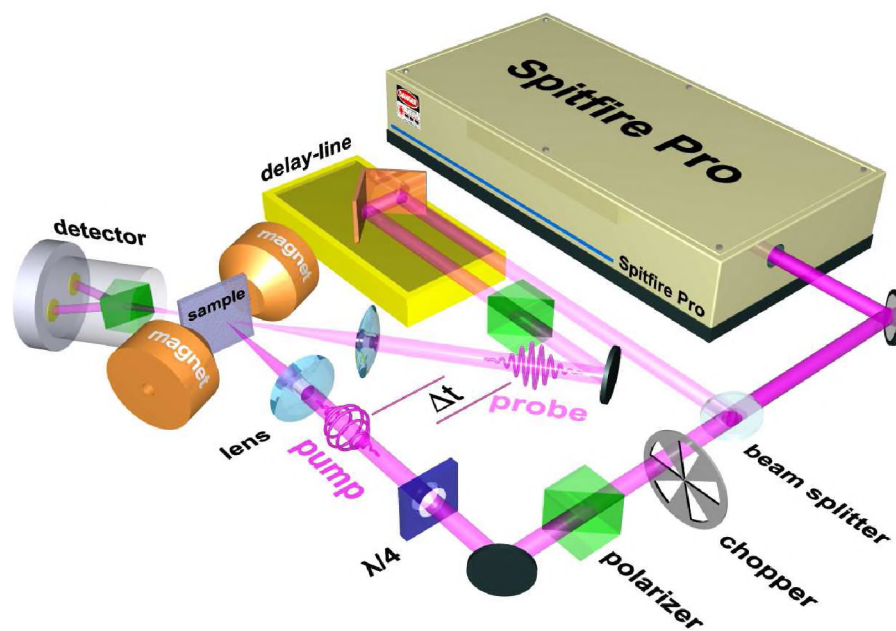


Figure 3.5: Experimental configuration of the all-optical time-resolved pump-probe technique. With the help of a beamsplitter, the laser beam from the *Spitfire Pro* is split into pump (intense) and probe (less intense) beams. By changing the position of the retro-reflector mounted on a motorized mechanical stage (delay-line), the time delay required between pump and probe is achieved to monitor magnetic changes in the sample which is located between the poles of an electromagnet. After the excitation by pump pulses, the magnetic state is detected via the Faraday rotation of the probe pulses.

changed, the transmitted probe beam is detected by a balanced photodiode detector, where the probe pulse is split into two parts with intensities I_1 and I_2 by a Wollaston prism. These two beams are detected by two separate photodiodes. In such a way, the Faraday rotation of the probe is detected as a slight imbalance of the intensities ($I_1 - I_2$). The difference current is then amplified by a *SR830* lock-in amplifier and integrated by a boxcar averager from Stanford Research Systems Inc., triggered by the 1 kHz reference frequency from the *Spitfire Pro*. The sample excitation is modulated by chopping the pump beam at 500 Hz such that every second pump pulse is blocked. Therefore, the lock-in amplifier can be used for phase-sensitive detection of subsequent pump induced changes. In such an experiment the magnetic system has time (1 ms) to relax back to the initial equilibrium state. A shot by shot data acquisition scheme is shown in Figure 3.6.

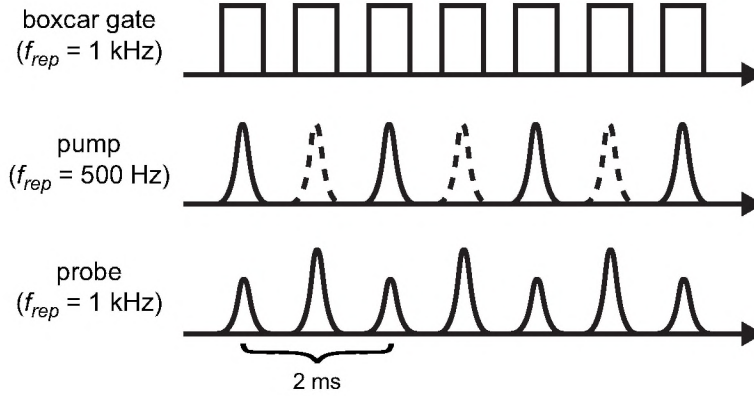


Figure 3.6: Schematic diagram for the detection scheme of time-resolved pump-probe spectroscopy. A boxcar averager triggered by the laser system (f_{rep}) and a lock-in amplifier were used to record the probe signal. Every second pump pulse is blocked by driving an optical chopper with half of the laser repetition rate ($f_{rep}/2$).

3.4 Single-shot time-resolved magneto-optical imaging technique

Although earlier experiments [17–20] showed the possibility of magnetization reversal with a subpicosecond stimulus, the actual speed and mechanism of such a magnetization reversal had remained an unexplored issue. To address these questions, we developed a single-shot time-resolved magneto-optical microscopy setup, providing a 100 fs temporal and 1 μm spatial resolution. A schematic illustration of this setup is shown in Figure 3.7. This approach is based on a principle used earlier in high speed domain wall dynamics studies [10, 21, 22]. In our experiment a single 100 – 2100 fs optical pump pulse with a central wavelength at $\lambda = 800 \text{ nm}$ was used to excite the magnetic films. A single, less intense, 100 fs optical probe pulse ($\lambda = 640 \text{ nm}$), delayed with respect to the pump pulse, was used to obtain the magneto-optical image of the sample (as explained in Section 3.2.2). Repeating such a single pump - single probe measurement for various values of the delay time we obtained images of the magnetic state of the samples at various moments after the arrival of the pump pulse. The same setup was also used to study the final state of the samples after the action of a single pump pulse. For this we were either separating the pumping and probing events by a longer time delay of several seconds or even used a lamp as a probe.

As discussed in Section 3.3.1, we used femtosecond laser pulses which were generated by a Ti:Sapphire laser system at a central photon energy of $E_0 = 1.54 \text{ eV}$ and a repetition rate of 1 kHz. Each pulse had a Gaussian temporal profile, full width at half maximum of which could be varied from 40 fs up to 2100 fs, using an internal

grating-based pulse compressor in the amplifier. The duration of the pulses was monitored using an autocorrelator. The intensity of the pulses was estimated from the averaged power of the pump beam measured by a power-meter. A less intense probe beam with a central photon energy of 1.94 eV and duration of 100 fs was generated by the OPA (see Section 3.3.1) Note that in contrast to a similar setup described in Ref. [23], we employed a two-color pump-probe scheme, which allows straightforward analysis of the obtained images. Using a chopper we reduced the repetition rate of the pulses down to 10 Hz. Behind the chopper we placed a mechanical shutter with an opening time of 100 ms. The combination of the chopper and the shutter, both of which were synchronized with the amplifier, allowed getting a single pump and a single probe pulse. A retro-reflector placed on the translational stage was used to introduce a delay between pump and probe pulses. This delay could be varied up to 3.8 ns, with the minimal step of 10 fs. By introducing extra mirrors in the path of the

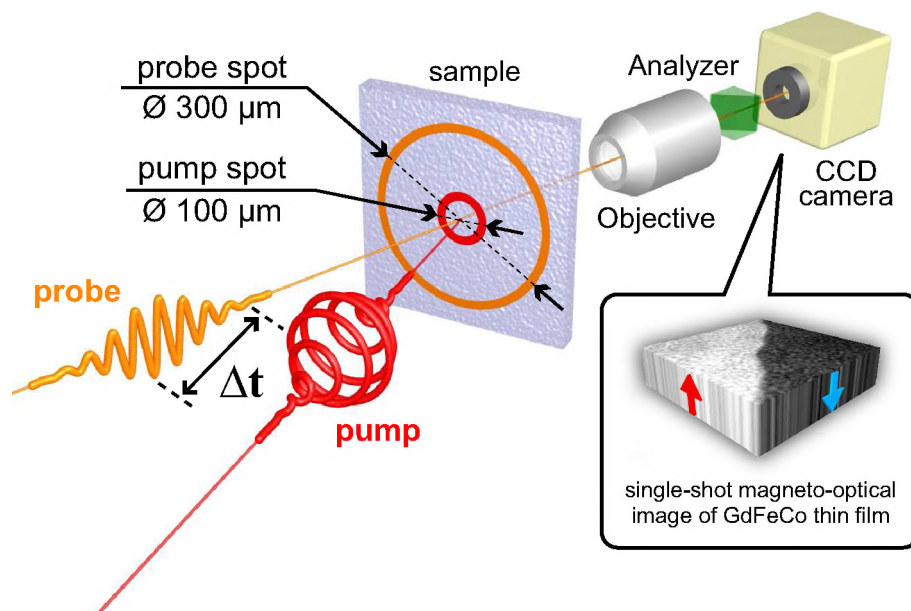


Figure 3.7: Sketch of the single-shot time-resolved magneto-optical microscopy experiment. The magneto-optical image is obtained at a CCD camera for a delay Δt_{delay} after an action of a single pump pulse ($\lambda = 800 \text{ nm}$) by using a single linearly polarized probe pulse ($\lambda = 640 \text{ nm}$) passing through the microscope objective and analyzer, the transmission axis of which is perpendicular to the polarization plane of the probe pulse. Circles on the sample indicate sizes of the pump and probe spots.

probe beam we could extend the delay time between pump and probe pulses up to 25 ns. The pump pulse was directed at normal incidence to the sample and focused into a spot of about $100\ \mu\text{m}$ in diameter (see Figure 3.7). The polarization of the pump pulses was controlled by a quarter-wave plate. Linearly polarized probe pulses are focused to a larger area of about $300\ \mu\text{m}$ and had an oblique angle of incidence of about 20° . To obtain magneto-optical images the sample was placed between two crossed polarizers (see Section 3.2.2). A thermoelectrically cooled CCD (charged coupled devices) camera and objectives with magnifications of 10 or 20 times, depending on the conditions of the experiment, were used to register the images. After obtaining each image, the sample was brought to the initial homogeneous magnetic state by applying a pulse of external magnetic field. Low temperature measurements were performed using an optical cold-finger cryostat.

3.5 Time-resolved X-ray spectroscopy

Up to now, we described the experimental measurement techniques that are used to characterize the magnetic properties of the materials and to investigate the magnetization dynamics induced and probed by ultrashort laser pulses. Since the laser system in our lab operates in the visible or infrared wavelength region ($0.4\text{--}3\ \mu\text{m}$), all of these studies are mainly sensitive to optical transitions in metals within the valance band (discussed in more details in Section 5.3.1). However, all of these transitions are quite broad and not very element-specific. In particular because most of our studies involve magnetic alloys with different magnetic sublattices, it would be interesting to be able to identify the magnetic contribution of each element. This is possible with methods based on X-ray absorption spectroscopy (XAS). In the X-ray spectral range between 400 and 1400 eV, atoms of transition and rare-earth metals have electronic transitions between $2p \rightarrow 3d$ and $3d \rightarrow 4f$ states ($L_{2,3}$ and $M_{4,5}$), respectively. Therefore, an element-specific probe of the magnetic properties of a medium can be obtained from spin-dependent X-ray absorption spectra, exploiting the X-ray magnetic circular dichroism (XMCD) [24–26].

Because of these advantages of X-rays, the static and stroboscopic magneto-optical techniques are extended to the X-ray region. The new synchrotron radiation sources provide X-rays with tunable energy and polarization (linearly or circularly polarized). Examples of such sources are the *Advanced Light Source* (ALS) in Berkeley, USA, the *Swiss Light Source* (SLS) in Villigen, Switzerland, the *French National Synchrotron Facility* (SOLEIL) in Paris, France and the *Berlin Electron Storage Ring Society for Synchrotron Radiation* (BESSY II) in Berlin, Germany. A schematic illustration of SOLEIL synchrotron storage ring is shown in Figure 3.8. The working principle is briefly explained as follows. Electrons are injected from an electron gun into a linear accelerator (*LINAC*, see Figure 3.8), which is required as a pre-accelerator for the *booster synchrotron*. The electrons can be accelerated here to an energy of up

to 1.7 GeV, and are finally injected into the *storage ring*, in which they circulate at almost the speed of light. The radiation emitted by the electrons is called *synchrotron radiation* and it is particularly intense and very directional when electrons traveling at close to the speed of light are bent in magnetic fields, thus requiring greater energy to alter their paths and releasing greater energies in response.

The bending magnets are needed to keep the electrons in orbit, or insertion devices such as wigglers and undulators that are placed in the straight sections of the storage ring. The undulator consists of two pairs of planar magnet arrays above and below the electron beam, as shown in Figure 3.9. As the electron beam passes between these magnet arrays, it changes directions and wiggles left and right. Any wiggling electric charge emits electromagnetic radiation covering the whole spectral range from microwaves to hard X-rays. The wavelength of the radiation is tunable by cutting out a narrow band of a wavelength for particular experiment with monochromator crystals that selectively allow the wavelength of choice. The photon energy emitted

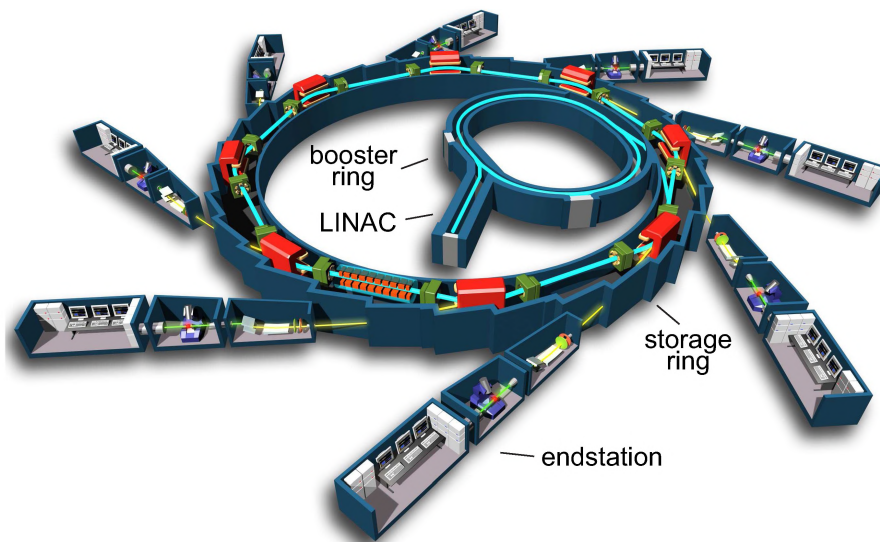


Figure 3.8: Schematic drawing of a synchrotron radiation storage ring. Electrons produced by an electron gun (LINAC) are pre-accelerated in the booster ring and then injected into the storage ring. Due to the acceleration experienced in the bending magnets or insertion devices, the electrons emit an intense white radiation ranging from microwaves to hard X-rays. The radiation is monochromated to a narrow band width in the beam line optics and finally reaches into the several endstations simultaneously (from [27]).

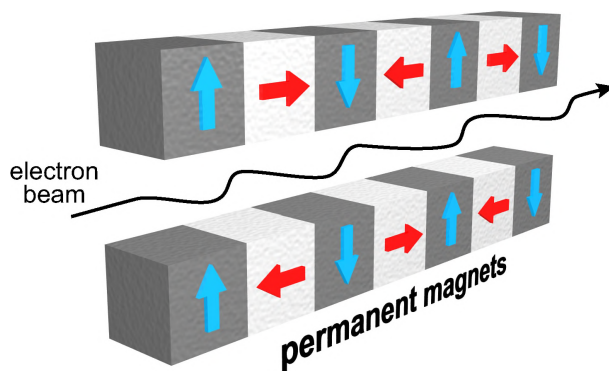


Figure 3.9: The undulator is an array of permanent magnets, designed to generate electromagnetic radiation. When an electron beam runs through the undulator (or wigglers), it experiences wavy path due to the periodic alternating vertical (or horizontal) magnetic field. These so-called “insertion devices” can be used to produce synchrotron light which is tuned for particular experiment.

from the undulator can be tuned by changing the strength of the magnetic field, which can be done by changing the vertical gap distance between the upper and lower pairs of magnet arrays. The polarization state of the X-rays depends on the position between the magnetic array in each pair. The undulator forces the electron beam to follow a helical path to emit elliptical polarized radiation and provides polarised radiation, with emissions in the first, third and fifth harmonics, in the energy range of 90 – 1500 eV. By driving the undulator and the monochromator simultaneously, the maximum of the undulator peak and the energy are selected and the undulator provides X-ray radiation with a high photon flux and constant circular polarization required for XAS and XMCD measurements.

The X-rays travel through various pin holes, slits, and focusing units in the beamline. These components are employed to prepare the beam properly throughout the beamline. The combination of a plane grating and the first two mirrors in the beamline is used to get the desired photon energy through the exit slit. Behind the exit slit a horizontally deflecting conical mirror refocuses the X-ray beam onto the sample [28].

If one gets a source of femtosecond pulses of polarized X-ray radiation, it would be an elegant way to probe ultrafast magnetization dynamics in an element-selective way. We employed such an element-specific time-resolved X-ray magnetic circular dichroism (TR-XMCD) with subpicosecond temporal resolution, available at BESSY II (Berliner Elektronenspeicherring-Gesellschaft für Synchrotronstrahlung m. b. H.) in Berlin-

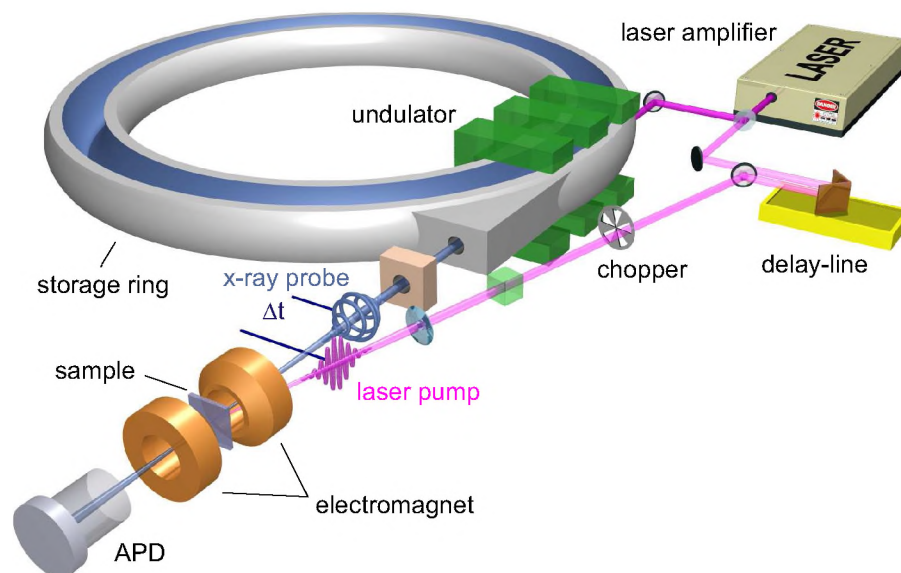


Figure 3.10: Schematic layout of the UE56/1-ZPM beamline and the experimental setup at BESSY II. The medium is irradiated by a femtosecond laser pulse. After a well-defined time delay, the X-ray pulses from the synchrotron are used to measure the changes in the magnetic state. The transmitted X-ray pulses are detected by a fast diode.

Adlershof, Germany [29]. Static and time-resolved XMCD measurements have been performed at the UE56/1-ZPM beam line where the X-rays are monochromatized by a reflection zone plate monochromator. Figure 3.10 shows schematically the layout of the UE56/1-ZPM beamline and the experimental setup. According to the time resolution of the electron wave packets in the storage ring, different modes can be used for the experiments. In the multi bunch mode, which is the normal operation mode, the duration of X-ray pulses is 50 ps while in the low- α mode, this can be improved to 10 ps. However, these durations are not short enough to study phase transitions which take place in subpicosecond time-scale. In the quest for shorter pulse duration at short wavelengths, by employing a special technique, so called “*femtoslicing*”, it is possible to produce X-ray pulses having a duration as short as 100 fs with continuously tunable photon energy from 400 to 1300 eV [30–35]. In this option, a femtosecond laser pulse is used to create a femtosecond time structure on a long electron bunch through energy modulation of an ultrashort slice of the bunch, which is induced by the electric field of a femtosecond laser pulse. The energy modulated electrons can be spatially separated from the rest of the electron bunch by a dipole bending magnet.

Picosecond radiation from the main bunch is blocked below a certain angle relative to the electron beam axis by front end apertures. Since the modulation is created by a femtosecond optical pulse, there is an absolute synchronization between the X-ray pulses and the pump pulses which trigger the dynamic processes. As the electron slice is created through interaction with the femtosecond laser pulse, the duration of the X-ray pulses produced by these electrons will be approximately the same as the laser pulse duration. With the help of this important capability of synchrotron sources, time-resolved XMCD measurements (laser pump – X-ray probe technique) were carried out to study element-specific magnetization dynamics.

For the dynamics studies, femtosecond laser pulses ($\sim 10\%$ of the laser pulse intensity) from an amplified Ti:Sapphire system¹ were used as the pump beam in our experiments (see Figure 3.10). About $\sim 90\%$ of the laser beam is guided into the electron storage ring to generate femtosecond X-ray pulses. The laser system (wavelength $\lambda = 800$ nm, pulse duration of 60 fs FWHM, pulse energy up to 2 mJ, and 3 kHz repetition rate) is synchronized intrinsically to the frequency of the synchrotron. The delay between the laser and X-ray pulses is controlled by the motorized delay-line stage. The transmitted X-ray intensity is recorded by a fast avalanche photodiode (APD). Using a boxcar integrator, which is triggered at the repetition rate of the laser, and a chopper allow to measure pumped and unpumped states. An electromagnet is used to apply an external magnetic field of ± 0.5 T to the sample for the dynamic XMCD measurements. The sample is placed in a UHV chamber where the sample position can be changed by a manipulator with four degrees of freedom (x, y, z , and θ for rotation). A commercial heating system is used to stabilize the temperature of the sample in the range $80 \text{ K} \leq T_{\text{sample}} \leq 800 \text{ K}$.

¹The femtosecond Ti:Sapphire laser system was similar to the one we used in our labs in Nijmegen.

References

- [1] P. N. Argyres, Phys. Rev. **97**, 334 (1955).
- [2] H. R. Hulme, Proc. R. Soc. A **135**, 237 (1932).
- [3] H. S. Bennett and E. A. Stern, Phys. Rev. **137**, A448 (1965).
- [4] A. K. Zvezdin and V. A. Kotov, *Modern Magneto-optics and Magneto-optical Materials* (Institute of Physics Publishing, London, 1997).
- [5] L. D. Landau, E. M. Lifshitz, and L. P. Pitaevskii, *Electrodynamics of Continuous Media*, vol. 8 of *Theoretical Physics* (Elsevier, 2006).
- [6] M. C. Langner, Ph.D. thesis, University of California, Berkeley (2009).
- [7] D. Y. Smith, J. Opt. Soc. Am. **66**, 454 (1976).
- [8] <http://physics.uwb.edu.pl/exp/domeny/>.
- [9] B. Petek, P. L. Trouilloud, and B. E. Argyle, IEEE Trans. Magn. **26**, 1328 (1990).
- [10] F. H. Liu, M. D. Schultz, and M. H. Kryder, IEEE Trans. Magn. **26**, 1340 (1990).
- [11] M. Du, S. Xue, W. Eppler, and M. H. Kryder, IEEE Trans. Magn. **31**, 3250 (1995).
- [12] D. E. S. Stanescu, Ph.D. thesis, Joseph Fourier University (2003).
- [13] J. Shah, *Ultrafast Spectroscopy of Semiconductors and Semiconductor Nanostructures*, vol. 115 (Springer Series in Solid-State Sciences, Springer, Berlin, 1996).
- [14] Spectra-Physics, *Tsunami: Mode-locked Ti:sapphire Laser, User's Manual* (Spectra-Physics, The Solid-State Laser Company, Mountain View, CA, U.S.A., 2002).
- [15] Spectra-Physics, *Spitfire Pro: Ti:Sapphire Regenerative Amplifier Systems, User's Manual* (Spectra-Physics, The Solid-State Laser Company, Mountain View, CA, U.S.A., 2005).
- [16] Spectra-Physics, *OPA-800C: Ultrafast Optical Parametric Amplifier, User's Manual* (Spectra-Physics, The Solid-State Laser Company, Mountain View, CA, U.S.A., 2003).
- [17] C. H. Back, D. Weller, J. Heidmann, D. Mauri, D. Guarisco, E. L. Garwin, and H. C. Siegmann, Phys. Rev. Lett. **81**, 3251 (1998).

-
- [18] C. H. Back, R. Allenspach, W. Weber, S. S. P. Parkin, D. Weller, E. L. Garwin, and H. C. Siegmann, *Science* **285**, 864 (1999).
- [19] I. Tudosa, C. Stamm, A. B. Kashuba, F. King, H. C. Siegmann, J. Stöhr, G. Ju, B. Lu, and D. Weller, *Nature* **428**, 831 (2004).
- [20] C. D. Stanciu, F. Hansteen, A. V. Kimel, A. Kirilyuk, A. Tsukamoto, A. Itoh, and T. Rasing, *Phys. Rev. Lett.* **99**, 047601 (2007).
- [21] M. V. Chetkin, S. N. Gadetskii, and A. I. Akhutkina, *JETP Letters* **35**, 459 (1982).
- [22] M. V. Chetkin, A. P. Kuz'menko, S. N. Gadetskii, V. N. Filatov, and A. I. Akhutkina, *JETP Letters* **37**, 264 (1983).
- [23] M. Elazar, M. Sahaf, L. Szapiro, D. Cheskis, and S. Bar-Ad, *Opt. Lett.* **33**, 2734 (2008).
- [24] J. Stöhr, *J. of Electr. Spectr. and Rel. Phenom.* **75**, 253 (1995).
- [25] J. Stöhr, *J. of Magn. Magn. Mater.* **200**, 470 (1999).
- [26] J. Stöhr and H. C. Siegmann, *Magnetism: From Fundamentals to Nanoscale Dynamics* (Springer-Verlag, Berlin, 2006).
- [27] The French National Synchrotron Facility (SOLEIL): <http://www.synchrotron-soleil.fr/>.
- [28] K. J. S. Sawhney, F. Senf, M. Scheer, F. Schäfers, J. Bahrtdt, A. Gaupp, and W. Gudat, *Nucl. Instrum. Meth. Phys. Res. A* **390**, 395 (1997).
- [29] BESSY II (Berliner Elektronenspeicherring-Gesellschaft für Synchrotronstrahlung m. b. H.): <http://www.helmholtz-berlin.de/>.
- [30] R. W. Schoenlein, S. Chattopadhyay, H. H. W. Chong, T. E. Glover, P. A. Heimann, C. V. Shank, A. A. Zholents, and M. S. Zolotarev, *Science* **287**, 2237 (2000).
- [31] A. Cavalleri, M. Rini, H. H. W. Chong, S. Fourmaux, T. E. Glover, P. A. Heimann, J. C. Kieffer, and R. W. Schoenlein, *Phys. Rev. Lett.* **95**, 067405 (2005).
- [32] K. Holldack, T. Kachel, S. Khan, R. Mitzner, and T. Quast, *Phys. Rev. ST Accel. Beams* **8**, 040704 (2005).
- [33] S. Khan, K. Holldack, T. Kachel, R. Mitzner, and T. Quast, *Phys. Rev. Lett.* **97**, 074801 (2006).

-
- [34] N. Pontius, C. Stamm, T. Kachel, R. Mitzner, T. Quast, K. Holldack, S. Khan, H. A. Dürr, and W. Eberhardt, in *Ultrafast Phenomena XVI* (Springer Berlin Heidelberg, 2009), vol. 92 of *Springer Series in Chemical Physics*, pp. 119–121.
- [35] C. Stamm, N. Pontius, T. Kachel, K. Holldack, T. Quast, R. Mitzner, S. Khan, M. Wietstruk, H. A. Dürr, and W. Eberhardt, in *Ultrafast Phenomena XVI* (Springer Berlin Heidelberg, 2009), vol. 92 of *Springer Series in Chemical Physics*, pp. 194–196.

All-optical magnetization reversal triggered by circularly-polarized laser pulses¹

4.1 Introduction

The fundamental and practical limit of the speed of magnetization reversal is a subject of vital importance for magnetic recording and information processing technologies as well as one of the most intriguing questions of modern magnetism [1–9]. The conventional way to reverse the magnetization \mathbf{M} is to apply a magnetic field \mathbf{H} antiparallel to \mathbf{M} . In this collinear M-H geometry the reversal occurs via precession accompanied by damping that channels the associated angular momentum into the lattice. Although this process is perfectly deterministic it is also unavoidably slow, typically of the order of nanoseconds, due to the required angular momentum transfer [1].

Alternatively, the driving field can be applied orthogonal to \mathbf{M} , so that the created torque $[\mathbf{M} \times \mathbf{H}]$ leads to a rapid change of the angular momentum and a possible switching of the magnetization [2, 4, 5, 10]. However, such precessional switching requires a magnetic field pulse precisely tuned to half of the precession period. The fastest precessional reversal demonstrated so far using an external magnetic field [2, 6]

¹Adapted from: K. Vahaplar, A. M. Kalashnikova, A. V. Kimel, D. Hinzke, U. Nowak, R. Chantrell, A. Tsukamoto, A. Itoh, A. Kirilyuk and Th. Rasing, *Phys. Rev. Lett.* **103**, 117201 (2009), and K. Vahaplar, A. M. Kalashnikova, A. V. Kimel, S. Gerlach, D. Hinzke, U. Nowak, R. Chantrell, A. Tsukamoto, A. Itoh, A. Kirilyuk and Th. Rasing, *submitted to Phys. Rev. B*.

or a spin-polarized current [7, 8, 11] is limited to 100 ps. On such a time scale the magnetization dynamics can be fully described in terms of adiabatic and macrospin approximations. Moreover, it has been shown that for field pulses shorter than 2.3 ps such a switching becomes nondeterministic [6, 12]. Furthermore, the dynamics of spins on such a short time scale is not fully understood so far.

One of the most intriguing alternatives to magnetic field-induced magnetization switching is making use of a subpicosecond laser pulse. Ultrafast laser-induced heating of a magnetic material is known to stimulate the transfer of angular momentum from spins to lattice on a femtosecond time scale. Already the first observation of subpicosecond demagnetization of a thin Ni film subjected to a 60 fs laser pulse [13] suggested that such a pulse represents a powerful stimulus which is able to cause ultrafast changes in the magnetic state of matter. At the same time, this and the following studies of the various effects occurring in magnetic media under the action of ultrashort laser pulses rose a number of important fundamental questions [14–19]. A closer look at these questions reveals that a strong external perturbation, i.e. a femtosecond laser pulse, brings the magnetic medium into a strongly nonequilibrium state, where a conventional description of magnetic phenomena in terms of thermodynamics and adiabatic approximations is no longer valid. In the subpicosecond time domain, typical time of such a perturbation is comparable to or even shorter than the characteristic times of equilibration between different reservoirs of energy and angular momentum. Therefore, from the point of theoretical physics, there is a need for developing novel approaches and approximations capable of an adequate description of the ultrafast spin dynamics at extremely short time scales. From the experimental point of view, studies of such a dynamics also require techniques which combine subpicosecond time resolution with a sensitivity to changes of the magnetic ordering. Consequently, attempts to understand ultrafast light-induced magnetization dynamics have yielded a burst in the development of various experimental [15, 20–25] and theoretical [26–31] approaches (for a recent review, see Ref. [32]).

Recently, it has been demonstrated that a 40 fs circularly polarized optical laser pulse can reverse the magnetization in a collinear M-H geometry [33], as if it acts as an equally short magnetic field pulse $\mathbf{H}_{\text{eff}} \sim [\mathbf{E} \times \mathbf{E}^*]$ (where \mathbf{E} is the electric field of light) pointing along the direction of light [34]. Both the experimental investigation of the details of this *all-optical helicity-dependent magnetization reversal* and its theoretical description constitute a number of challenging issues [35]. In order to address these issues, we performed comprehensive studies of the all-optical reversal of magnetization by subpico- and picosecond circularly-polarized laser pulses in ferrimagnetic metallic rare earth – transition metal (RE–TM) alloys.

This chapter is organized as follows. The structure, magnetic and magneto-optical properties of the GdFeCo alloys are described in Section 4.2. In Section 4.3, we describe the details of the single-shot time-resolved magneto-optical microscopy experiments and the multiscale calculations. This is followed by a discussion and compar-

ison between the experimental and the modeling results in Sections 4.4.1 and 4.4.2. Then we show how the all-optical reversal changes as a function of the laser pulse duration and polarization (Sec. 4.4.3) and the ferrimagnetic properties of the samples (Sec. 4.4.4). Finally, we present an outlook (Sec. 4.5), where we specify the most important open questions left.

4.2 Samples

The magnetic materials studied in this work are 20 nm thick films of the ferrimagnetic rare earth – transition metal (RE–TM) amorphous alloy $\text{Gd}_x\text{Fe}_{90-x}\text{Co}_{\sim 10}$ ($14 < x < 30$). The samples were grown by magnetron sputtering in the following multilayer structure: glass | AlTi(10 nm) | SiN(5 nm) | GdFeCo(20 nm) | SiN(60 nm). The AlTi layer serves as a heat sink and the SiN as buffer and capping layers. The latter one also serves as an antireflection coating.

$\text{Gd}_x\text{Fe}_{100-x-y}\text{Co}_y$ alloys are ferrimagnets, where the Fe and Gd sublattices are coupled antiferromagnetically, while the Co magnetic moments are parallel to those of iron. These alloys are widely used in magneto-optical recording and known for their strong magneto-optical effects [36, 37]. Depending on RE ions concentration RE–TM alloys can exhibit magnetization (T_M) and angular momentum compensation temperatures (T_A), where the magnetizations (angular momenta) of the RE and TM sublattices are equivalent and, consequently, the net magnetization (angular momentum) is zero (see Chapter 2). For the case of Gd-containing alloys the magnetization compensation point may be expected below the Curie point (T_C) if $x = 20\% \dots 30\%$ [38]. The angular momentum compensation point is typically ~ 50 K above T_M [39]. Along with T_M , a number of other magnetic properties, such as magnetic anisotropy and coercive field, are defined by the Gd concentration [38]. The Co ions, substituting for 0% \dots 30% of Fe ions in $\text{RE}_x\text{Fe}_{100-x-y}\text{Co}_y$ alloys, on the one hand, enhance T_C of the alloys and, on the other hand, increase their magneto-optical susceptibility [40, 41].

We investigated the magnetic and magneto-optical properties of the GdFeCo samples with Gd ions concentration x in the range from 14 to 30%. For this purpose the magneto-optical Faraday effect in the samples was measured at a photon energy of 1.52 eV as a function of applied magnetic field and sample temperature. The Curie temperature for all studied samples was found to be $T_C \approx 550$ K. We found that GdFeCo films exhibited perpendicular magnetic anisotropy in the range of Gd concentrations $20 < x < 28\%$. In this work we discuss the results obtained for the alloys $\text{Gd}_{20}\text{Fe}_{70}\text{Co}_{10}$, $\text{Gd}_{22}\text{Fe}_{68.2}\text{Co}_{9.8}$, $\text{Gd}_{24}\text{Fe}_{66.5}\text{Co}_{9.5}$, $\text{Gd}_{26}\text{Fe}_{64.7}\text{Co}_{9.3}$ and $\text{Gd}_{28}\text{Fe}_{63}\text{Co}_9$.

Figure 4.1(a) shows the temperature dependence of the Faraday rotation of these samples at saturation. The value of the Faraday rotation is of the order of 1° (i.e. 5×10^7 deg/m). This value decreases with an increase of the Gd concentration x . In the studied range of temperatures $T = 10 - 420$ K the Faraday rotation exhibits a weak

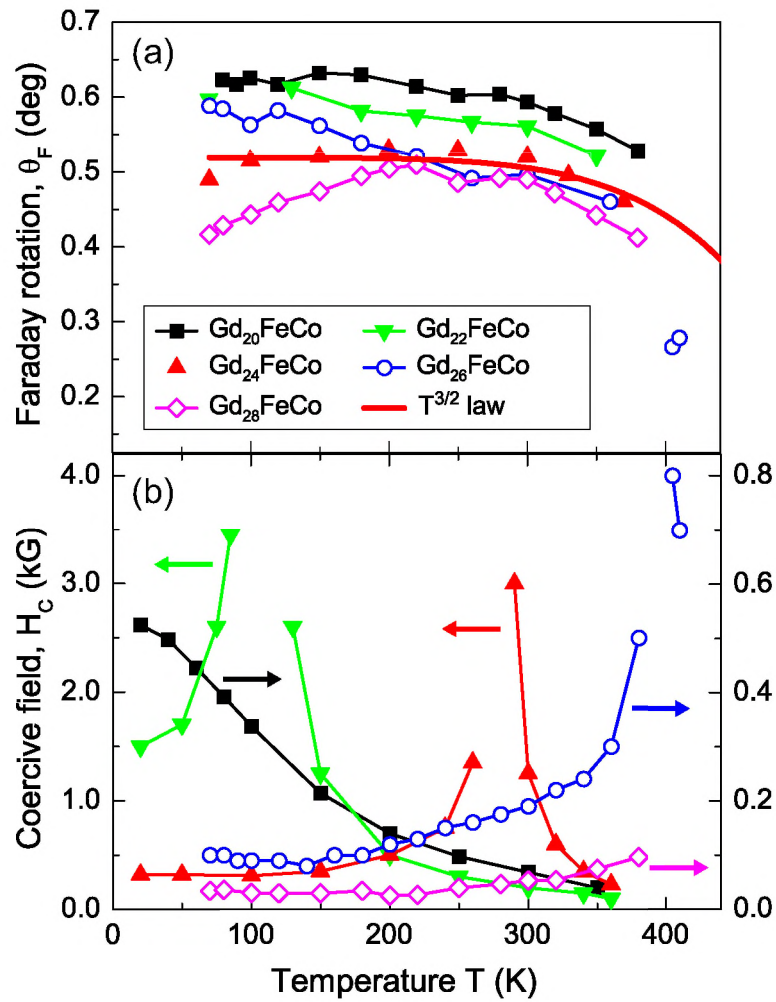


Figure 4.1: (a) Amplitude of the Faraday rotation θ_F and (b) coercive field H_c versus temperature T for the samples Gd_xFeCo , where $x = 20, 22, 24, 26, 28\%$, as obtained from the field dependence of the Faraday rotation measured at different temperatures for a photon energy of 1.52 eV.

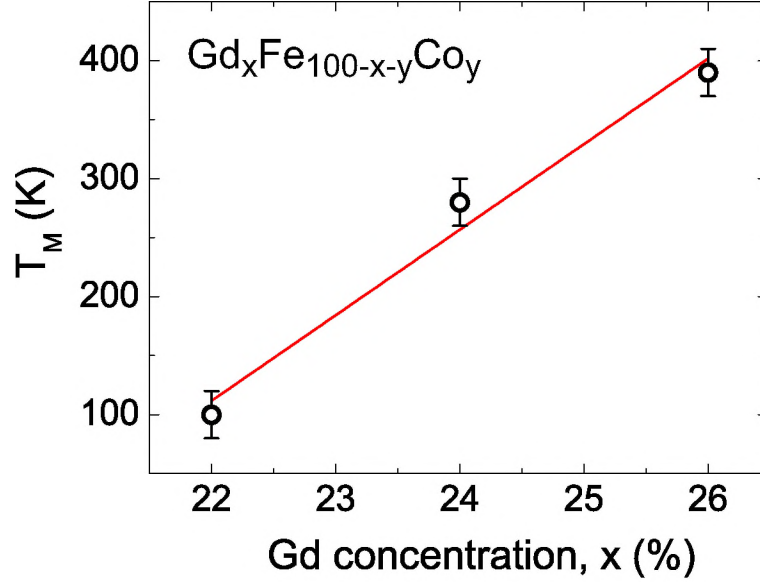


Figure 4.2: The dependence of the compensation temperature T_M on the concentration of the Gd ions. The red line is a linear fit ($T_M = -1483 + 72.5x$).

temperature dependence. It is conventionally assumed that in the visible spectral range the magneto-optical signal is dominated by contributions originating from the iron sublattice. Therefore, the change of the Faraday rotation with temperature, shown in Figure 4.1(a) reflects the magnetization changes of the iron sublattice with temperature.

In order to determine the compensation temperatures T_M we extracted the values of the coercive field H_c from the hysteresis loops measured as a function of temperature [Figure 4.1(b)]. The compensation temperatures are taken as those temperatures where the coercive fields $H_c(T)$ diverge [35]. As one can see from Figure 4.2, T_M increases with an increase of Gd concentration, in agreement with the data from the literature [38]. For the samples $\text{Gd}_{20}\text{FeCo}$ and $\text{Gd}_{28}\text{FeCo}$ no compensation point was observed in the range $10\text{ K} < T < 420\text{ K}$. The dependence of H_c on T for $\text{Gd}_{20}\text{FeCo}$ shows that the magnetization of the FeCo sublattice exceeds the magnetization of the Gd sublattice in the whole temperature range. In the sample $\text{Gd}_{28}\text{FeCo}$ the situation is opposite.

4.3 Methods

4.3.1 Experimental technique

For studying the ultrafast magnetization dynamics during the process of all-optical reversal, we developed a single-shot time-resolved magneto-optical microscopy setup providing a 100 fs temporal and 1 μm spatial resolution (described in more details in Section 3.4) [35]. In our experiments, ferrimagnetic 20 nm $\text{Gd}_x\text{Fe}_{100-x-y}\text{Co}_y$ amorphous films with perpendicular anisotropy [33] were excited by a single circularly polarized laser pulse (FWHM of 100 – 2100 fs, a central wavelength at $\lambda = 800$ nm). A single linearly polarized probe pulse (FWHM = 100 fs, $\lambda = 640$ nm) delayed with respect to the pump was used for ultrafast imaging of the magnetic domain structure by means of the magneto-optical Faraday effect (see Section 3.2.2). Magnetic domains with magnetization parallel (“up”) or antiparallel (“down”) to the sample normal are seen as white or black regions, respectively, in an image on a CCD (charged coupled devices) camera. After each “write-read” event, the initial magnetic state was restored by applying a magnetic field pulse. Taking images of the magnetic structure for different delays between the pump and probe pulses we were able to visualize the dynamics of the laser-induced magnetic changes in the material.

4.3.2 Theoretical methods

The description of the dynamics of a magnetic medium during and after the excitation with a subpicosecond laser pulse comprises a complicated theoretical task. First of all, it requires an adequate model, which describes the interaction of the laser pulse with the medium. Furthermore, as the excitation with such a short laser pulse brings a medium to a transient nonequilibrium state, description of the spin dynamics of such a state goes beyond conventional macrospin approximations in magnetism. A new approach to this problem was developed in the groups of Prof. Roy Chantrell (University of York) and Prof. Ulrich Nowak (University of Konstanz). Below a brief description of this so-called *atomistic spin model* will be given.

Modeling a laser pulse impact on a medium

As the starting point for developing a model, we assume a two fold-action of a laser pulse on the medium. First of all, we take into account the fact that a circularly polarized subpicosecond laser pulse can act on spins as an effective light-induced magnetic field, the direction of which is determined by the helicity of the light [9, 34]. Thus, one part of the impact of a laser pulse on a medium is represented by this *opto-magnetic field*, \mathbf{H}_{OM} . Secondly, subpicosecond laser pulses are known to lead to a rapid increase of the electronic temperature followed by ultrafast demagnetization

in metals [13]. Therefore, this part of the laser pulse impact enters our model as a short *heat pulse* resulting in a rapid increase of the electronic temperature T_{el} .

We introduce the opto-magnetic field pulse using an expression derived on the basis of the phenomenological consideration of the interaction of the electric field of light with a medium [42]:

$$\mathbf{H}_{\text{OM}}(t, r) = \frac{\varepsilon_0}{\mu_0} \beta \left[\mathbf{E}(t, r) \times \mathbf{E}^*(t, r) \right] \sim p \beta P_0 f(t) e^{-\frac{r^2}{2r_0^2}} \mathbf{n}. \quad (4.1)$$

where ε_0 and μ_0 are the vacuum permittivity and permeability, respectively. \mathbf{n} is the unit vector in the direction of the wavevector of light. The coefficient p gives the degree of circular polarization and is equal to ± 1 and 0 , for a right-, left-handed circularly-polarized and linearly-polarized light, respectively. In other words, the field \mathbf{H}_{OM} is directed along the wave-vector of light and reverses its polarity when the helicity of the laser pulse is reversed.

The amplitude of the field $\mathbf{H}_{\text{OM}} \sim \beta P_0$ is defined by the magneto-optical susceptibility β and the peak pump pulse power P_0 . The latter is related to the experimental laser pulse fluence² F (J/m²) as $P_0 \approx F/\tau d$, where τ is the full width at the half maximum (FWHM) of the laser pulse and d is the thickness of the film. Thus, the value of this field can be estimated from the strength of the Faraday effect [see Figure 4.1(a)]. For instance, for a pump pulse fluence of 0.25 mJ/cm² and a duration of 100 fs, the amplitude of \mathbf{H}_{OM} in GdFeCo is of the order of ~ 20 T.

The light-induced effective field is introduced in the calculations as having a Gaussian spatial profile with a radius r_0 , which coincides with the spatial profile of the pump pulse. The temporal profile of this field $f(t)$ has the following form:

$$f(t) = \begin{cases} e^{-\frac{(t-t_0)^2}{\tau^2/4 \ln 2}}, & t < t_0 \\ e^{-\frac{(t-t_0)^2}{(\tau+2\tau_{\text{decay}})^2/4 \ln 2}}, & t > t_0 \end{cases} \quad (4.2)$$

Thus, regarding the duration of this field, we assumed the time profile as shown in Figure 4.3. The effective light-induced magnetic field \mathbf{H}_{OM} builds up with no delay with respect to the laser pulse electric field. The decay time of \mathbf{H}_{OM} is, in turn, assumed to be slower and is given by the decay time of the process responsible for the emerging of \mathbf{H}_{OM} . Considering possible microscopic origins of this effective field we estimated the limits for the decay of \mathbf{H}_{OM} . The lower limit for the decay of the light-induced field is, supposedly, given by an optical coherence time, which is well below 100 fs in metals [43, 44]. The upper limit was roughly estimated based on the data of a polarization-dependent THz emission from a thin iron film subjected to a 50 fs laser pulse excitation [45]. We took into account that one of the possible reasons

²Fluence can also be described as energy density W which is a term used for the amount of energy stored in the system per unit volume (J/m³).

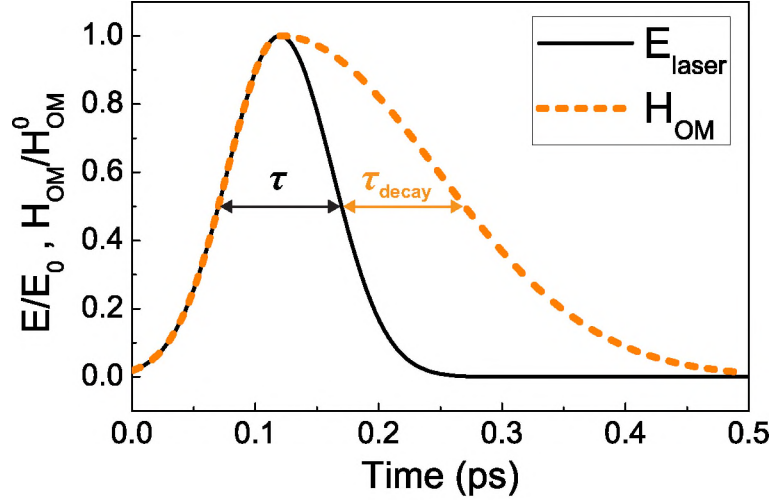


Figure 4.3: The temporal profiles of the laser pulse (solid line) and of the opto-magnetic light-induced field, \mathbf{H}_{OM} (open circles). τ is the FWHM of the laser field, while $\tau_{\text{OM}} = \tau + \tau_{\text{decay}}$ is the FWHM of the laser-induced effective magnetic field pulse, \mathbf{H}_{OM} . The decay time is in the range of $20 \text{ fs} < \tau_{\text{decay}} < 3000 \text{ fs}$.

for a THz yield and for the appearance of the light-induced effective magnetic field is a circular light-induced current. Consequently, half a period of the lower mode of oscillations observed in the polarization-dependent THz emission can be used as a measure of the duration of the effective light-induced magnetic field, which is 3 ps for the case of the iron film [45].

The second contribution to the laser pulse impact on the medium is introduced as a heat pulse, the duration of which is defined by the laser pulse duration. As in the case of the opto-magnetic pulse, the spatial profile of the heat pulse is Gaussian and coincides with the profile of the laser pulse,

$$P(t) = P_0 e^{-\frac{r^2}{2r_0^2}} e^{-\frac{(t-t_0)^2}{\tau^2/4 \ln 2}}. \quad (4.3)$$

The action of this pulse results in a rapid increase of the electron temperature T_{el} of the system. To calculate this response we used the two-temperature model [46]:

$$C_{\text{el}}(T_{\text{el}}) \frac{dT_{\text{el}}}{dt} = -G_{\text{el-ph}}(T_{\text{el}} - T_1) + P(t, r), \quad (4.4a)$$

$$C_1(T_1) \frac{dT_1}{dt} = -G_{\text{el-ph}}(T_1 - T_{\text{el}}) - C_1 \frac{T_1 - T_0}{\tau_{\text{th}}}, \quad (4.4b)$$

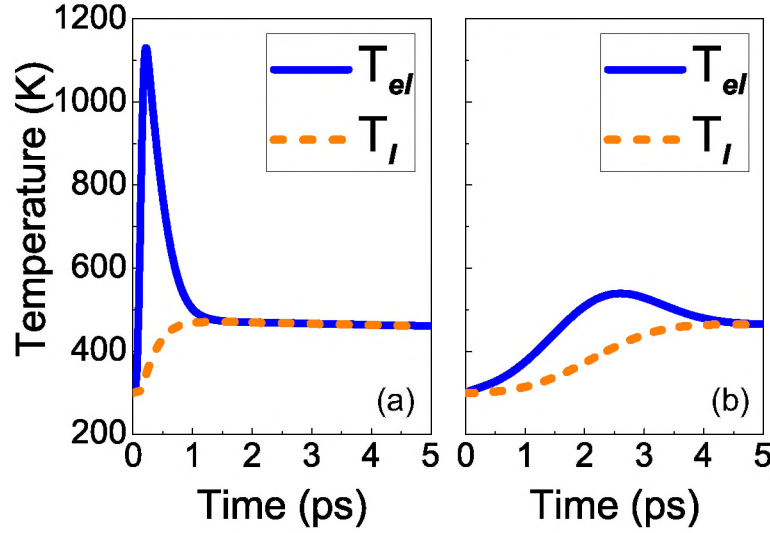


Figure 4.4: Time evolution of the electronic T_{el} (solid line) and lattice T_l (open circles) temperatures after an excitation with (a) 100 fs and (b) 2000 fs laser pulse as calculated from the two-temperature model.

where T_{el} and T_l are the temperatures of the electronic and lattice reservoirs, C_{el} and C_l are the electronic and lattice specific heats, respectively, and G_{el-ph} is the electron-phonon coupling constant. The time constant $\tau_{th} = 50$ ps describes the relaxation back to the initial temperature T_0 . The parameters used in the model were assumed to be typical for a transition metal [47]. In this model after the action of a laser pulse the electron temperature T_{el} increases from the initial temperature (equilibrium temperature of the sample) up to T_{el}^* within the duration of the laser pulse. The value of T_{el}^* is defined by the fluence of the laser pulse and by the electron heat capacity C_{el} , which is $C_{el} = \gamma T_{el}$ with $\gamma = 700 \text{ J/m}^3\text{K}^2$. The increase is followed by a decrease of T_{el} due to the electron-phonon relaxation. The characteristic time of this relaxation is determined by the electron-phonon coupling constant G_{el-ph} , which is assumed to be $1.7 \times 10^{18} \text{ J/Ks}$. In Figure 4.4(a,b) we show the calculated dynamics of the T_{el} for heat pulses of durations 100 and 2000 fs.

Modeling ultrafast nonequilibrium spin dynamics

Atomistic simulations may allow one to calculate the response of the spin system to the combined action of the ultrafast heating and the opto-magnetic field \mathbf{H}_{OM} . In this approach the spin system interacts with a heat-bath, the temperature of which is

defined by the electron temperature. The latter changes in time according to the two-temperature model [Eqs. (4.4a, 4.4b)] [46]. The dynamics of each spin is described by the stochastic Landau-Lifshitz-Gilbert (LLG) equation where the total effective field entering the LLG equation contains three contributions from Heisenberg exchange, a crystalline anisotropy and the opto-magnetic field \mathbf{H}_{OM} . This atomistic approach, however, does not allow to calculate the behavior of a large ensembles of spins. Nevertheless, it allows to calculate the equilibrium magnetization, the perpendicular and parallel magnetic susceptibilities, as well as the exchange stiffness of the spin system, required for the description of the magnetization dynamics in the case, when neither the length nor even the equilibrium value of the magnetization are conserved [27].

In our multiscale model the behavior of the averaged magnetization \mathbf{m} after the action of the laser pulse is described using the Landau-Lifshitz-Bloch (LLB) equation [27, 48]:

$$\begin{aligned} \dot{\mathbf{m}}_i = & -\tilde{\gamma}(\mathbf{m}_i \times \mathbf{H}_{\text{eff}}^i) + \frac{\tilde{\gamma}\alpha_{\parallel}}{m_i^2} [\mathbf{m}_i \cdot (\mathbf{H}_{\text{eff}}^i + \zeta_{\parallel}^i)] \mathbf{m}_i \\ & - \frac{\tilde{\gamma}\alpha_{\perp}}{m_i^2} \mathbf{m}_i \times [\mathbf{m}_i \times (\mathbf{H}_{\text{eff}}^i + \zeta_{\perp}^i)], \end{aligned} \quad (4.5)$$

The temperature dependence of the uniaxial anisotropy constant K_{u} is introduced via a temperature dependent transverse susceptibility [27]. The room-temperature value of K_{u} is taken to be $6.05 \times 10^5 \text{ J/m}^3$ and the exchange stiffness is chosen such that it leads to the Curie temperature of 500 K. The microscopic Gilbert damping constant is assumed to be 0.1. Solely ferromagnetic behavior is considered here so that the details of the ferrimagnetic spin structure cannot be simulated. All methods used are described in details in Ref. [27].

Using this micromagnetic approach developed by the group of Prof. Ulrich Nowak (University of Konstanz), we are able to perform calculations of the spin dynamics of extended systems accounting for spatially inhomogeneous excitation process on a micrometer length scale. This approach takes long range dipolar interactions into account, which are calculated with the aid of the well-established fast-Fourier transformation. The parallelized code used in the calculations allowed to simulate systems with up to 10^7 macro-spins (cells). The volume of the modeled spin system is up to $10 \mu\text{m} \times 10 \mu\text{m} \times 5 \text{ nm}$, which is comparable to the size of the systems, studied in the experiments. For these micromagnetic simulations the heat pulse and the pulse of the opto-magnetic field were modeled by a Gaussian spatial profile as explained above. In addition to this computation time demanding large-scale simulations we also performed single-macrospin simulations, where the macrospin represents a single-domain volume of $(30 \text{ nm})^3$. Note, that at this stage we neglect the spatial distribution of the \mathbf{H}_{OM} in Eq. (4.1) and of T_{el} .

4.4 Results and discussion

4.4.1 Determination of the laser pulse fluence dependence for the helicity dependent reversal

Experiment

To investigate how the process of all-optical magnetization reversal depends on the laser pulse fluence, we studied the final state of the magnetization after the action of a single laser pulse as a function of the laser pulse fluence. Figure 4.5(a) shows the steady-state magneto-optical images of the $\text{Gd}_{26}\text{FeCo}$ sample obtained after the sample was subjected to single circularly polarized pulses of various fluences.

As one can see from Figure 4.5(a), the change of the laser pulse fluence (F) leads to a change of the magnetic state observed after the action of the pulse. If F is below $\sim 3.14 \text{ mJ/cm}^2$, no reversal is observed (not shown). If F is about 3.14 mJ/cm^2 , all-optical helicity-dependent reversal is observed. As F is increased by a relatively small value, the reversal of magnetization is observed after the action of laser pulses of both helicity, and even a linearly polarized pulse can trigger the reversal. However, the size of the reversed spot appears to be slightly larger, if the helicity of the laser pulse favors the helicity-dependent reversal at lower fluence. This is demonstrated in the last row in Figure 4.5(a). At laser fluences above $\sim 4.5 \text{ mJ/cm}^2$ the formation of a multidomain state is observed. We note in Figure 4.5(b) that in the Gaussian spatial profile of the laser pulses of high fluence ($F > 4.5 \text{ mJ/cm}^2$) we can distinguish four regions, corresponding to the four types of the impact of a laser pulse on the magnetic medium: [I] fluence range where no all-optical reversal is observed; [II] helicity-dependent all-optical reversal; [III] helicity-independent reversal and [IV] the formation of a multidomain state.

An analogous dependence of the reversal on the laser pulse fluence was observed in several other samples, with absolute values of the fluence being slightly different, as discussed in Section 4.4.4. To examine the range, where the helicity-dependent reversal is observed, we studied the laser pulse fluence dependence of the probability for the magnetization to be reversed after the action of a single right- [$P(\sigma^+)$] or left-handed [$P(\sigma^-)$] circularly polarized pulse [35]. The result for the sample $\text{Gd}_{26}\text{FeCo}$ is shown in Figure 4.6, where these probabilities and the all-optical switchability, that is, $P(\sigma^+) - P(\sigma^-)$, are plotted as a function of the laser pulse fluence. As one can see, there is a narrow range of laser pulse fluences ($\sim 10\%$), where the switchability is non-zero $P(\sigma^+) - P(\sigma^-) > 0$, i.e. the probability for a helicity-dependent reversal to occur is finite. In the middle of this window the switchability reaches 100%. At these conditions the direction of the magnetization in the final state is unambiguously determined by the helicity of the laser pulse. When the laser pulse fluence is above the reversal window, the reversal into a single domain state still occurs, but appears to be independent of the helicity of the laser pulse.

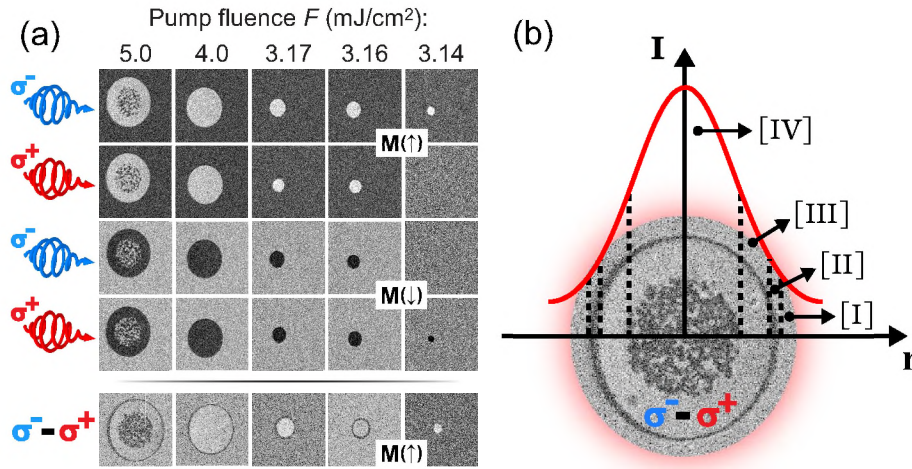


Figure 4.5: (a) Rows 1-4: Steady-state magneto-optical images of the sample $\text{Gd}_{26}\text{FeCo}$ at room temperature obtained after the action of single 100 fs σ^+ - and σ^- -polarized laser pulses with fluence F . The initial direction of magnetization was “up” for images in rows 1-2, and “down” in rows 3-4. Each of the images is the result of the subtraction of the image obtained before the excitation with the single laser pulse from the image obtained at ~ 2 s after the excitation. Images were obtained using a white light source. Before each irradiation event, the sample was brought to a single-domain state by applying a magnetic field pulse. The last row shows the subtraction of the images in rows 1-2 obtained with pulses of opposite helicities ($\sigma^- - \sigma^+$) for each specific fluence. (b) Schematic presentation of the laser fluence distribution and the reversal for $F = 5$ mJ/cm²: [I] no reversal; [II] helicity-dependent reversal; [III] helicity-independent reversal and [IV] multidomain state.

Thus, from the study of the impact of laser pulses of various fluences and helicities on magnetization of the GdFeCo alloy, we can conclude that the all-optical reversal occurs only when the medium is subjected to a circularly polarized pulse with its fluence being within a narrow range, or *reversal window*. Below this window no reversal occurs. Above this window the reversal is insensitive to the polarization of the laser pulse, which is a manifestation of the fact that the information about the light polarization is lost. In the following theory section we only focus on all-optical helicity-dependent magnetization reversal.

Modeling

In order to understand how the observed helicity-dependent magnetization reversal can occur, we performed multiscale calculations of the dynamics of the ferromagnetically coupled spins subjected to the combined action of the heat and opto-magnetic pulse, as described in Section 4.3.

In the two-temperature model the action of the 100 fs laser pulse leads to a rapid increase of the electron temperature T_{el} from 300 K up to T_{el}^* . This increase is followed by a relaxation of T_{el} due to the electron-phonon interactions with a characteristic time of 0.5 ps. The quasi-equilibrium electronic temperature achieved after this relaxation is determined by the peak electronic temperature T_{el}^* , as shown in Figure 4.7(a). Figure 4.7(b) shows the calculated dynamics using the LLB equation of a single macro spin, representing the averaged magnetization of a $(30 \text{ nm})^3$ spin system for three different peak temperatures T_{el}^* and opto-magnetic field amplitude H_{OM} for

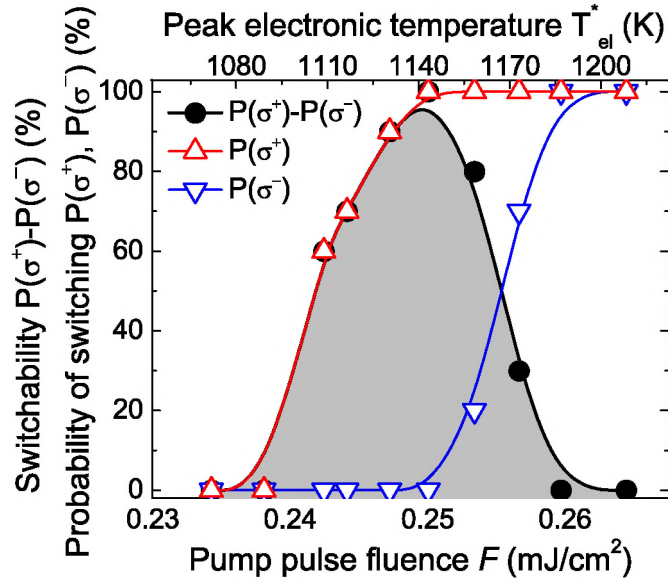


Figure 4.6: Probabilities that the magnetization is reversed after the action of a single left- $[P(\sigma^-)]$ and right-handed $[P(\sigma^+)]$ circularly polarized laser pulse (open triangles) and all-optical switchability $P(\sigma^+) - P(\sigma^-)$ (closed circles) versus F in the sample $\text{Gd}_{22}\text{FeCo}$ [35]. For the sake of clarity, we show also the values of the peak electronic temperature, which were calculated from the laser peak fluence using the electronic heat capacity $C_e = 1.8 \times 10^6 \text{ J/Km}^3$ being typical for a metal [47].

a field duration of $\tau_{\text{OM}} = 250$ fs. This field is directed antiparallel with respect to the initial orientation of the magnetization. As one can see, for the particular value of $T_{\text{el}}^* = 1129$ K the magnetization reverses. The reversal occurs via a *linear* path and does not involve precession, i.e. the transverse components of the magnetization remain zero (not shown). Instead, at the very early stage of the reversal process the magnetization is nearly quenched. As it was shown previously [49], for the linear dynamics of the spin system, achieving a nearly quenched magnetization state is crucial. In this state, the dynamics of the spins is governed by the longitudinal damping. This favors the reversal of magnetization by the short strong pulse of the opto-magnetic field \mathbf{H}_{OM} directed antiparallel with respect to \mathbf{M} . We note that this is in contrast to the precessional switching of the magnetization, which is governed by the transverse damping.

As it can be seen from Figure 4.7(b), the final state of the magnetization is mainly defined by T_{el}^* . For the low peak electron temperature (e.g. $T_{\text{el}}^* = 970$ K) the spin system reaches a state with nearly-quenched magnetization, but later on relaxes back to the initial state, i.e. magnetization reversal does not occur. Thus, for the given amplitude and duration of \mathbf{H}_{OM} , the temperature T_{el} achieved within the duration of the effective field pulse is not sufficient for the occurrence of the linear reversal. The spin system relaxes into the state with reversed magnetization only for certain intermediate values of T_{el}^* . If T_{el}^* is too high, the calculations give a final state with zero magnetization. This shows that the highly-nonequilibrium state, with T_{el} sufficient for the linear reversal, should not persist for too long after the end of the effective magnetic field pulse. Otherwise the effect of the field pulse action, namely the nucleation of the phase with the reversed magnetization, will be lost. In the latter case the system is expected to relax back to a state with random orientation of magnetization, yielding a multidomain state.

The width of the electronic temperature range, or the *reversal window*, where the magnetization reversal via the linear mechanism can occur, is strongly influenced by changes of the parameters of the opto-magnetic field pulse \mathbf{H}_{OM} . In Figure 4.8(a) we examine the state of nano-element 10 ps after the combined action of the heat and opto-magnetic pulses for different laser fluences and opto-magnetic field pulse durations. The laser pulse duration was fixed at 100 fs. As can be seen from Figure 4.8(a), there is a region in that parameter space where the reversal occurs. As the duration of the effective field pulse increases, the reversal occurs in a broader window of the laser fluences. The lower limit of τ_{OM} , at which the reversal can be realized, is strongly influenced by the material constants entering the calculations (see Section 4.3). In particular, an increase of the electron-phonon coupling constant $G_{\text{el-ph}}$, governing the dynamics of electronic and lattice response to the heat pulse, leads to a reduction of the minimum field pulse duration. For the parameters used in the calculations, the minimal duration of the opto-magnetic field, for which the reversal occurs, is 250 fs. Therefore, despite the fact that the parameters of the laser-induced effective field

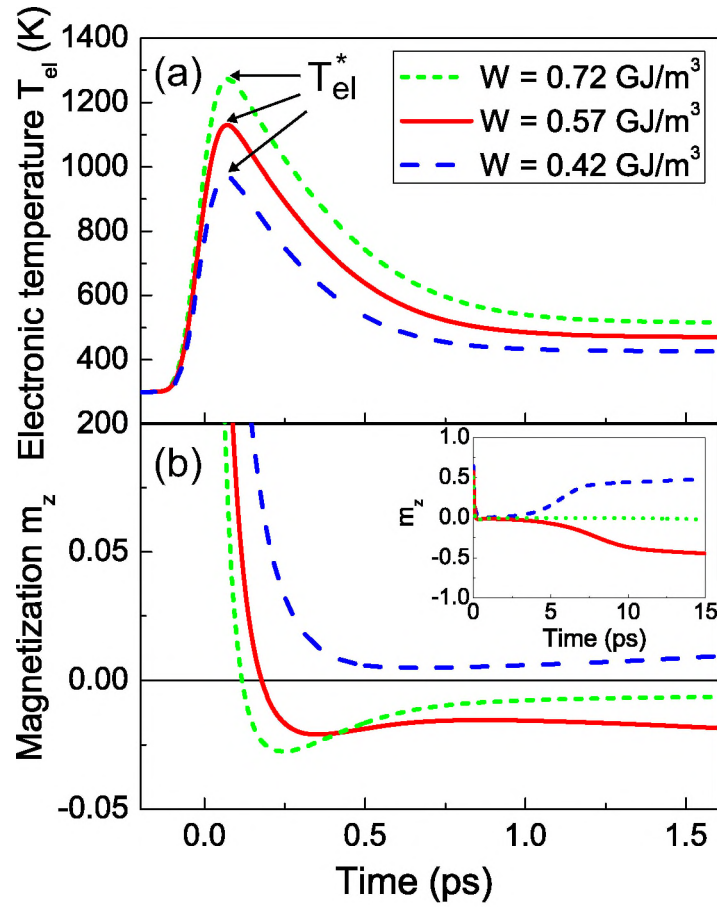


Figure 4.7: (a) Electronic temperature as a function of time, as calculated from the two-temperature model for the peak electronic temperatures $T_{el}^* = 970 \text{ K}$ (triangles), 1129 K (circles) and 1273 K (squares) (b) Dynamics of the longitudinal component of the magnetization for these three different peak electronic temperatures and corresponding opto-magnetic field amplitudes ($H_{eff} = 18.8 \text{ T}$ for the lowest fluence) with duration $\tau_{OM} = 250 \text{ fs}$. The inset shows the dynamics for a time scale up to 15 ps .

\mathbf{H}_{OM} are not fully defined at this stage, the results in Figure 4.8(a) show that the regime of linear reversal is achievable for a rather wide range of opto-magnetic field parameters.

For any opto-magnetic pulse durations τ_{OM} there is a laser pulse fluence, above which the calculated final state for the magnetization is zero [see Figure 4.8(a)]. Detailed analysis of the dynamics of the $(30\text{ nm})^3$ spin ensemble at $W = 0.8\text{ GJ/m}^3$ shows that there are equal probabilities for the magnetization to reemerge in both $+z$ and $-z$ directions after an excitation with such a pulse. This is illustrated in Figure 4.8(b), where the statistics of the time evolutions of the m_z component is shown. It is seen that at high laser pump fluences the final state of the magnetization is defined by neither opto-magnetic field pulse nor by the initial magnetic state. The latter fact corresponds to the loss of the magnetic memory studied in [27].

To summarize, the model shows that the action of laser pulses with a duration above a certain limit results in magnetization reversal. In good agreement with our experimental results, this process can be realized only in a narrow range of the laser pulse fluences. Most importantly, our model shows that the magnetization during the reversal process follows a linear trajectory passing through a state with no net magnetization. The latter can be seen as a distinct feature of the laser-induced reversal process. The model also provides quite intriguing predictions about the dynamics of the all-optical magnetization reversal, showing that it may occur within just a few picoseconds. As it can be seen from Figure 4.7(b), under the conditions favoring linear reversal ($T_{\text{el}}^* = 1129\text{ K}$) almost 50% of the state with reversed magnetization is reconstructed already after $\sim 10\text{ ps}$. In order to verify whether the all-optical reversal indeed occurs via a demagnetized state and whether its dynamics is indeed that fast, time-resolved experimental studies should be performed.

4.4.2 Dynamics of the all-optical helicity-dependent reversal

Experiment

In order to identify the path which the magnetization follows after excitation with a circularly polarized pulse with the fluence (Figure 4.6), we employed the single-shot time resolved microscopy technique, described in Sections 4.3.1 and 3.4.

Figure 4.9(a) shows the single-shot magneto-optical images of the $\text{Gd}_{24}\text{FeCo}$ sample obtained at room temperature at various time delays between pump and probe pulses [35]. Experiments have been performed for various combinations of the pump pulse polarization and two initial orientations of the magnetization. It is seen that within the first picosecond, pump pulses of both helicities bring the originally magnetically ordered medium into a strongly non-equilibrium state with no measurable net magnetization, seen as a gray area [see the second column of Figure 4.9(a)]. In the following few tens of picoseconds either the medium relaxes back to the initial state or a small ($\sim 5\text{ }\mu\text{m}$) domain with a reversed magnetization is formed. We especially

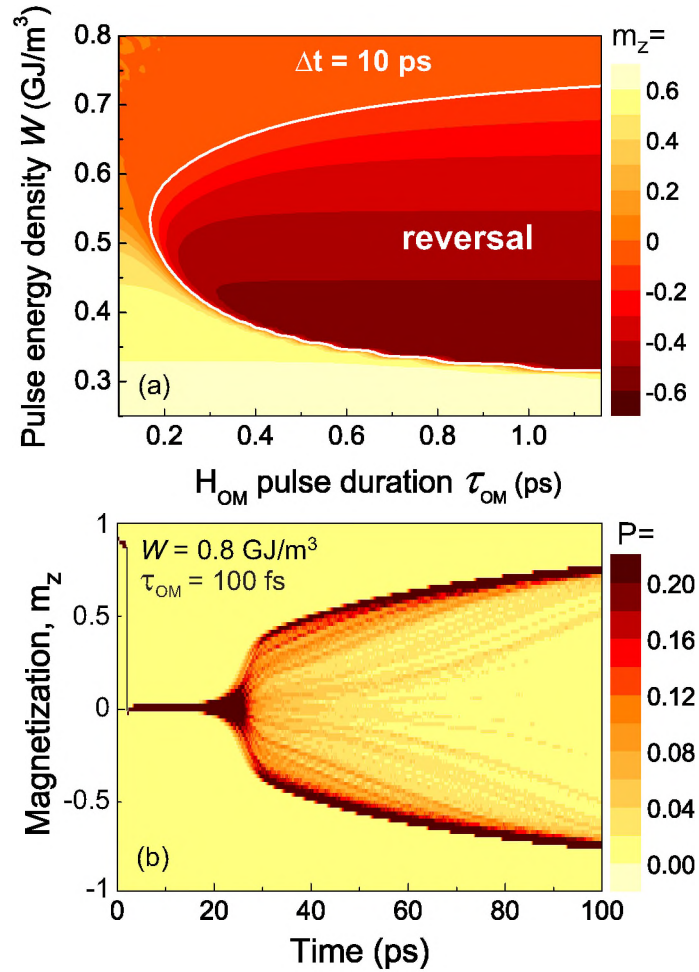


Figure 4.8: (a) Phase diagram showing the z -component of the averaged magnetization m_z of the $(30\text{ nm})^3$ volume at 10 ps after the action of the laser pulse with given energy density and opto-magnetic pulse duration. The laser pulse duration τ is considered to be 100 fs. The color code for the m_z values is given on the right hand side of the figure: yellow, red and blue colors respectively correspond to a positive, zero and negative values of m_z . The initial value of m_z is +1. The solid line corresponds to $m_z = 0$ and separates the region with finite probability for the final state to be reversed. (b) Statistical analysis of the time evolutions of the m_z at high pulse energy density ($W = 0.8$ GJ/m³). The color code for the probabilities P for m_z to have a certain value at a certain time delay is shown on the right-hand side of the figure (in %). The resulting average value of m_z at such a laser pulse fluence is zero at any time delay, as shown in (a) and Figure 4.7(b).

note that we see no sign of precession during the whole reversal process. Due to the oblique incidence of the probe beam (see Section 3.4), the appearance of an in-plane component of the magnetization during the precession might become visible in the time-resolved images in Figure 4.9(a). Therefore, we assume that the gray areas seen at short delay times correspond to the quenching of both out-of-plane and in-plane components of magnetization. It appears that the all-optical helicity-dependent reversal proceeds via a state with nearly quenched magnetization [35, 50]. This observation fully agrees with our model of linear reversal.

From the results shown in Figure 4.9(a) it follows that the reversal process is inhomogeneous across the area subjected to the laser pulse. In order to characterize the observed dynamics quantitatively and to estimate the actual switching time, we calculated the averaged value of the magnetization at the various delays in the area of $\sim 5 \mu\text{m}$. This area corresponds to the domain with the reversed magnetization in the final state [the columns on the right-hand side in Figure 4.9(a)]. The result is shown in Figure 4.9(b). Already at delays shorter than 100 ps, a clear magnetic contrast is observed between the states reached after excitations with different helicities. This contrast is slightly different from the contrast between the final states [the last column in Figure 4.9(a)], as clearly seen from Figure 4.9(b). This can be ascribed to the laser-induced heating of the sample followed by a slow ($> 1 \text{ ns}$) heat diffusion. To take into account the heat-induced change of the magnetization in the metastable magnetization states, we introduce two asymptotic levels [see dashed lines in Figure 4.9(b)]. The characteristic time of switching τ_{sw} can be identified as the time required to reconstruct 63% ($1 - e^{-1}$) of the difference between the two metastable states. After $1.5\tau_{\text{sw}}$ the difference reaches 80%. Figure 4.9(a) shows that this time can indeed be reliably assumed as the period required for a write-read event. Thus, we can conclude that the switching time and the write-read time for the case shown in the Figure 4.9(a,b) are $\tau_{\text{sw}} = 60 \text{ ps}$ and $\tau_{\text{w-r}} = 90 \text{ ps}$, respectively.

Modeling

Experimental results shown in Figure 4.9(a,b) clearly demonstrate that the all-optical helicity-dependent reversal indeed possesses the main features expected for the linear reversal as described in the previous Section 4.4.1. However, one can notice a clear discrepancy between reversal times observed numerically [Figure 4.8(a)] and experimentally [Figure 4.9(b)]. These calculations were done for a small magnetic element, neglecting spatial inhomogeneities of both opto-magnetic and heating pulses. In order to investigate the linear reversal in a magnetic film of μm size under realistic excitation conditions, we performed multi-macrospin LLB calculations (see Section 4.3). We considered a $10 \mu\text{m} \times 10 \mu\text{m} \times 5 \text{ nm}$ ferromagnetic film subjected to a heat pulse and opto-magnetic field pulse (Eq. 4.1) of Gaussian spatial profile with $r_0 = 2.1 \mu\text{m}$. The laser fluence and duration as well as the opto-magnetic field duration are chosen to favor linear reversal (see Figure 4.7). The calculated distributions of the magne-

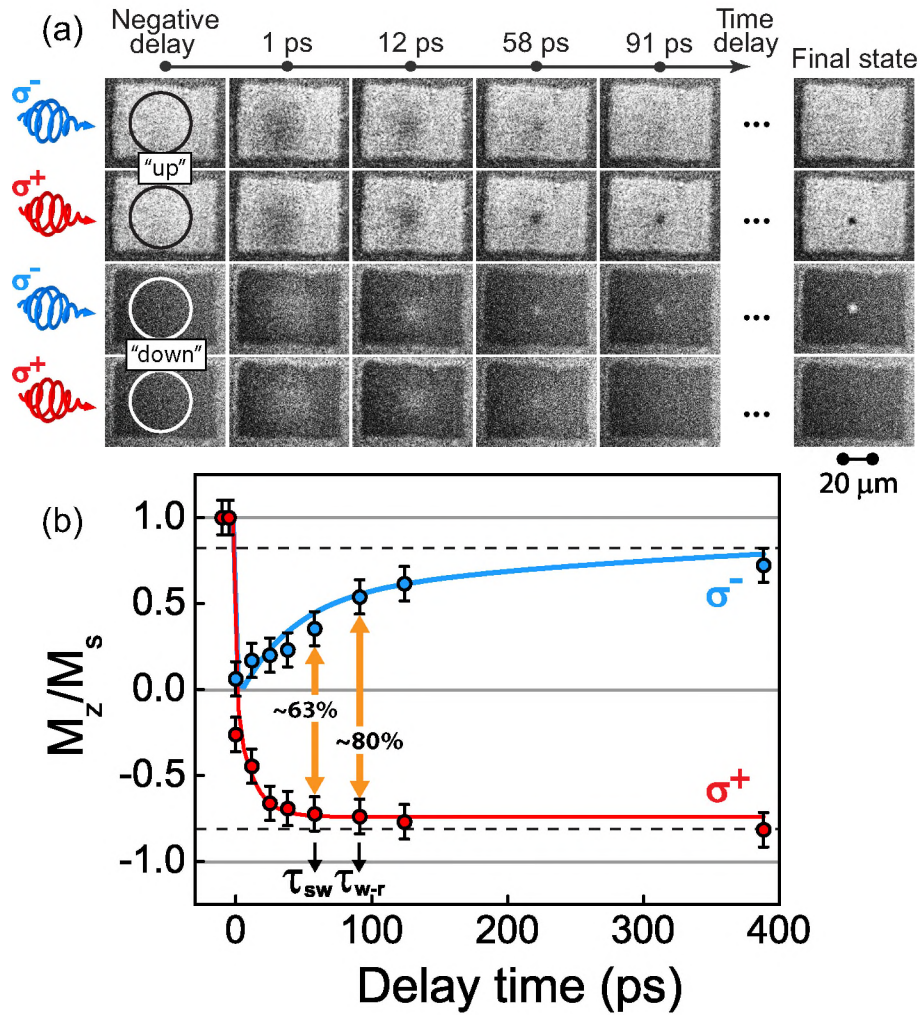


Figure 4.9: (a) The magnetization evolution in $\text{Gd}_{24}\text{Fe}_{66.5}\text{Co}_{9.5}$ after the excitation with σ^+ and σ^- circularly polarized pulses at room temperature. The domain is initially magnetized up (white domain) and down (black domain). The last column shows the final state of the domains after a few seconds. The circles show areas actually affected by pump pulses. (b) The averaged magnetization in the switched areas ($\sim 5 \mu\text{m}$) after σ^+ and σ^- laser pulses, as extracted from the single-shot images in (a) for the initial magnetization up [35].

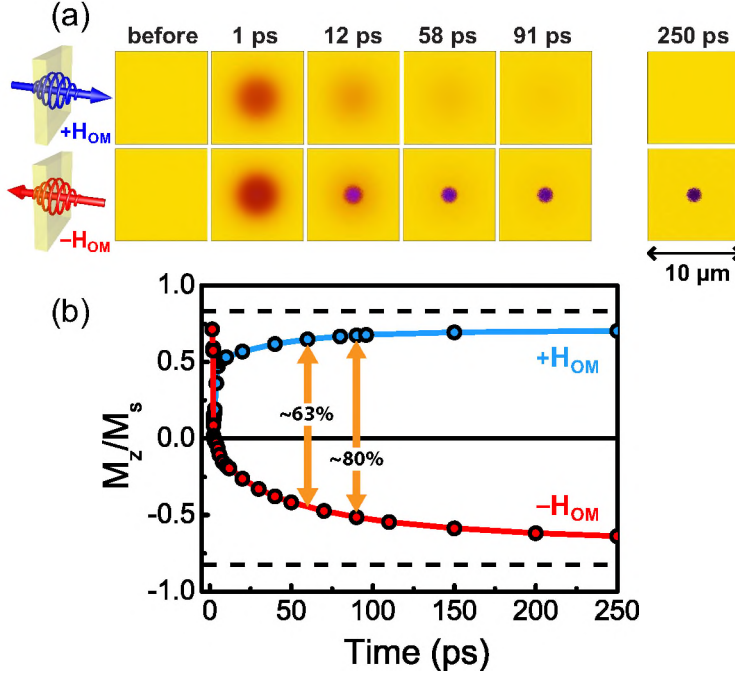


Figure 4.10: (a) Distributions of the z -component of the magnetization across the $10 \mu\text{m} \times 10 \mu\text{m} \times 5 \text{nm}$ ferromagnetic film at different time delays after the combined action of a 100 fs long laser pulse and a 250 fs long opto-magnetic field pulses as obtained from the multi-macrospin simulations. The peak electronic temperature is $T_{el}^* = 1129 \text{K}$. Yellow, red and blue regions respectively correspond to positive, zero and negative values of m_z . (b) The averaged magnetization in the switched areas ($\sim 0.5 \mu\text{m}$) versus time.

tization at various time delays for two opposite \mathbf{H}_{OM} are shown in Figure 4.10(a). Figure 4.10(b) shows the calculated time evolution of the z -component of the magnetization in the center of the magnetic element shown in Figure 4.10(a). Comparison of the calculated and experimental results shows that the spatial profile of the process of the relaxing magnetic state is determined by the spatial distribution of the laser pulse fluence, which defines the distribution of both the electronic temperature and the opto-magnetic field. The switching times obtained for the larger element appears to be close to those obtained in the experiment [see Figs. 4.9(b) and 4.10(b)].

Thus, using both experimental results and multiscale modeling we confirm that the all-optical helicity-dependent reversal can be a result of ultrafast laser-induced heating accompanied by the action of the effective laser-induced magnetic field. The latter is

responsible for the helicity-dependence of the reversal. In this process of the all-optical reversal, the magnetization follows a novel linear path, not involving precessional motion but passing through the state with no net magnetization [35]. Simulations show that the nucleation of the phase with the reversed magnetization happens on an ultrafast time scale of just ~ 1 ps, which is followed by a slower relaxation to the equilibrium state. Even though, the write-read time achieved in the experiment appears to be comparable to the fastest switching in an external magnetic field or by a spin-polarized current, our model shows that the write-read time can be even faster and reach values as low as ~ 10 ps.

Our consideration, however, leaves two important questions open. First, as the realistic parameters, strength and duration, of the laser-induced effective field \mathbf{H}_{OM} are still under discussion, it is important to investigate what would happen to the helicity-dependent all-optical reversal when these parameters are changed. Second, so far neither in the experiments nor in the modeling, the ferrimagnetic structure of the GdFeCo alloys was taken into account. Consequently, it is interesting to verify if the ferrimagnetism of GdFeCo plays a role in the reversal process. In particular, whether the write-read times close to those predicted by the model can be improved by tailoring the properties of the medium.

4.4.3 Helicity-dependent all-optical reversal as a function of the laser pulse parameters

Parameters of a laser pulse affect both the demagnetization process and the opto-magnetic field (Eq. 4.1). Therefore, it is natural to expect that the all-optical magnetization reversal, being a result of the interplay between these two effects, should possess a high sensitivity to the parameters of the laser pulse. We have already shown in Section 4.4.1 that the laser fluence is one of the crucial parameters for the all-optical reversal, because it defines the electronic temperature increase and, consequently, the degree of demagnetization. Moreover, the calculations suggest that the reversal should be feasible with picosecond laser pulses as well. In order to explore how the all-optical helicity-dependent reversal process depends on the laser pulse parameters we studied the reversal for the case of laser pulses of various durations and ellipticities.

Effect of the laser pulse polarization: experiment

As we have shown, the all-optical helicity dependent magnetization reversal is very sensitive to the changes of the laser pulse fluence. As it follows from the two temperature model [Eqs. (4.4a, 4.4b)] and the phenomenological expression for the effective field \mathbf{H}_{OM} (Eq. 4.1), the change of the fluence of a laser pulse leads to changes of both the peak electronic temperature T_{el}^* and the amplitude of the field \mathbf{H}_{OM} . Therefore, it would be interesting to examine which of these two factors is especially crucial for the reversal. In order to do so, we have to be able to vary T_{el}^* and \mathbf{H}_{OM} independently.

This can be done by studying the all-optical reversal for laser pulses of various polarizations. As can be seen from Eq. 4.1, the value of the light-induced effective field is determined in particular by the coefficient p , which gives the degree of the circular polarization. It varies gradually from -1 to +1 when the polarization of the laser pulse is changed from left- to right-handed circular. Therefore, in the experiments it is possible to change the value of the effective field without changing the peak power of the laser pulse and, consequently, without affecting the demagnetization process [16].

In Figure 4.11 we show the switchability as a function of the laser pulse fluence measured for circularly polarized, elliptically polarized and linearly polarized laser pulses. Here the switchability $P(\mathbf{M} \uparrow) - P(\mathbf{M} \downarrow)$ is determined as the difference between the probabilities for the laser pulse of the given polarization to reverse the magnetization from two opposite initial states “up” [$P(\mathbf{M} \uparrow)$] and “down” [$P(\mathbf{M} \downarrow)$]. Surprisingly, the all-optical reversal could still be observed when the degree of the circular polarization was significantly reduced down to $p \approx 0.15$. This result shows that there exists a lower limit for the amplitude of \mathbf{H}_{OM} , which is substantially below the peak value used above. This limit is estimated and found from our phenomenological model of the inverse Faraday effect to be of the order of 3 T for $p = 0.15$ (given $H_{\text{OM}} = 20$ T for the circularly polarized pulse $p = 1$). Even more importantly, it clearly demonstrates that in our experiments with the circularly polarized pulses, the changes of the all-optical reversal with the laser pulse fluence [see e.g. Figure 4.5(b)] are mostly determined by the changes in the ultrafast demagnetization process and not by the changes of the amplitude of the effective field.

Effect of the laser pulse duration: experiment

In order to investigate experimentally how the change of the laser pulse duration influences the reversal process, we measured the all-optical switchability $P(\sigma^+) - P(\sigma^-)$ as a function of the laser pulse fluence for different laser pulse durations. The results for the samples $\text{Gd}_{24}\text{FeCo}$ and $\text{Gd}_{26}\text{FeCo}$ are shown in Figure 4.12. In Figure 4.12(a,b) we have plotted the dependence of the laser pulse fluence F_{sw} and the laser peak power P_0 which corresponds to 100% switchability on the laser pulse duration. The width of the reversal window ΔF_{sw} as a functions of the laser pulse duration is shown in Figure 4.12(c,d). As one can see, the reversal window is getting wider as the laser pulse duration increases. Such a behavior is in qualitative agreement with the phase diagram $W - \tau_{\text{OM}}$ [Figure 4.8(a)]. Our experimental data also show that the all-optical switching of the magnetization requires more laser pulse fluence as the pulse duration increases [Figure 4.12(a,b)]. Note that the overall increase of the required laser pulse fluence F_{sw} with the pulse duration is rather small. As a result, the corresponding peak power P_0 required for the reversal decreases with an increase of the laser pulse duration. The effects of the laser pulse duration on the reversal are qualitatively the same in $\text{Gd}_{24}\text{FeCo}$ and $\text{Gd}_{26}\text{FeCo}$ alloys. However, in the case of

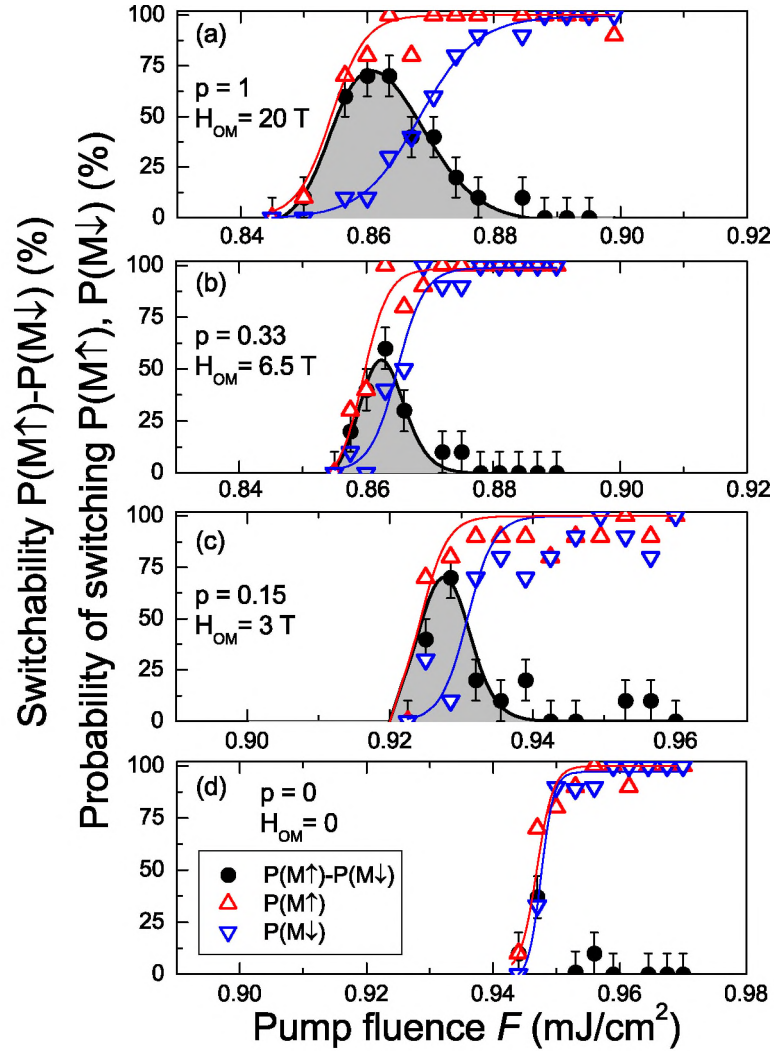


Figure 4.11: The switchability $P(M\uparrow) - P(M\downarrow)$ (closed circles) measured for the sample $\text{Gd}_{24}\text{FeCo}$ for (a) the circularly-, (b,c) elliptically- ($p = 0.33, 0.15$), and (d) linearly-polarized ($p = 0$) 100 fs single laser pulses. Also shown are the probabilities of the reversal for the initial states with magnetization “up” [$P(M\uparrow)$] or “down” [$P(M\downarrow)$] (open triangles). Solid lines are guides to the eye.

Gd₂₄FeCo, the all-optical reversal is observed only when the laser pulse duration is shorter than 1700 fs. For longer pulses we have observed either no effect (in the case of low pump fluence) or the formation of a multidomain state (in the case of high pump pulse fluence). In the sample Gd₂₆FeCo the reversal is observed in the whole range of the studied pulse durations up to 2100 fs.

Effect of the laser pulse duration: modeling

It is natural to expect that an increase of the laser pulse duration will result in an increase of the duration of the opto-magnetic field (see Figure 4.3). The former, however, also affects the time profile of the electronic temperature. This is illustrated in Figure 4.3(b,c), which shows the dynamics of the electronic temperature calculated from the two-temperature model for laser pulse durations 100 fs and 2000 fs. To understand the observed dependence of the magnetization reversal on the laser pulse duration, we simulated the dynamics of the magnetization of a (30 nm)³ sample in a single-macrospin approximation. We took into account the scaling of the opto-magnetic field and the change of the electronic temperature T_{el} profile with the change of the laser pulse duration (Eq. 4.1). Figure 4.13 shows the magnetic state of the sample 100 ps after the action of the laser pulse with fluence F and duration τ .

As one can see from the presented phase diagram, there is a range of laser pulse durations and fluences, where the probability for the all-optical reversal of the magnetization is nonzero. Similar to the experiment (see Figure 4.12), the magnetization reversal by a longer laser pulse requires a higher fluence. Again, similar to the experiment [Figure 4.12(a,b)] this means that longer pulses can reverse the magnetization with lower peak power P_0 . As it follows from Eq. 4.1, the peak power of the laser pulse defines the amplitude of the effective field. Thus, from our experimental and simulated results we can conclude that, when the effective light-induced field \mathbf{H}_{OM} has a longer duration, the amplitude of this field can be lower than for the case of shorter pulses. Moreover, as it follows from the two temperature model (Figure 4.4), the dynamics of the electronic temperature T_{el} is also affected by the duration of the laser pulse. Consequently, longer pulses allow to achieve the conditions required for the all-optical switching at lower T_{el}^* . This also results in a decrease of the peak power P_0 required for the reversal. Our calculations show (see Figure 4.13) that the width of the reversal window decreases as the pulse duration increases and after certain pulse duration all-optical reversal cannot be realized. This agrees partly with our experimental data which show the disappearance of the all-optical reversal in sample Gd₂₄FeCo for pulses longer than 1700 fs [Figure 4.12(a)]. Moreover, the disappearance of the magnetization reversal for laser pulses with longer duration agrees well with the fact that ultrafast demagnetization cannot be realized when the laser pulse duration becomes too long [51–53].

We would like to note, however, that the proposed model is genuinely not capable of accounting for the difference between the magnetization reversal by longer pulses

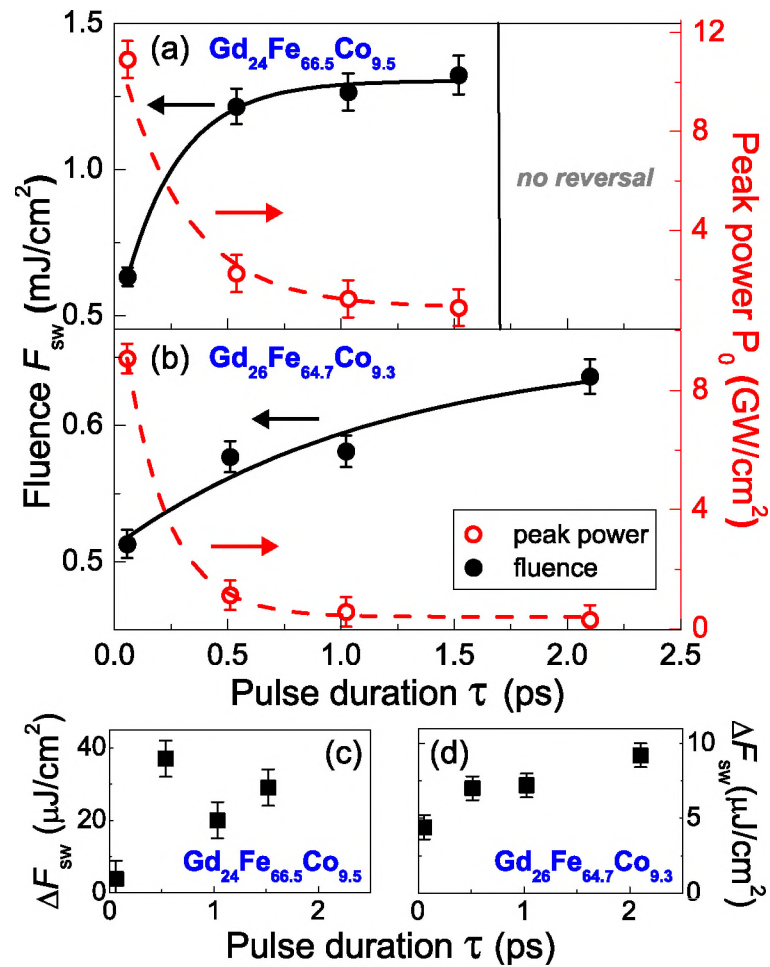


Figure 4.12: (a,b) The laser pulse fluence F_{sw} and peak power P_0 at the center of the reversal window and (c,d) the width of the reversal window ΔF_{sw} versus the duration of the laser pulse τ as obtained for the samples $Gd_{24}FeCo$ (a,c) and $Gd_{26}FeCo$ (b,d) from the fluence dependencies of the switchability measured for different laser pulse durations. Note that in the sample $Gd_{24}FeCo$, after the action of the laser pulses with duration $\tau > 1.7$ ps, no reversal was observed. Lines are the guides for an eye.

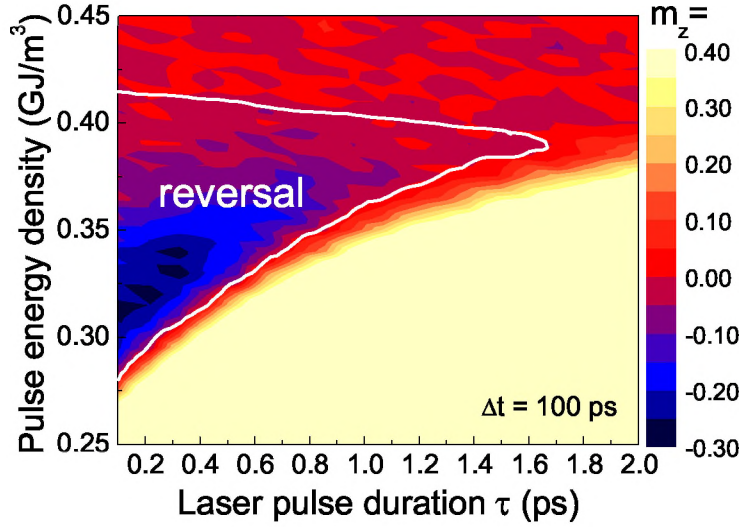


Figure 4.13: Calculated phase diagram showing the magnetization of the $(30\text{nm})^3$ element 100 ps after the action of a laser pulse of fluence F and duration τ . The parameters of the opto-magnetic fields are scaled with the parameters of the laser pulse as discussed in Section 4.3. Yellow, red and blue regions respectively correspond to positive, zero and negative values of m_z . The solid line separates the region where $m_z < 0$, i.e. where the probability of the reversal is > 0 . The initial state corresponds to $m_z = +1$.

in the samples with different concentrations of Gd ions [see Figure 4.12(a,b)], as it treats the medium as a ferromagnetic ensemble of spins.

As it was discussed in Section 4.2, the GdFeCo alloys with different Gd concentrations possess different magnetic properties, such as compensation temperature and coercivity. The difference in the all-optical reversal process revealed in the samples with different Gd contents suggests, that the actual magnetic structure plays an important role in the laser-induced magnetic dynamics. The model of the all-optical reversal in a ferrimagnetic medium is still a challenge. Nevertheless, here we experimentally investigated the effect of the ferrimagnetic structure of the GdFeCo alloys on the speed and efficiency of the all-optical helicity-dependent magnetization reversal.

4.4.4 Helicity-dependent all-optical reversal in various ferrimagnetic alloys of GdFeCo

Efficiency of the helicity-dependent reversal

If one compares the results of the action of a laser pulse of the same fluence, duration and polarization on samples with different concentration of Gd ions, a striking difference is clearly seen. Figure 4.14(a) shows that at a pump fluence $F = 3.14 \text{ mJ/cm}^2$ the all-optical magnetization reversal is observed only in the sample $\text{Gd}_{26}\text{FeCo}$, while in the samples $\text{Gd}_{22(24)}\text{FeCo}$ a laser pulse of the same fluence leads to a polarization-independent reversal. All-optical helicity-dependent reversal in these samples was also observed but at somewhat lower pump fluences. Surprisingly, in the sample $\text{Gd}_{20}\text{FeCo}$ the action of a single pulse of any polarization results only in the formation of a multidomain state. No all-optical reversal was observed in this sample at room temperature.

The main difference between these samples is the compensation temperature T_M (see Figure 4.2). We have studied the all-optical reversal in these samples at different temperatures. As a quantitative parameter, describing the all-optical reversal, we have chosen the fluence required for the all-optical reversal F_{sw} , falling approximately in the center of the reversal window. As a reference parameter, we also measured the minimum fluence required for the formation of a multi-domain final state F_{md} . This study reveals plenty of differences between the samples. In $\text{Gd}_{22}\text{FeCo}$, F_{sw} drops as the temperature decreases (similar dependence of F_{sw} on temperature in the $\text{Gd}_{22}\text{FeCo}$ alloy was reported in [54]). In sample $\text{Gd}_{20}\text{FeCo}$, which possessed no reversal at room temperature, a decrease of the temperature below $T = 200 \text{ K}$ leads to the appearance of all-optical reversal. In contrast, in $\text{Gd}_{24}\text{FeCo}$ and $\text{Gd}_{26}\text{FeCo}$ samples, a temperature decrease had an opposite effect, leading to an increase of F_{sw} . The dependence of F_{md} on temperature for all samples showed the same trend. At lower temperatures higher fluences were required for the formation of the multidomain state.

This diverse behavior of the reversal in the studied samples becomes unified if one plots the minimum fluence F_{sw} required for the all-optical reversal as a function of the difference between the temperature of the sample T and its compensation temperature T_M , as shown in Figure 4.14(b). From this figure one can see that for all studied samples, F_{sw} shows a minimum near the compensation point (at $T - T_M = 0$). The larger the deviation of the sample temperature from the compensation temperature, the higher the fluence required for switching.

Note that, the linear reversal implies that the fluence of the laser pulse is sufficient to increase the electronic temperature from its equilibrium value up to T_{e}^* . Consequently, one can expect that F_{sw} should be higher when the equilibrium electron temperature, i.e. sample temperature, decreases. The experimental data, however, show that this condition is satisfied only below T_M . [55] The observed dependence on

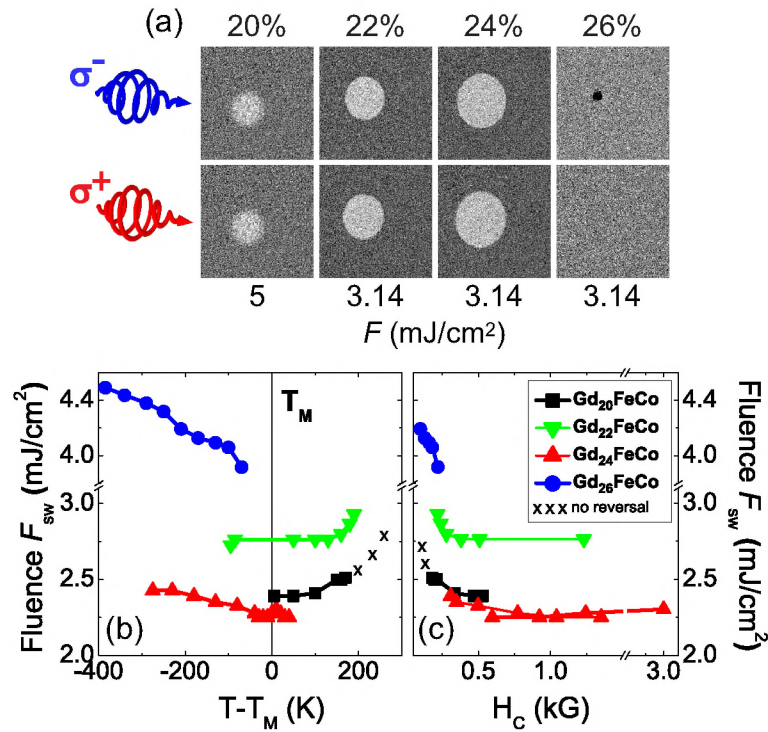


Figure 4.14: (a) Steady-state magneto-optical images of the samples Gd_xFeCo , $x = 20, 22, 24, 26\%$ obtained after the action of a single 100 fs circularly-polarized laser pulse. The fluence of the laser pulse was 3.14 mJ/cm^2 for all samples except for $\text{Gd}_{20}\text{FeCo}$, where no effect was observed for such an fluence. Before the irradiation all samples were saturated by applying an external magnetic field of the same direction. Because of the magneto-optical imaging, the orientation of the FeCo sublattice is visualized. Thus, black and white areas correspond to the orientation of the FeCo-sublattice magnetization “up” and “down.” It is oriented differently for the sample $\text{Gd}_{26}\text{FeCo}$, because this sample is below the compensation point and, consequently the FeCo sublattice is antiparallel to the magnetic field. Thus, in all shown cases the initial orientation of the total bulk magnetization is the same. The laser pulse fluence required for the all-optical reversal F_{sw} as a function of (b) the relative temperature $T - T_M$ and (c) coercive field H_c for the same samples. The pulse duration in these measurements was $\tau = 100 \text{ fs}$. The value of T_M at $T \approx 0 \text{ K}$ for the sample $\text{Gd}_{20}\text{FeCo}$ was obtained from the extrapolation of T_M vs. x dependence (see Figure 4.2). Crosses indicate the absence of the all-optical reversal for the sample $\text{Gd}_{20}\text{FeCo}$.

temperature shows that the ferrimagnetic properties of the medium, which have not been taken into account in our model, strongly affects the reversal process.

It is also important to note that, by taking into account the multi-sublattice nature of the GdFeCo alloys, one can see that there is an unequivocal correlation between the coercivity of the medium and the fluence required for the reversal [see Figure 4.14(c)]. It is known that the coercivity determines, in particular, the minimum stable size of a domain which can exist in a medium. Hence, as a result of this, one of the possible reasons for the observed disappearance of the reversal in the samples with low coercivity is that the domain created by the laser pulse of a given spot size cannot be sustained in the medium.

Therefore, the study of the efficiency of the all-optical helicity-dependent reversal clearly shows that choosing temperature in the vicinity of the compensation temperature T_M is very important for the reversal process. A lower pump fluence is required to switch magnetization near T_M , while far away of the compensation point all-optical magnetization reversal may become not feasible.

Speed of the all-optical reversal in GdFeCo alloys

It can be shown that along with the efficiency of the all-optical reversal, the switching time appears to be strongly affected by the composition of the GdFeCo alloy. Figure 4.15 shows the evolution of the magnetic state during the reversal process in the samples Gd₂₂FeCo and Gd₂₆FeCo at ambient temperature. As one can see, the switching time for Gd₂₆FeCo is around 100 ps and comparable with the time obtained for Gd₂₄FeCo. However, the magnetization switching in Gd₂₂FeCo happens on a much longer time scale of 16 ns.

In order to investigate this effect further we studied the speed of the reversal as a function of temperature in these three alloys. The write-read time τ_{w-r} [as defined in Figure 4.9(b)] is plotted in Figure 4.16 as a function of the difference between the sample temperature and the compensation point $T - T_M$. Figure 4.16 shows that the reversal appears to be the fastest for temperatures below T_M . In particular, by decreasing the temperature of Gd₂₂FeCo one can tune τ_{w-r} from 16 ns at room temperature down to 30 ps at 10 K ($T - T_M = -90$ K) [35].

As we have shown in Section 4.4.2, the all-optical helicity-dependent magnetization reversal is a linear reversal, occurring when the sample is brought to a strongly non-equilibrium state with no net magnetization. This is followed by a relaxation of the sample to an equilibrium mono-domain state including, among other processes, the growth of the domains with the reversed magnetization. The speed of the latter process, naturally, depends on the mobility of the domain walls, which in GdFeCo alloys is strongly temperature dependent. Moreover, the speed is very high in the vicinity of the angular momentum compensation temperature T_A [56–58]. When a sample being below T_A is subjected to a circularly polarized laser pulse, the laser excited area always contains domains brought close to T_A where the domain wall

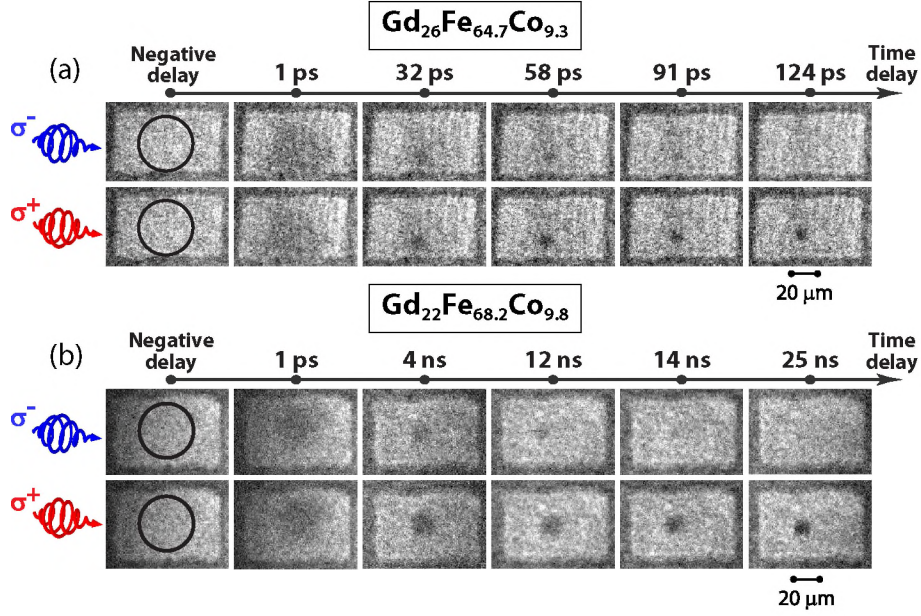


Figure 4.15: Single-shot magneto-optical images of Gd_xFeCo for (a) $x = 26$ and (b) 22% at room temperature obtained at different time delays after excitation with a single 100 fs circularly polarized laser pulses.

mobility is the largest. Then, it is the mobility at T_A which dominates the averaged domain walls speed in the photoexcited area and, thus, determines the write-read time. Above T_A , all-optical magnetization reversal can still be realized but the write-read time increases with temperature, as the optical excitation brings the system even further from T_A (see Figure 4.16).

4.5 Conclusions

Combining the experimental technique of single-shot time-resolved magneto-optical microscopy with multiscale modeling of the non-equilibrium spin dynamics, we have revealed a path for the reversal of the magnetization by a single circularly-polarized laser pulse. In particular, we have demonstrated experimentally that in order to reverse the magnetization, the laser pulse should bring the spin system within 1 ps into a strongly non-equilibrium state characterized by a nearly quenched net magnetization. Multiscale modeling of the dynamics of the spin system at this state shows that

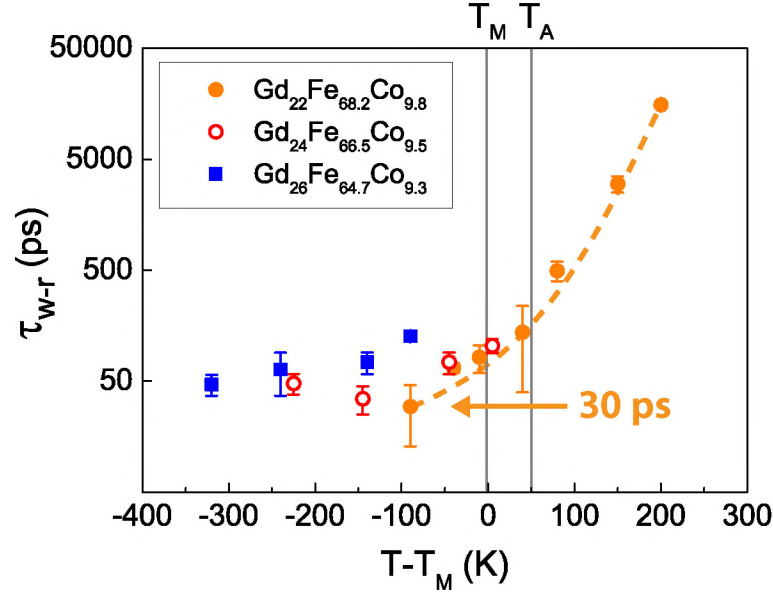


Figure 4.16: Write-read time τ_{w-r} versus relative temperature $T - T_M$ for $\text{Gd}_{22}\text{Fe}_{68.2}\text{Co}_{9.8}$ ($T_M = 100$ K), $\text{Gd}_{24}\text{Fe}_{66.5}\text{Co}_{9.5}$ ($T_M = 280$ K) and $\text{Gd}_{26}\text{Fe}_{64.7}\text{Co}_{9.3}$ ($T_M = 390$ K). We achieved magnetization reversal within 30 ps for $\text{Gd}_{22}\text{Fe}_{68.2}\text{Co}_{9.8}$ at 10 K [35]. The dashed line is a guide to the eye.

the simultaneous action of a strong and short heat pulse in connection with a pulse of magnetic field favors the magnetization to follow a so-called *linear* path, governed by longitudinal relaxation process. Experimentally such a two-fold action can be obtained using circularly-polarized laser pulses.

By examining, experimentally and computationally, the reversal process for various laser pulses we have shown that the helicity-dependent magnetization switching occurs in a narrow range of laser pulse fluences. Below this range the conditions for linear reversal are not satisfied, as the latter can occur only when the magnetization is nearly quenched [49]. Above this range, the degree of disorder brought to the spin system is too high and, thus, the strength and duration of the effective light-induced magnetic field are not sufficient for the reversal.

We have found that the all-optical reversal is feasible for a rather wide range of laser pulse durations up to 2100 fs. However, our experimental data and the proposed model suggest that there is an upper limit for the laser pulse duration required for the all-optical reversal. Based on our model, we expect that there should also be a lower limit. This, however, still has to be verified in future experiments with ultrashort

laser pulses.

The feasibility and the characteristics of the all-optical reversal process are also dependent on the magnetic properties of the GdFeCo alloys. Although the all-optical reversal can be observed above and below the compensation temperature of ferrimagnetic GdFeCo alloys, in the vicinity of T_M the reversal requires less laser pulse fluence. Moreover, the all-optical reversal disappears if the sample temperature is too high above the compensation temperature. These results suggest that the ferrimagnetic properties of the samples play a crucial role in the all-optical magnetization reversal. Consequently, development of comprehensive approaches for simulations of non-equilibrium spin dynamics in multi-sublattice magnets are urgently required.

We also demonstrated that the all-optical helicity-dependent magnetization reversal time is determined by the relaxation process from the strongly non-equilibrium state and by the mobility of the domain walls, in particular. This leads to a drastic decrease of the reversal time in the samples below their compensation temperature. Therefore, we expect that ferrimagnetic media with compensation points above room temperature are promising candidates for the realization of fast all-optical magnetic recording. We would like to mention that the achieved write-read time of 30 ps in one of the GdFeCo alloys (see Figure 4.16) is the shortest write-read time demonstrated for magnetic recording so far [35]. Moreover, our experimental studies and modeling suggest that this time can be reduced further by a proper tailoring of the magnetic and magneto-optical properties of recording medium.

As a concluding remark, we would like to stress that our study of the all-optical reversal in RE-TM alloys highlights the role of ferrimagnetism in the process. The write-read time depends dramatically on the difference between the sample temperature and the compensation point ($T - T_M$). Moreover, the experimental findings suggest that the ferrimagnetic structure of GdFeCo alloys also influences the features of linear reversal at ultrashort time scales. A further understanding how such a complex magnetic structure influences the ultrafast laser-induced spin dynamics will be a challenging task for both theoreticians and experimentalists. Development of models and theories capable of accounting for realistic interactions in a magnetic medium is required. For further experimental studies of the ultrafast dynamics in ferrimagnets, experiments with higher spatial and temporal resolution and with element specificity (to distinguish, for example, Gd from Fe and Co) will be desirable [59–61]. These studies are the main topic of Chapter 5.

References

- [1] J. Stöhr and H. C. Siegmann, *Magnetism: From Fundamentals to Nanoscale Dynamics* (Springer-Verlag, Berlin, 2006).
- [2] C. H. Back, R. Allenspach, W. Weber, S. S. P. Parkin, D. Weller, E. L. Garwin, and H. C. Siegmann, *Science* **285**, 864 (1999).
- [3] B. C. Choi, M. Belov, W. K. Hiebert, G. E. Ballentine, and M. R. Freeman, *Phys. Rev. Lett.* **86**, 728 (2001).
- [4] T. Gerrits, H. A. M. van den Berg, J. Hohlfeld, L. Bar, and T. Rasing, *Nature* **418**, 509 (2002).
- [5] S. Kaka and S. E. Russek, *Appl. Phys. Lett.* **80**, 2958 (2002).
- [6] I. Tudosa, C. Stamm, A. B. Kashuba, F. King, H. C. Siegmann, J. Stöhr, G. Ju, B. Lu, and D. Weller, *Nature* **428**, 831 (2004).
- [7] T. Devolder, A. Tulapurkar, Y. Suzuki, C. Chappert, P. Crozat, and K. Yagami, *J. Appl. Phys.* **98**, 053904 (2005).
- [8] Y. Acremann, J. P. Strachan, V. Chembrolu, S. D. Andrews, T. Tyliczszak, J. A. Katine, M. J. Carey, B. M. Clemens, H. C. Siegmann, and J. Stöhr, *Phys. Rev. Lett.* **96**, 217202 (2006).
- [9] A. Kimel, A. Kirilyuk, and T. Rasing, *Laser & Photon. Rev.* **1**, 275 (2007).
- [10] H. W. Schumacher, C. Chappert, P. Crozat, R. C. Sousa, P. P. Freitas, J. Militat, and J. Ferre, *IEEE Trans. Magn.* **38**, 2480 (2002).
- [11] J. C. Slonczewski, *J. of Magn. Magn. Mater.* **159**, L1 (1996).
- [12] A. Kashuba, *Phys. Rev. Lett.* **96**, 047601 (2006).
- [13] E. Beaurepaire, J.-C. Merle, A. Daunois, and J.-Y. Bigot, *Phys. Rev. Lett.* **76**, 4250 (1996).
- [14] B. Koopmans, M. van Kampen, J. T. Kohlhepp, and W. J. M. de Jonge, *Phys. Rev. Lett.* **85**, 844 (2000).
- [15] C. Stamm, T. Kachel, N. Pontius, R. Mitzner, T. Quast, K. Holldack, S. Khan, C. Lupulescu, E. F. Aziz, M. Wietstruk, et al., *Nature Materials* **6**, 740 (2007).
- [16] F. Dalla Longa, J. T. Kohlhepp, W. J. M. de Jonge, and B. Koopmans, *Phys. Rev. B* **75**, 224431 (2007).

-
- [17] C. Boeglin, E. Beaurepaire, V. Halte, V. Lopez-Flores, C. Stamm, N. Pontius, H. A. Durr, and J.-Y. Bigot, *Nature* **465**, 458 (2010).
- [18] M. Battiato, K. Carva, and P. M. Oppeneer, *Phys. Rev. Lett.* **105**, 027203 (2010).
- [19] M. S. Si and G. P. Zhang, *J. Phys.: Condens. Matter* **22**, 076005 (2010).
- [20] B. Koopmans, J. E. M. Haverkort, W. J. M. de Jonge, and G. Karczewski, *J. Appl. Phys.* **85**, 6763 (1999).
- [21] J.-Y. Bigot, L. Guidoni, E. Beaurepaire, and P. N. Saeta, *Phys. Rev. Lett.* **93**, 077401 (2004).
- [22] E. Beaurepaire, G. M. Turner, S. M. Harrel, M. C. Beard, J.-Y. Bigot, and C. A. Schmuttenmaer, *Appl. Phys. Lett.* **84**, 3465 (2004).
- [23] J. Gdde, U. Conrad, V. Jhnke, J. Hohlfeld, and E. Matthias, *Phys. Rev. B* **59**, R6608 (1999).
- [24] M. Aeschlimann, M. Bauer, S. Pawlik, W. Weber, R. Burgermeister, D. Oberli, and H. C. Siegmann, *Phys. Rev. Lett.* **79**, 5158 (1997).
- [25] A. Scholl, L. Baumgarten, R. Jacquemin, and W. Eberhardt, *Phys. Rev. Lett.* **79**, 5146 (1997).
- [26] L. Cywiski and L. J. Sham, *Phys. Rev. B* **76**, 045205 (2007).
- [27] N. Kazantseva, D. Hinzke, U. Nowak, R. W. Chantrell, U. Atxitia, and O. Chubykalo-Fesenko, *Phys. Rev. B* **77**, 184428 (2008).
- [28] G. Lefkidis, G. P. Zhang, and W. Hbner, *Phys. Rev. Lett.* **103**, 217401 (2009).
- [29] B. Koopmans, G. Malinowski, F. Dalla Longa, D. Steiauf, M. Fahnle, T. Roth, M. Cinchetti, and M. Aeschlimann, *Nature Materials* **9**, 259 (2010).
- [30] G. P. Zhang, Y. Bai, and T. F. George, *Phys. Rev. B* **80**, 214415 (2009).
- [31] V. N. Gridnev, *Phys. Rev. B* **77**, 094426 (2008).
- [32] A. Kirilyuk, A. V. Kimel, and T. Rasing, *Rev. Mod. Phys.* **82**, 2731 (2010).
- [33] C. D. Stanciu, F. Hansteen, A. V. Kimel, A. Kirilyuk, A. Tsukamoto, A. Itoh, and T. Rasing, *Phys. Rev. Lett.* **99**, 047601 (2007).
- [34] A. V. Kimel, A. Kirilyuk, P. A. Usachev, R. V. Pisarev, A. M. Balbashov, and T. Rasing, *Nature* **435**, 655 (2005).

-
- [35] K. Vahaplar, A. M. Kalashnikova, A. V. Kimel, D. Hinzke, U. Nowak, R. Chantrell, A. Tsukamoto, A. Itoh, A. Kirilyuk, and T. Rasing, *Phys. Rev. Lett.* **103**, 117201 (2009).
- [36] M. Mansuripur, *The Physical Principles of Magneto-Optical Recording* (Cambridge University Press, Cambridge, 1995).
- [37] X. Jiang, L. Gao, J. Z. Sun, and S. S. P. Parkin, *Phys. Rev. Lett.* **97**, 217202 (2006).
- [38] Y. Mimura, N. Imamura, T. Kobayashi, A. Okada, and Y. Koshiro, *J. Appl. Phys.* **49**, 1208 (1978).
- [39] C. D. Stanciu, A. V. Kimel, F. Hansteen, A. Tsukamoto, A. Itoh, A. Kirilyuk, and T. Rasing, *Phys. Rev. B* **73**, 220402 (2006).
- [40] H. Tsujimoto, M. Shouji, A. Saito, S. Matsushita, and Y. Sakurai, *J. Magn. Soc. Jpn.* **7**, 119 (1983).
- [41] N. Endo, S. Masui, T. Kobayashi, S. Tsunashima, and S. Uchiyama, *J. Magn. Soc. Jpn.* **8**, 101 (1984).
- [42] P. S. Pershan, *Phys. Rev.* **130**, 919 (1963).
- [43] H. Petek and S. Ogawa, *Prog. in Surf. Sci.* **56**, 239 (1997).
- [44] V. V. Kruglyak, R. J. Hicken, M. Ali, B. J. Hickey, A. T. G. Pym, and B. K. Tanner, *Phys. Rev. B* **71**, 233104 (2005).
- [45] D. J. Hilton, R. D. Averitt, C. A. Meserole, G. L. Fisher, D. J. Funk, J. D. Thompson, and A. J. Taylor, *Opt. Lett.* **29**, 1805 (2004).
- [46] M. I. Kaganov, I. M. Lifshitz, and L. V. Tanatarov, *Sov. Phys. JETP* **4**, 173 (1957).
- [47] G. Zhang, W. Hübner, E. Beaurepaire, and J.-Y. Bigot, *Spin Dynamics in Confined Magnetic Structures I, Topics in Applied Physics*, vol. 83 (Springer, New York, 2002).
- [48] D. A. Garanin, *Phys. Rev. B* **55**, 3050 (1997).
- [49] N. Kazantseva, D. Hinzke, R. W. Chantrell, and U. Nowak, *Europhys. Lett.* **86**, 27006 (2009).
- [50] R. Hertel, *Physics* **2**, 73 (2009).

-
- [51] M. Agranat, S. Anhitkov, A. Kirillin, V. Fortov, S. Anisimov, A. Granovskiĭ, and P. Kondratenko, *JETP Letters* **67**, 953 (1998).
- [52] M. B. Agranat, S. Ashitkov, A. Granovsky, and G. Rukman, *Zh. Eksp. Teor. Fiz.* **86**, 1376 (1984).
- [53] A. Vaterlaus, D. Guarisco, M. Lutz, M. Aeschlimann, M. Stampanoni, and F. Meier, *J. Appl. Phys.* **67**, 5661 (1990).
- [54] J. Hohlfeld, C. D. Stanciu, and A. Rebei, *Appl. Phys. Lett.* **94**, 152504 (2009).
- [55] We note that the decrease of F_{sw} with temperature in $Gd_{22}FeCo$, reported in [54], leads the authors to the conclusion that the all-optical reversal has an athermal character and does not involve the process of ultrafast laser-induced demagnetization. Our results clearly show that the observed behavior is only typical for samples above the compensation temperature T_M .
- [56] T. Miyama, S. Matsushita, H. Tsujimoto, and Y. Sakurai, *IEEE Trans. Magn.* **14**, 728 (1978).
- [57] R. Weng and M. Kryder, *IEEE Trans. Magn.* **29**, 2177 (1993).
- [58] V. Randoshkin, V. Polezhaev, N. Sysoev, and Y. Sazhin, *Physics of the Solid State* **45**, 513 (2003), 10.1134/1.1562240.
- [59] S. Eisebitt, J. Luning, W. F. Schlotter, M. Lorgen, O. Hellwig, W. Eberhardt, and J. Stohr, *Nature* **432**, 885 (2004).
- [60] B. Koopmans, *Nature Materials* **6**, 715 (2007).
- [61] C. Gutt, S. Streit-Nierobisch, L.-M. Stadler, B. Pfau, C. M. Günther, R. Könnecke, R. Frömter, A. Kobs, D. Stickler, H. P. Oepen, et al., *Phys. Rev. B* **81**, 100401 (2010).

Element-specific studies of ultrafast magnetization reversal in ferrimagnetic GdFeCo alloys¹

5.1 Introduction

Since the first observation of ultrafast demagnetization in a Ni film subjected to 60 fs laser pulses [1], processes triggered by such ultrashort pulses in magnetic matter have become an issue of intensive theoretical and experimental investigations [2, 3]. Since then it became commonly accepted that processes in magnetically ordered media excited by femtosecond laser pulses constitute a complex interplay between the dynamics of spins, electrons and lattice, with distinct characteristic times and various strengths of cross-interactions. More specifically, the transfer of energy and angular momentum between these three reservoirs required for the ultrafast demagnetization became one of the most debated topics in modern magnetism [4–8]. Attempts to resolve these issues yielded a burst in the development of various experimental [5, 9–11] and theoretical [12–15] approaches to the studies of spin dynamics on the pico- and subpicosecond time scales.

Within these developments, the dynamics of the magnetization, which is sensitive to the polarization of the laser pulses, attracted considerable interest. On the one hand, it was demonstrated that a fs laser pulse can act as the equivalent of a magnetic

¹Adapted from: I. Radu, K. Vahaplar, C. Stamm, T. Kachel, N. Pontius, H. A. Dürr, T. A. Ostler, J. Barker, R. F. L. Evans, R. W. Chantrell, A. Tsukamoto, A. Itoh, A. Kirilyuk, Th. Rasing, and A. V. Kimel, *Nature* **472**, 205–208 (2011).

field pulse of remarkably high amplitude [2, 16–18] and a direction controlled by the polarization of the laser pulse. On the other hand, the characteristics of this light-induced effective field go beyond the properties of ordinary magnetic fields [19] and, thus, allow new types of magnetic excitations [20], including *all-optical* reversal of the magnetization in a thin metallic ferrimagnetic film by a single circularly polarized laser pulse [21]. However, due to the complexity of the physics of the elementary processes occurring in the magnetic medium during and after the excitation with an ultrashort laser pulse, the only conclusion which was drawn about the mechanism of the all-optical reversal was that it involves both, ultrafast demagnetization and a non-thermal, i.e. polarization-dependent, impact of the fs laser pulse on the magnetic medium.

As it was discussed in the previous chapter, using a novel experimental approach to study the all-optical reversal, we were able to identify the time required for the switching of the magnetization by a single femtosecond laser pulse [22]. Moreover, performing recently developed multiscale modeling [13] we proposed that the mechanism of the reversal has a linear character. In other words, this mechanism is not based on precession, as does the conventional switching in a magnetic field [23, 24] or spin-polarized current [25–27], but involves ultrafast laser induced demagnetization combined with a light-induced effective field. We showed that in GdFeCo alloys the compensation temperature T_M plays a major role in the switching speed of the magnetization and has a significant effect on such parameters as the fluence required for helicity-dependent switching and the speed of the reversal. Aeschlimann *et al.* reported already in the early 1990's that at a temperature $T < T_M$, laser excitation in an external dc magnetic field can reverse the magnetization by increasing the temperature above T_M [28, 29]. In 2001, Hohlfeld *et al.* also investigated the fast magnetization reversal induced by femtosecond laser pulses in GdFeCo alloys [30]. In the presence of an external magnetic field with a strength smaller than the coercive field, femtosecond laser excitation was followed by a subpicosecond demagnetization and a slow recovery of the magnetic order with the magnetization reversed. Moreover, it was demonstrated that an ultrafast laser-induced heating of the GdFeCo ferrimagnetic system over its compensation point under an applied magnetic field results in a subpicosecond magnetization reversal [31, 32].

Based on these studies, an understanding of ultrafast magnetization dynamics and revealing the switching speed of the magnetization are crucial to identify the processes responsible for high speed magnetization reversal in such systems. Although it is well known that exchange interaction, being the strongest force in magnetism, is responsible for ferromagnetic or antiferromagnetic spin ordering [33–35], virtually nothing is known about the behavior of spins in a magnetic material immediately after being excited on a time scale faster than that corresponding to the exchange interaction ($\sim 10 - 100$ fs), i.e. in a non-adiabatic way. To study this transient regime of spin dynamics where novel coupling phenomena can emerge, one faces two challenges: 1)

How to probe the response of one magnetic moment relative to another and 2) How to bring the moments out of equilibrium on a time scale corresponding to the exchange interaction? In order to identify the magnetic contribution of each element in such systems, replacing the optical probe with X-rays offers a great opportunity to obtain element-specific information by using X-ray magnetic circular dichroism (XMCD).

This chapter is organized as follows: first we describe our studies of the optically induced ultrafast spin dynamics and magnetization reversal in the rare earth - transition metal ferrimagnetic alloy GdFeCo. The measurements were performed using an all-optical pump-probe technique, which was described in Section 3.3.2. Second, we will focus on the time- and element-resolved XMCD measurements, where we used a laser pump – X-ray probe technique to probe the magnetic response of one element relative to another.

5.2 Switching over the compensation point

Since the GdFeCo ferrimagnetic amorphous alloys exhibit a high perpendicular uniaxial anisotropy and a large MO effect, they have been extensively used as the storage layer in magneto-optical storage media [36]. For the experiments, a thin film of ferrimagnetic GdFeCo alloy with a thickness of 20 nm was prepared by magnetron sputtering in the following multilayer structure: glass | AlTi(10 nm) | SiN(5 nm) | GdFeCo (20 nm) | SiN(60 nm). As described in details in Section 4.2, by tuning the composition of the ferrimagnet, magnetic properties, such as compensation temperature (T_M) and Curie point (T_C), can be changed in RE-TM alloys. The composition effect for various GdFeCo alloys can be seen in Figure 4.1(b) in Section 4.2. The sample composition analyzed in this work was $\text{Gd}_{26}\text{Fe}_{64.7}\text{Co}_{9.3}$. As it is shown in Figure 5.1, extracting the coercive field H_c values from the hysteresis loops, we defined $T_M \approx 390$ K and $T_C \approx 550$ K. The inset plots show that the hysteresis loops change sign as one passes T_M from one side to the other (see hysteresis loops in Figure 5.1 below and above the magnetization compensation temperature). The magnetization easy axis is perpendicular to the sample surface.

The analysis of the magnetization dynamics has been performed at ambient temperature, below T_M , with an amplified Ti:Sapphire laser system, generating 50 fs linearly-polarized pulses with 800 nm (1.54 eV) wavelength. The repetition rate of the pulses is 1 kHz. The dynamics investigations have been carried out via a pump-probe technique with the pump beam focused to a spot size of a few hundreds of μm and an average fluence of a few mJ/cm^2 . The ratio of pump to probe in the fluence was around 100. The pump beam was at normal incident whereas the probe beam was incident at a small angle of 10° with respect to the normal and focused onto the same spot as the pump, with a spot size of at least less than half the one of the pump. In order to study magnetization dynamics in our sample, we employed pump pulses that change the magnetic system by heating across the compensation point

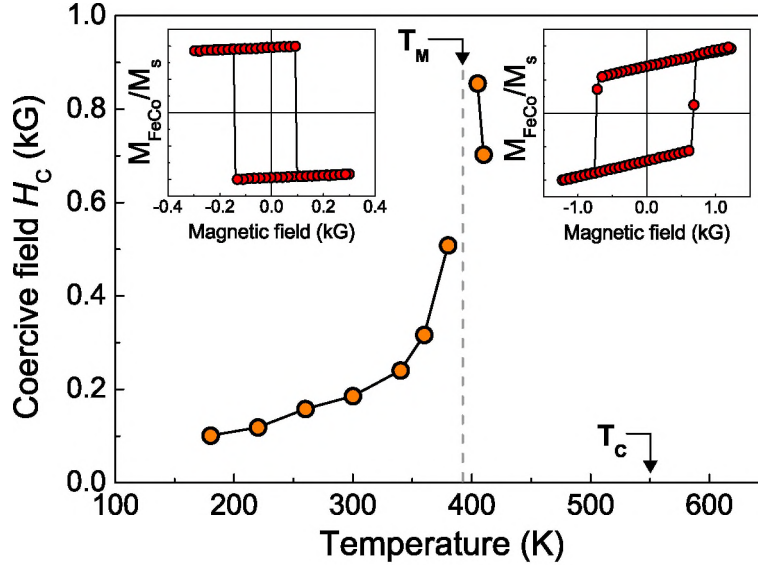


Figure 5.1: The coercive field H_c as a function of temperature in $\text{Gd}_{26}\text{Fe}_{64.7}\text{Co}_{9.3}$ alloy. The divergence of H_c indicates the magnetization compensation temperature at $T_M = 390$ K. The inset hysteresis plots show magneto-optical hysteresis loops below and above T_M , indicating the behavior of FeCo sublattice.

T_M , by altering the equilibrium direction of the magnetization. In the experiments a magnetic field $H_{\text{ext}} \sim 0.5$ kG larger than the coercive field H_c at ambient temperature was applied to initialize the magnetic state after each pump pulse.

The pump fluence dependence of the ultrafast laser-induced magnetization reversal and recovery dynamics of GdFeCo films were studied experimentally. The dynamic magnetization processes are shown in Figure 5.2 for different pump fluences. For the excitations with fluences lower than 0.34 mJ/cm^2 , the heating by the femtosecond pump pulse leads to a change in the magnitude of the magnetization, indicating the ultrafast demagnetization [37, 38]. The larger pump fluences increase the transient signal and consequently the demagnetization ratio increases. Additionally, the magnetization recovery process to the initial state becomes slower as the pump fluence increases, shown in Figure 5.2. However, for pump fluences higher than 0.34 mJ/cm^2 , the magnetic system first relaxes in the opposite direction. Note that, at a longer time scale (> 1 ns) the system cools down back to the initial magnetic state. The occurrence of this relaxation in the opposite direction originates from the sample temperature rising over T_M [31, 39, 40]. Since the applied magnetic field is larger than the coercive field of the sample, $H_{\text{ext}} > H_c$, below T_M , following cooling down, the re-

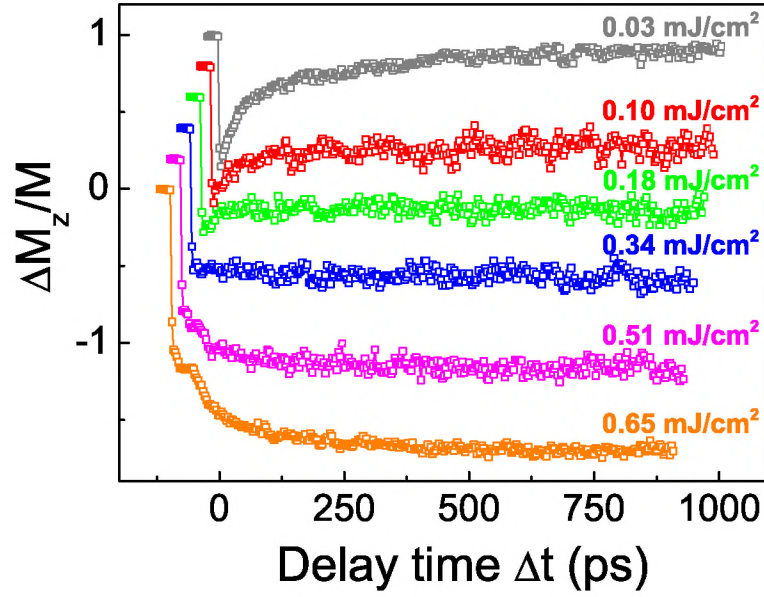


Figure 5.2: The pump fluence dependence of ultrafast laser-induced magnetization recovery and reversal dynamics in $\text{Gd}_{26}\text{Fe}_{64.7}\text{Co}_{9.3}$ alloy. For clarity, the data are offset.

versed magnetization will switch back to the initial state for each pump pulse. It can be also clearly seen that the degree and the rate of the magnetization reversal increase with pump fluence, revealing the nucleation and growth of the reversed domain.

In order to determine the time of reversal across T_M , we measured the magnetization dynamics at short time scales for the pump fluence of 0.65 mJ/cm^2 , where the system first switches and then returns to the initial state. As one can see from Figure 5.3, the signal changes sign after $\sim 800 \text{ fs}$, which agrees with the time Stanciu *et al.* measured [31]. This observation reveals that laser-induced magnetization reversal across T_M is indeed faster than that across T_C . Note that the Faraday rotation signal here reflects mainly the net magnetization of the transition metal (TM) atoms in GdFeCo . Therefore, this sign change of the transient rotation signal indicates the switching of the transition metal (FeCo) sublattice direction along the applied magnetic field. Since the response time of the Gd sublattice has not been studied so far, it is an interesting question if Gd also follows such an ultrafast reorientation of its magnetization.

Recently, it has been reported that laser pulses excite only the TM moment, which is mostly carried by the spin-split $3d$ band near the Fermi level, while Gd does not exhibit an orbital momentum in the $4f$ shell, which is half full [41]. Using an X-ray

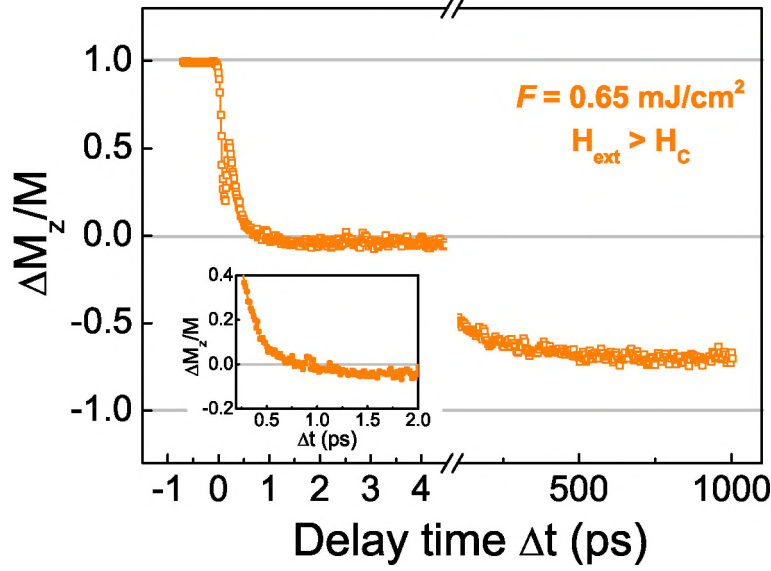


Figure 5.3: The laser-induced magnetization reversal dynamics in $\text{Gd}_{26}\text{Fe}_{64.7}\text{Co}_{9.3}$ alloy for a pump fluence of 0.65 mJ/cm^2 . The magnetic system first switches and recovers in the opposite direction, then cools down back to the initial magnetic state. The inset shows the magnetization change on a shorter time scale.

streak camera with the time resolution of 2.5 ± 0.5 ps, Bartelt *et al.* [42] demonstrated a simultaneous demagnetization time for Fe (1.9 ± 0.5 ps) and Gd (2.2 ± 0.6 ps). Furthermore, a faster demagnetization time of 0.76 ± 0.25 ps has been observed by Wietstruk *et al.* for Gd [43]. Comparing these ultrafast processes, one can notice that the demagnetization time in $4f$ rare earth elements is slower than in $3d$ transition metals [1, 5, 15, 44] and it should be noted that these laser-induced demagnetization experiments rely on crossing the Curie point T_C . Alternatively, crossing the magnetization compensation point T_M by a laser-induced heating might allow us to investigate the magnetization dynamics in a fundamentally different regime.

What would be the relative response of the spins of the two sublattices in a antiferromagnetically ordered material if the coupled spins are excited on a time scale comparable with the characteristic time of their exchange interaction? To answer this question, in the next section we study the magnetization dynamics of the two sublattices in the ferrimagnetic alloy GdFeCo by using advanced experimental (femtosecond optical excitation combined with ultrafast X-ray measurements) and computational (localized atomistic spin model) approaches.

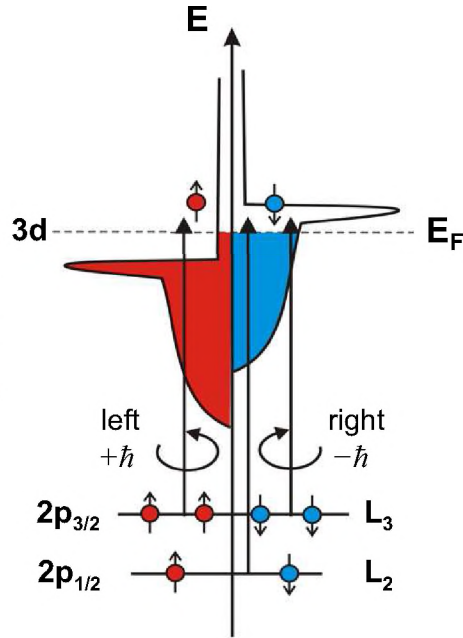
5.3 Nonequilibrium spin dynamics of magnetic sublattices in ferrimagnetic GdFeCo alloy

Probing the relative response of exchange coupled spins that are excited on a time scale that is equivalent to their exchange interaction energy is a great challenge for the research in magnetism and magnetic ordering. Ferrimagnetic materials are ideal candidates to address this challenge. First, in contrast to elementary ferromagnets, such as Fe, Ni or Co, and typical antiferromagnets like NiO, where all the spins are equivalent, ferrimagnets consist of two (or more) non-equivalent and antiferromagnetically coupled spin sublattices [45]. This non-equivalence of the sub-lattices in combination with an element-specific detection technique like X-ray Magnetic Circular Dichroism (XMCD) allows one to “colour” spins in the magnet and to probe the response of one moment relative to another. Second, ultrafast heating of a ferrimagnet over its compensation point in an external magnetic field allows the initiation of the fastest spin reversal reported so far [28, 31]. The simplest ferrimagnet, consisting of two collinear magnetic sublattices, may possess magnetization and angular momentum compensation temperatures denoted as T_M and T_A , respectively. A small difference between the gyromagnetic ratio of the two sublattices leads to an angular momentum compensation point T_A slightly above T_M [46]. At T_A no angular momentum is associated with the magnetization which can thus be moved by the slightest torque. Therefore spin dynamics in the vicinity of T_A may become infinitely fast [45, 47]. As it has been experimentally demonstrated in the previous section, heating the ferrimagnetic Gd(FeCo) alloy with sub-picosecond laser pulses triggers the reversal of the FeCo-sublattice within 800 fs. Looking at the Gd sublattice during ultrafast spin reversal of the antiferromagnetically coupled FeCo sublattice would thus be a promising approach to generate and study a state with decoupled behavior and different dynamics of the two sublattices.

5.3.1 X-ray magnetic circular dichroism (XMCD)

In 1975, the first theoretical investigation of X-ray magnetic dichroism (XMD) was done by Erskine and Stern [48] who performed a band structure calculation and predicted a XMD at the $M_{2,3}$ absorption edges of ferromagnetic nickel. Unfortunately, no serious attempts were made to check this theory experimentally over the next 10 years. Thole *et al.* [49] reported in 1985 strong predictions which concluded the existence of quite significant XMD at the $M_{4,5}$ edges of magnetic rare-earth materials. They showed that the magnitude and the orientation of the local rare-earth magnetic moments can be determined efficiently by using the polarization vector of X-rays. One year later, the first experimental evidence was given by van der Laan *et al.* [50] who measured a strong XMD at the Tb $M_{4,5}$ absorption edges in the ferrimagnetic terbium iron garnets by using linearly polarized synchrotron radiation.

Figure 5.4: Schematic illustration of X-ray magnetic circular dichroism (XMCD) in a generic band structure for a $3d$ ferromagnet. In the first step, spin-polarized photoelectrons are generated by circularly polarized X-rays. In the second step, the polarized photoelectrons are detected by the spin-split valence band.



Shortly later, the existence of X-ray magnetic circular dichroism (XMCD) was first proposed experimentally by G. Schütz *et al.* [51] in 1987 as the difference in absorption between left- and right-handed circularly polarized X-rays at the K edge in an Fe foil. Chen *et al.* measured in 1990 larger XMCD effects at the $L_{2,3}$ edges of Ni [52], Co, and Fe [53]. In 1998, a detailed understanding of the presence of circular dichroism in the X-ray absorption spectra in magnetic elements was described by J. Stöhr and R. Nakajima [54]. It was shown that in the soft X-ray region, XMCD is able to distinguish the magnetic contributions of different atoms in complex elements. Therefore, XMCD has been widely used in the last 10 years to improve the understanding of magnetism further in thin transition metals, rare-earths, and multilayer structures.

In principle, this method is very similar to the magneto-optical Kerr or Faraday effects, but with higher energy X-rays and can be explained with a simple two-step model, as illustrated in Figure 5.4 (for $3d$ transition metals). In the first step, a circularly polarized X-ray photon that carries an angular momentum ($+\hbar$ for right-handed photons and $-\hbar$ for left-handed photons) transfers its angular momentum to a core electron from the $2p$ level depending on the edge (L_3 or L_2) [55]. These edges are separated by the spin-orbit coupling energy and they are denoted by capital letters depending on the principal quantum numbers and core level involved (see Figure 5.4). Since the $p_{3/2}$ (L_3) and $p_{1/2}$ (L_2) levels have opposite spin-orbit coupling ($j = l + s$ and $j = l - s$, respectively), the spin polarization will be opposite at the two edges.

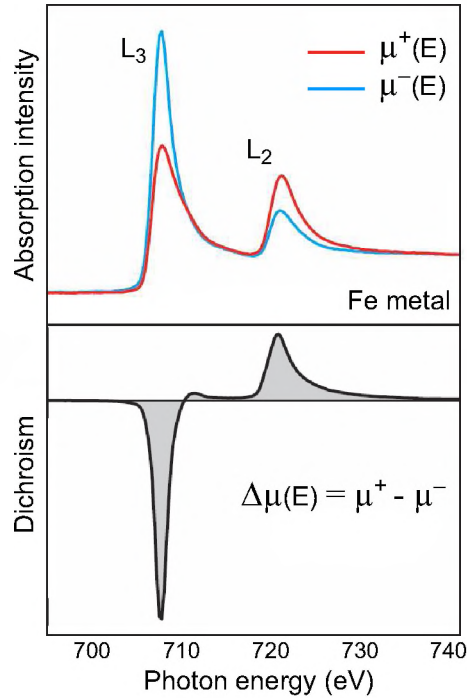


Figure 5.5: X-ray magnetic circular dichroism (XMCD) spectrum for L_3 and L_2 edges of Fe. Circularly polarized X-rays are aligned parallel or antiparallel to the magnetization direction of the medium [55].

As can be seen from Figure 5.4, according to the optical selection rules, left-handed circularly polarized photons ($+\hbar$) excite spin-up photoelectrons, whereas spin-down photoelectrons are created by right-handed circularly polarized photons ($-\hbar$).

In the second step, any imbalance in either spin or orbital momentum in the final states will immediately give rise to a dichroic effect [56]. The absorption of circularly polarized X-rays are a probe for the magnetic properties of the unoccupied density of states of a magnetic medium, where spin and orbital contributions can be detected separately from each other. In other words, the spin-split valance band acts as a sensitive “*spin-detector*” of the spin-polarized photoelectrons. The maximum dichroism effect is observed if the photon spin direction and the magnetization direction are parallel or antiparallel², as shown in Figure 5.5 [57–62]. In this case, due to the spin conservation, the photoelectrons excited from $2p_{3/2}$ by spin-down photons probe mostly the spin-down states above the Fermi level. Therefore, the absorption of right-handed circularly polarized X-rays ($-\hbar$) will be enhanced at the L_3 edge and reduced

²Circularly polarized light can be thought of carrying an angular momentum of $l = 1$ directed along the k -vector. Left-handed circularly polarized light carries an axial angular momentum equal $+1$, while right-handed circularly polarized light has -1 .

at the L_2 edge. The opposite effect occurs for left-handed circularly polarized X-rays ($+\hbar$). From the combinations of the measured L_3 and L_2 dichroism intensities and the total absorption spectra, the spin and orbital moments of the final-state can be directly determined [63, 64]. Thus, the XMCD effect of a magnetic medium can be obtained as the difference between two absorption spectra measured with left- and right-handed circularly polarized X-rays, or equivalently as the difference between two spectra measured with fixed helicity of X-rays and opposite directions of external magnetic field. This is defined as:

$$\Delta\mu(E) = \mu^+(E) - \mu^-(E). \quad (5.1)$$

where $\mu^+(E)$ and $\mu^-(E)$ are the absorption coefficients which denote the absorption as a function of photon energy for right- and left-handed circularly polarized X-rays, respectively. Time- and element-resolved XMCD measurements can be performed with an experimental design similar to that of an all-optical pump-probe experiment. Polarized X-ray pulses are used as the probe to study magnetization dynamics with element-specificity [5, 65].

5.3.2 Experimental details

Our sample was an amorphous ferrimagnetic 30 nm $\text{Gd}_{25}\text{Fe}_{65.6}\text{Co}_{9.4}$ thin film deposited by magnetron sputtering on a free-standing Al foil of 500 nm thickness, as described in Section 2.3. To avoid oxidation of the GdFeCo layer, Si_3N_4 films of 100 nm and 60 nm thickness were used as buffer and capping layers, respectively. In this medium, Gd and FeCo represent two antiferromagnetically coupled collinear magnetic sublattices [66]. The presence of Co in the GdFeCo alloy leads to a stronger out-of-plane magnetic anisotropy and to larger coercive fields (see Section 2.2). The latter ones are necessary to have a well defined initial and final magnetic state during the pump-probe cycles in the time-resolved XMCD measurements.

In order to probe independently the magnetizations of the two sublattices, we employed the element-specific XMCD technique. Soft X-ray light covering the $L_{2,3}$ absorption edges of Fe and Co and the $M_{4,5}$ edges of Gd has been employed to measure the magnetic response of the elements in the composite alloy. Static and dynamic XMCD measurements have been performed in transmission for opposite orientations of the external magnetic field (± 0.5 T) and at a fixed X-ray light helicity. As in the experimental setup shown in Figure 5.6, the magnetic field is oriented perpendicular to the sample and parallel with the X-ray propagation direction. The element-specific hysteresis curves have been recorded by setting the X-ray photon energy at the maximum absorption edge (L_3 edge of Fe and M_5 edge of Gd) and sweeping the external magnetic field between ± 0.5 T.

A typical data set of XMCD spectra measured at Fe and Gd edges as the sample is thermally driven through the compensation temperature (here $T_M = 300$ K) is shown

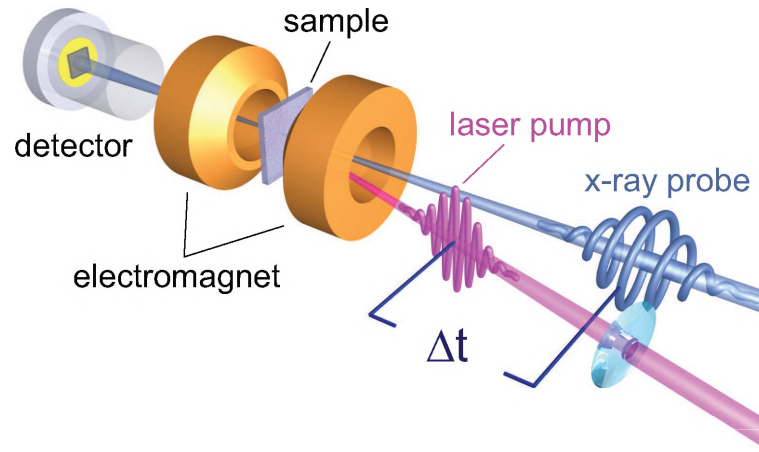


Figure 5.6: Scheme of the experimental setup for time- and element-resolved X-ray magnetic circular dichroism (XMCD). The X-ray light with a fixed helicity is directed perpendicular to the sample normal. The magnetic field (± 0.5 T) is oriented parallel with the X-ray propagation direction. There is ~ 1 degree angle between X-ray and the visible laser beam. This maintains the time resolution of the measurements down to the intrinsic pulse duration of the X-ray pulse.

in Figure 5.7. We observe clearly the antiferromagnetic coupling of Fe and Gd and the sign change of XMCD upon crossing the compensation point T_M [67].

The out-of-plane magnetic anisotropy of GdFeCo samples has been deduced from the measured element-specific hysteresis curves. As it is shown in Figure 5.8, the measured hysteresis curves show an antiferromagnetic alignment of Fe and Gd magnetic moments. Similar coercive fields are measured at the Co edge compared to both Fe and Gd as the sample is thermally driven through the magnetization compensation point. Below the magnetization compensation temperature $T_M = 250$ K, the magnetization of the Gd sublattice is larger than that of Fe and in an external magnetic field the Gd-sublattice is aligned along the field (see drawings at the bottom of Figure 5.8). Above $T_M = 250$ K, the magnetization of Gd is smaller than that of Fe and the spin system favours anti-parallel orientation of Gd with respect to the external magnetic field. The angular momentum compensation temperature T_A occurs at a temperature of about 50 K above T_M [66]. The exchange interaction between the sublattices is so strong that both sublattices have the same Curie temperature of ~ 550 K.

In the time-resolved experiments, we photo-excite electrons of the hybridized Fe $3d$ and Gd $5d6s$ bands with 60 fs laser pulses at a photon energy of 1.55 eV. A schematic drawing of the excitation mechanism is shown in Figure 5.9. The binding energy of the

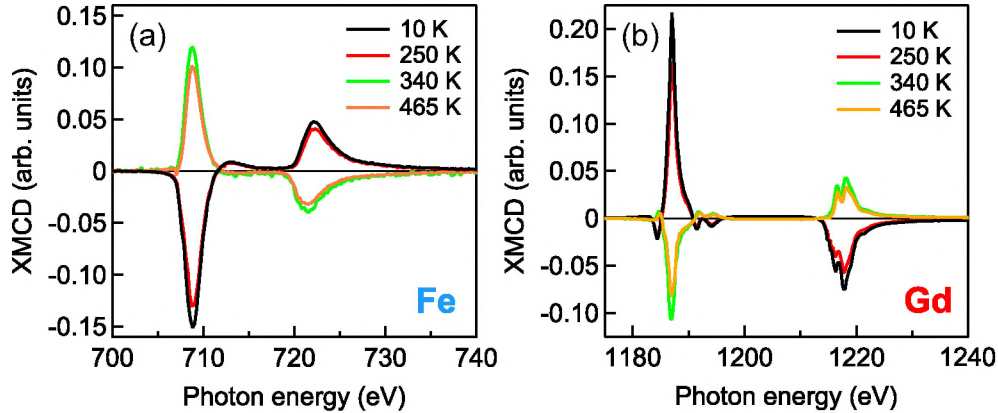


Figure 5.7: XMCD spectra of Fe and Gd as a function of temperature. XMCD spectra measured at Fe and Gd edges as a function of temperature for a sample with magnetization compensation point at $T_M = 300$ K. The XMCD polarity change appears upon crossing T_M [67].

occupied spin-up $4f$ state is around 9 eV, that is, much larger than the energy of the photons in the pump. Subsequent laser-induced dynamics is probed by measuring the magnetization-dependent absorption of circularly polarized 100 fs X-ray pulses at the Fe- L_3 absorption edge (photon energy 707 eV) and at the Gd- M_5 edge (photon energy 1189 eV). At these energies we probe the dynamics of the $3d$ magnetic moment of Fe and the $4f$ moment of Gd. Varying the delay between the pump and probe pulses, we were able to perform an element specific study of the laser-induced magnetic changes with sub-picosecond temporal resolution. The measurements were performed at the femto-slicing facility [5, 68–70] at BESSY II [71], which provides femtosecond soft X-ray pulses with variable polarization (see Section 3.5).

The laser-induced changes of X-ray transmission were measured for opposite orientations of the magnetic field using an avalanche photodiode (APD) and a gated boxcar detection [5, 69, 70]. Thereby, we were able to measure the time evolution of the pumped (in the presence of laser excitation) and un-pumped (in absence of laser excitation) signals. From the transmission changes measured for opposite magnetic fields we obtained the absorption changes and from the difference of the latter ones the dynamic XMCD curves. The typical size of the laser beam in focus was 0.8×0.4 mm².

The energy resolution of the time-resolved XMCD experiment is ~ 5 eV, which means that the measured transient XMCD signal is essentially integrated over the entire absorption edge, that is, over all available final states for the X-ray transitions. The moderate laser fluence used in the experiment together with the above argument

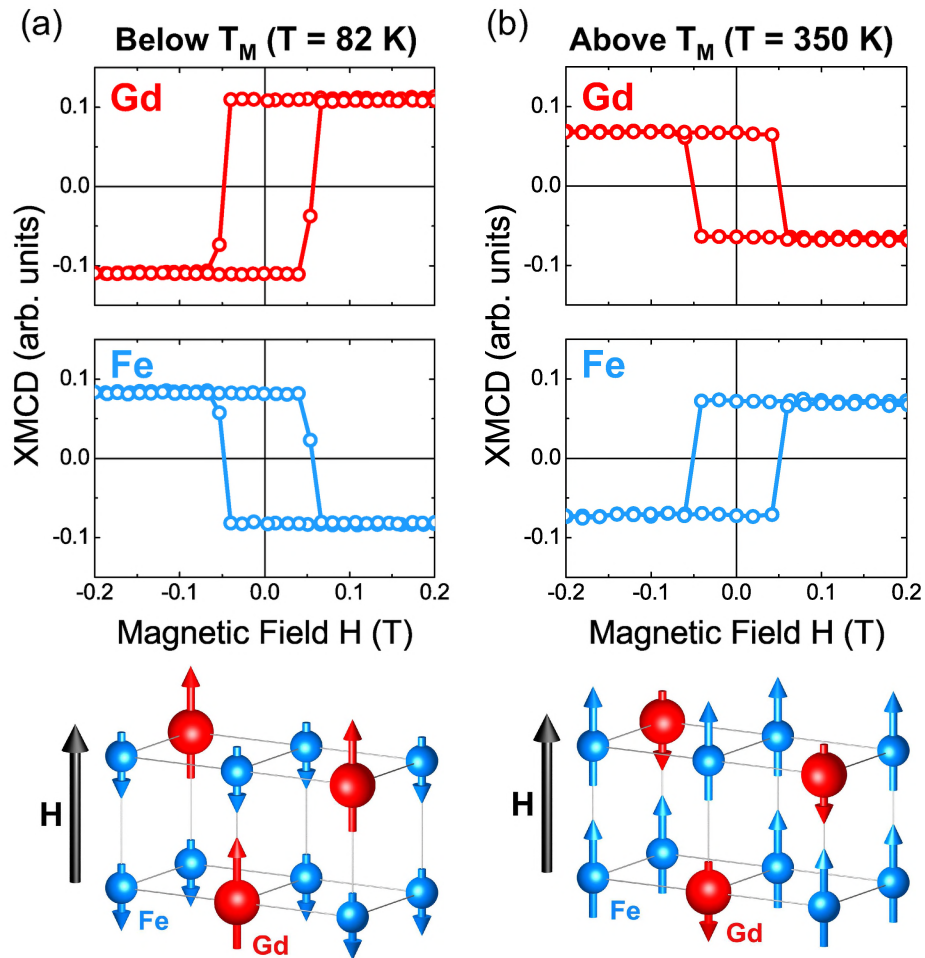
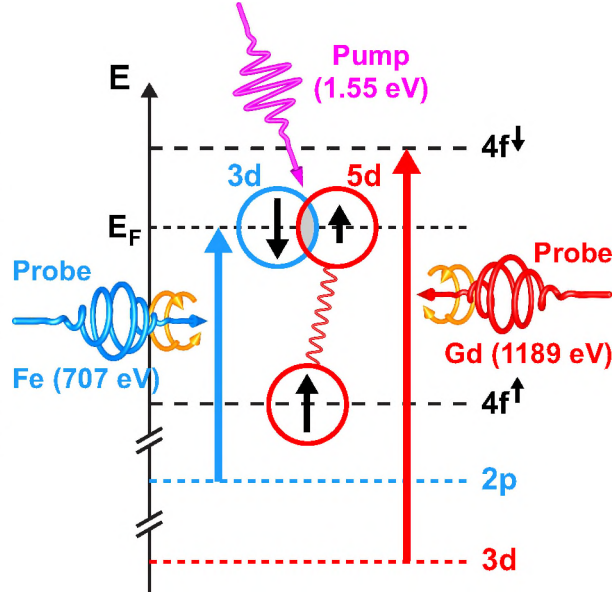


Figure 5.8: Ferrimagnetic alignment of the Fe and Gd magnetic moments as measured by element-specific XMCD hysteresis. (a,b) Top, XMCD signals measured at the Fe and Gd absorption edges as a function of applied magnetic field (a) below and (b) above the magnetization compensation point (T_M), demonstrating the ferrimagnetic alignment of the Fe and Gd magnetic moments. (a,b) Bottom, a generic ferrimagnet showing the alignment of the magnetic moments of the constituent sub-lattices with respect to the external magnetic field, H [67].

Figure 5.9: Pumping and probing mechanism in the schematic electronic structure of GdFeCo alloy. For Fe, spin polarized electrons are excited at the $2p$ level with a polarization depending on the edge (L_3 or L_2) and on the polarization of the light. The d band then acts as a spin detector, depending on the number of available empty states of a given spin. The same mechanism occurs in Gd for $3d \rightarrow 4f$ states depending on the edge (M_4 or M_5) [67].



lead us to conclude that optical bleaching effects are highly unlikely.

5.3.3 Theoretical methods

The localized atomistic spin model

In this section, we will present theoretical investigations of the dynamics of a spin system in a strongly nonequilibrium state by using the localized atomistic spin model. The underlying equation governing the magnetization dynamics is the Landau-Lifshitz-Gilbert (LLG) equation with Langevin dynamics. In the latter approach, the electron temperature is estimated from a two-temperature model calculation and the electrons are assumed to act as heat bath for the spin system [72]. Regarding the experiments, Langevin dynamics is responsible for reproducing the rapid decrease of the magnetization:

$$\frac{\partial \mathbf{S}_i}{\partial t} = -\frac{\gamma_i}{(1 + \lambda_i^2)\mu_i} \left\{ \mathbf{S}_i \times \left[\mathbf{H}_i(t) + \lambda_i (\mathbf{S}_i \times \mathbf{H}_i(t)) \right] \right\}. \quad (5.2)$$

Here S_i is the atomic localized spin at the atomic site i , which is normalized to unity. γ_i is the gyromagnetic ratio associated with the spin at site i , μ_i is the magnetic moment associated with each species, and λ_i is a microscopic damping parameter, which couples the spin system to the heat bath. \mathbf{H}_i is the effective field at each site

determined by our Hamiltonian, which we choose to be of the generic Heisenberg form, given by:

$$\mathcal{H} = - \sum_{\langle ij \rangle} J_{ij} (\mathbf{S}_i \cdot \mathbf{S}_j) - K \sum_i (S_i^z)^2 - \sum_i \mu_i \mathbf{B} \cdot \mathbf{S}_i. \quad (5.3)$$

where J_{ij} is the exchange integral between neighboring spins, K is the anisotropy energy constant, which we assume to be uniaxial and is 0.807243×10^{-23} J/spin, which is large enough to support a perpendicular magnetization. The \mathbf{B} is the applied magnetic field. The on-site effective field is then given by:

$$\mathbf{H}_i = - \frac{\partial \mathcal{H}}{\partial \mathbf{S}_i}. \quad (5.4)$$

which leads to the expression for the fields:

$$\mathbf{H}_i = \sum_{ij} \mathbf{S}_j + K S_i^z + \mu_i \mathbf{B}. \quad (5.5)$$

This field must be evaluated for each spin at each step of the numerical integration. The damping term in the LLG equation allows for dissipation of energy away from the spin system. We augment the effective field using a stochastic term included into the effective field to mimic thermal fluctuations. This allows for heat to flow into the spin system. The correlator, with stochastic term ζ_i , is given by:

$$\langle \zeta_i^a(t) \zeta_j^b(t') \rangle = 2 \delta_{ij} \delta_{ab} \delta(t - t') \frac{\lambda_i k_B T_e \mu_i}{\gamma_i \Delta t}. \quad (5.6)$$

In the model we assume that GdFeCo is a two sub-lattice system, with FeCo being described by a generic transition metal (TM) and Gd described by rare earth (RE). Experimentally GdFeCo is amorphous, which is extremely difficult to characterize fully. However, we can make a simplification in the model by assuming that we have a fixed face centered cubic (fcc) lattice. The fcc lattice is then populated randomly with TM species and RE species to mimic the amorphous nature of the system. The exchange constants were obtained by fitting static XMCD data for the Fe and Gd sublattices, the values are stated per link and do not take into account the number of neighbors of each species. They were $J_{\text{Fe-Fe}} = 2.835 \times 10^{-21}$ J/link, $J_{\text{Gd-Gd}} = 1.260 \times 10^{-21}$ J/link (corresponding to the Curie temperature of bulk Gd) and $J_{\text{Fe-Gd}} = -1.09 \times 10^{-21}$ J/link. Taking into account the number and type of neighbors, the effective Fe-Fe exchange is 1.96×10^{-20} J per spin (~ 35 fs), the Gd-Gd effective exchange is 8.72×10^{-22} J per spin (~ 760 fs) and the Fe-Gd effective exchange is 4.77×10^{-20} J per spin (~ 140 fs). The gyromagnetic ratios of each species were set to adjust the angular momentum compensation point ($T_A = 283$ K) above the magnetization compensation point ($T_M = 250$ K), $\gamma_{\text{TM}} = 1.05\gamma$ and $\gamma_{\text{RE}} = 1.00\gamma$, with

$\gamma = 1.76 \times 10^{11} \text{ T}^{-1}\text{s}^{-1}$. The number of spins in the simulations is 500.000 in a cubic structure with periodic boundary conditions on all sides as the samples used are much larger than that simulated. The spins are equilibrated before the application of any temperature to ensure that the magnetization is at equilibrium. Following Ref. [72] we couple the spin system to the electron temperature that is calculated using the so-called *two-temperature model* [73] [see Eqs. (4.4a, 4.4b) in Section 4.3.2]. To focus on the magnetic properties, the model assumes the same electron temperature and the same damping constants for Gd and Fe ($\lambda_{\text{TM}} = \lambda_{\text{RE}} = 0.05$) [67].

5.4 Results and discussion

We have confirmed from the static XMCD measurements that XMCD serves as an element specific probe of spins in this GdFeCo ferrimagnetic alloy (see Figure 5.8). In order to trigger ultrafast spin dynamics in this alloy, we initiated the reversal of the magnetizations of the two sublattices by ultrafast heating the sample over T_{M} using a linearly polarized 60 fs laser pulse with photon energy of 1.55 eV. As was described in Section 5.3.2, the dynamics of the Fe and Gd magnetic moments were independently probed using 100 fs soft X-ray pulses. Figure 5.10 shows the results of time-resolved measurements of the dynamics of the Fe and Gd sublattice magnetizations. The measurements were performed with an incident laser fluence of 4.4 mJ/cm² and a sample temperature of 83 K, which is well below $T_{\text{M}} = 250$ K.

First, the net magnetizations of both sublattices rapidly decrease. However, whereas the net magnetization of Fe has collapsed within 300 fs, the demagnetization of Gd takes as long as 1.5 ps [67]. Remarkably, in spite of the exchange coupling between the rare earth (RE) and transition metal (TM) sublattices, they apparently lose their net magnetizations independently, as would be the case for two decoupled TM and RE ferromagnets [15, 74]. To retrieve the time constants of the involved processes we have used a double exponential fit function convoluted with the time resolution of the experiment of 100 fs, depicted by the Gaussian curve in Figure 5.10, given by:

$$f(t) = G(t) \times \left\{ A - B \times [1 - \exp(-t/\tau_1)] - C \times [1 - \exp(-t/\tau_2)] \right\}. \quad (5.7)$$

Here $G(t)$ describes the Gaussian function that accounts for the time resolution of 100 fs, A represents the value of the transient signal at negative delays, τ_1 and τ_2 are the time constants characterizing the two processes - the initial rapid drop and the slower remagnetization in the opposite magnetization direction - describing the temporal evolution of the data, and B and C are exponential amplitudes.

We find a time constant $\tau_{\text{Fe}} = 100 \pm 25$ fs for the Fe and $\tau_{\text{Gd}} = 430 \pm 100$ fs for the Gd magnetic moment, and thus a ratio $\tau_{\text{Gd}}/\tau_{\text{Fe}} \approx 4$, characterizing the fast initial

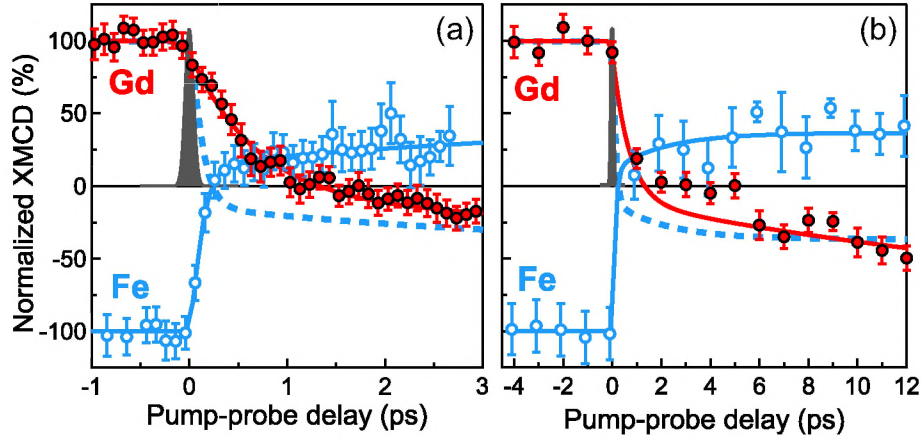


Figure 5.10: Element-resolved dynamics of the Fe and Gd magnetic moments measured by time-resolved XMCD with fs time-resolution. (a) Transient dynamics of the Fe (open circles) and Gd (filled circles) magnetic moments measured within the first 3 ps. (b) As in (a) but on a 12 ps time scale. Error bars of the experimental data represent the statistical standard error. The measurements were performed at a sample temperature of 83 K for an incident laser fluence of 4.4 mJ/cm^2 . Experimental time resolution of 100 fs is depicted by the solid Gaussian profile. The solid lines are fits according to a double exponential fit function. The dashed line in both panels depicts the magnetization of the Fe-sublattice taken with the opposite sign (i.e. opposite with respect to the sign of the measured Fe data) [67].

drop in the transient dichroic signal. Note that, the laser-induced dynamics studied here relies on crossing the compensation temperature T_M and thus is fundamentally different from the laser-induced demagnetization of pure Fe and Gd that relies on crossing the Curie point T_C [42, 43].

Second, the magnetizations of both sublattices switch their directions by crossing the zero signal level and rebuilding their net magnetic moments. Up to 10 ps, the Gd- and Fe-sublattices show a distinctly different switching dynamics. Even more surprisingly, within the time scale between the zero crossings of the Fe and Gd moments (i.e. between 300 fs and 1.5 ps), the net Fe and Gd moments are parallel aligned along the z -axis despite antiferromagnetic coupling of the spins in the ground state. Note that the net Fe and Gd moments in the “*transient ferromagnetic-like state*” are reaching rather large values of up to 25% of the equilibrium magnetization. This, together with the substantial laser-induced increase in temperature, indicates a rather strong transient parallel alignment of the Fe and Gd moments. All these observations mean that we have entered a thus far unexplored regime of magnetization dynamics

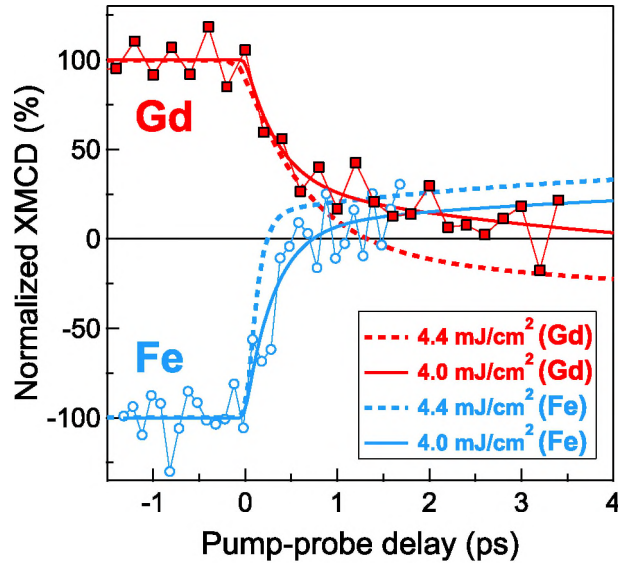


Figure 5.11: Fluence dependence of Fe and Gd switching dynamics. The change of the magnetization switching times for Fe and Gd moments upon varying the incidence laser fluence as labeled in the figure. The lines are fits to the data according to a bi-exponential fit function (Eq. 5.7) [67].

triggered by an ultrashort stimulus, where two exchange-coupled magnetic sublattices are not in equilibrium with each other, show different magnetization dynamics and store different amounts of energy. Consequently, the concept of a magnon (a quantized collective excitation of spins) in such a non-equilibrium ferrimagnetic state should be re-examined, as this state precedes the establishment of the collective Gd-Fe excitations and magnetic resonances in this material.

To further investigate the effect of the laser excitation on the degree of switching, we have also studied the dependence of the Fe and Gd dynamics on the laser fluence. As shown in Figure 5.11, we observe that slightly decreasing the fluence from 4.4 to 4.0 mJ/cm² leads to longer but still distinct switching times for Fe and Gd. This results in a longer lived transient ferromagnetic-like state, which spans the time range from 700 fs to about 4 ps for this lower fluence.

As discussed in Section 5.3.3, to obtain a better understanding of the origin of such strongly non-equilibrium spin dynamics, we have developed a model of a ferrimagnet comprising 10⁶ localized atomistic exchange-coupled spins and performed numerical simulations of the dynamics after ultra-short laser excitation.

Figure 5.12 shows the results of the simulations when applying a heat pulse with a

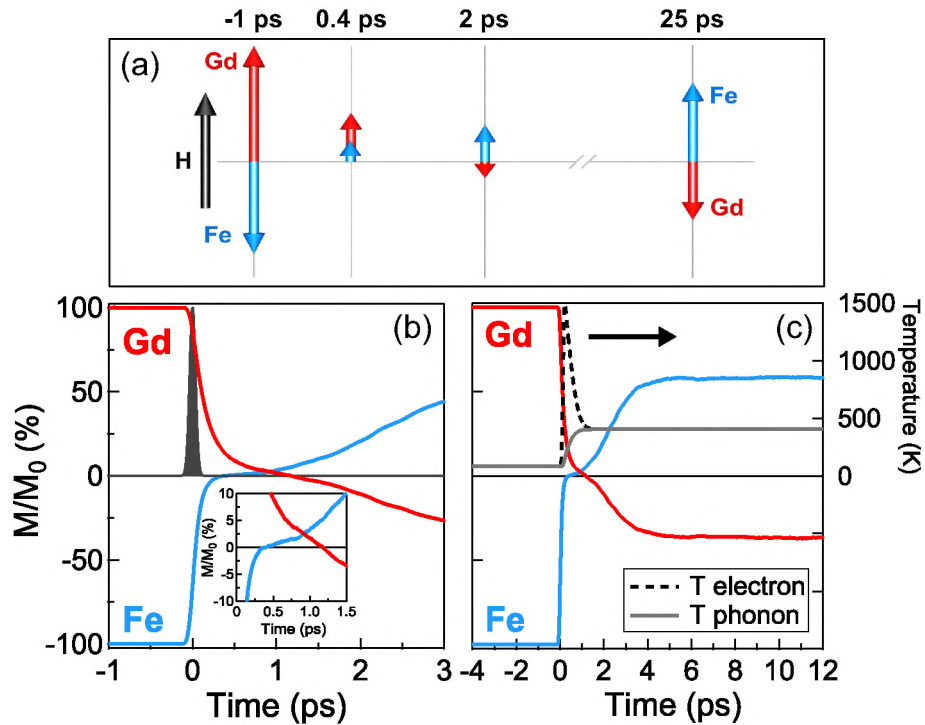


Figure 5.12: Computed time-resolved dynamics of the Fe and Gd magnetic moments from localized atomistic spin model. (a) Cartoon-like illustration of the non-equilibrium dynamics of the Fe and Gd magnetizations with respect to an external magnetic field \mathbf{H} . The lengths of the arrows are scaled to the magnitude of the transient XMCD signals shown in Figure 5.8. (b,c) Simulated dynamics for (b) the first 3 ps and (c) the first 12 ps after laser excitation. The calculations were performed for a peak electronic temperature of 1492 K with the corresponding transient electronic and phononic temperatures shown in (c). The transient magnetization changes are normalized to magnetization values at negative delays, i.e. to equilibrium values. As is clearly seen, the demagnetization of the Fe is much faster than that of the Gd [see inset in (b); axes same as main panel]. For a time of ~ 0.5 ps, we observe a parallel alignment of magnetizations of the sublattices. The agreement with the experimental data in Figure 5.8 is qualitatively excellent [67].

maximum electron temperature of 1492 K. First, the time evolution of the sublattice magnetization agrees very well with the experiments, and qualitatively reproduces the time scales for the demagnetization of each sublattice. The time required for the disappearance of the net magnetizations of the sublattices is found to be proportional to the ratio μ/γ , where μ and γ are respectively the magnetic moment of the ion and the damping constant of the sublattice.

Second, the ferromagnetic-like state is also reproduced, in a time window close to that observed experimentally. In addition, the reversal of the sublattice magnetizations is found to occur via the mechanism of linear reversal [74], that is, no transverse moment is observed. Note that even making the Gd-Gd exchange interaction in the simulations as strong as the Fe-Fe interaction does not lead to qualitative changes of the dynamics of the Fe and Gd sublattices. Figure 5.13 shows numerical results of the effect of changing the RE-RE exchange parameter, up to the strength of the TM-TM exchange. The distance between points on the red and blue lines show the time during which the system is in this transient ferromagnetic-like state. We see little difference in the behavior upon increase of the exchange interaction. Moreover, for the sake of argument the model ignores any differences in the electron temperature

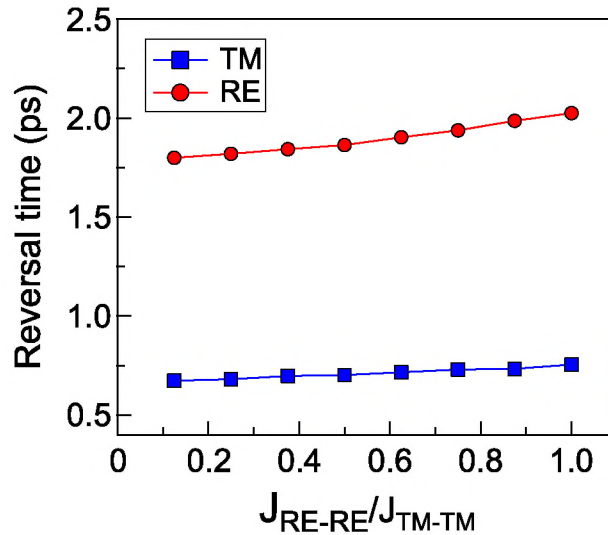


Figure 5.13: The variation of the reversal time for the RE and TM sub-lattices with the exchange interaction. Numerical calculations of reversal time in the FeCo (TM) and Gd (RE) systems (time for each sublattice to cross zero axis) as a function of the Gd-Gd exchange parameter. The effective Fe-Fe exchange is 1.96×10^{-20} J per spin [67].

and the damping constants for Gd and Fe ($\lambda_{TM} = \lambda_{RE} = 0.05$). However, even after such simplifications a good agreement between the experiment and the simulations is observed [67]. This is a strong indication that the novel magnetization dynamics reported here are an intrinsic property of the spins in a ferrimagnet excited by an ultrashort stimulus.

5.5 Conclusions

The ordering of magnetic spins allows one to manipulate them with the help of an external magnetic field and builds the basis of magnetic recording technologies. As the speed of these magnetic recording increases, it accordingly becomes necessary to understand the dynamics of spin ordering at ultrafast time scales. Hence, we have performed the first element specific studies of ultrafast magnetic switching by using advanced experimental and computational approaches.

Both approaches show that a “*ferromagnetic-like state*” emerges in the antiferromagnetic coupled sublattices of GdFeCo, owing to the substantially different dynamics of the TM and RE sublattices - in particular, the fact that the Fe reaches the state with zero net magnetization much faster than the Gd component. The dynamics of the Fe spins in the following time domain occur on the background of a reducing magnetization of the Gd. The exchange interaction between the Gd and Fe can flip an Fe spin when a Gd spin is reversed. As the exchange is antiferromagnetic, such a process will promote a growth of the net Fe magnetization in the direction parallel to the remaining magnetization of Gd. The simulations indeed confirm that the growth of the Fe magnetization in this time domain occurs with a speed similar (only slightly lower) to that at which the Gd magnetization decreases [see Figure 5.12(b) inset].

To conclude, our findings provide unexpected new insights into the fundamentals of ferrimagnetism, showing that two magnetic sublattices may have totally different spin dynamics even on a time scale much longer than the characteristic time of the exchange interaction between them. In the newly discovered transient ferromagnetic-like state, the magnetic system stores a large amount of energy in the intra- and inter-sublattice exchange interactions. Thus it is reasonable to hypothesize that the much weaker interaction of the spins with an external magnetic field hardly influences the spin dynamics in this ultrafast regime, leading to novel switching scenarios. The discovery of these dynamics is important for both the understanding of the physics of ultrafast magnetic phenomena on the time scale of the exchange interaction, and for the establishment of the fundamental limits on the speed of magnetic recording and information processing.

References

- [1] E. Beaurepaire, J.-C. Merle, A. Daunois, and J.-Y. Bigot, *Phys. Rev. Lett.* **76**, 4250 (1996).
- [2] A. Kimel, A. Kirilyuk, and T. Rasing, *Laser & Photon. Rev.* **1**, 275 (2007).
- [3] A. Kirilyuk, A. V. Kimel, and T. Rasing, *Rev. Mod. Phys.* **82**, 2731 (2010).
- [4] B. Koopmans, M. van Kampen, J. T. Kohlhepp, and W. J. M. de Jonge, *Phys. Rev. Lett.* **85**, 844 (2000).
- [5] C. Stamm, T. Kachel, N. Pontius, R. Mitzner, T. Quast, K. Holldack, S. Khan, C. Lupulescu, E. F. Aziz, M. Wietstruk, et al., *Nature Materials* **6**, 740 (2007).
- [6] F. Dalla Longa, J. T. Kohlhepp, W. J. M. de Jonge, and B. Koopmans, *Phys. Rev. B* **75**, 224431 (2007).
- [7] C. Boeglin, E. Beaurepaire, V. Halte, V. Lopez-Flores, C. Stamm, N. Pontius, H. A. Durr, and J.-Y. Bigot, *Nature* **465**, 458 (2010).
- [8] M. Battiato, K. Carva, and P. M. Oppeneer, *Phys. Rev. Lett.* **105**, 027203 (2010).
- [9] J.-Y. Bigot, L. Guidoni, E. Beaurepaire, and P. N. Saeta, *Phys. Rev. Lett.* **93**, 077401 (2004).
- [10] E. Beaurepaire, G. M. Turner, S. M. Harrel, M. C. Beard, J.-Y. Bigot, and C. A. Schmuttenmaer, *Appl. Phys. Lett.* **84**, 3465 (2004).
- [11] M. Elazar, M. Sahaf, L. Szapiro, D. Cheskis, and S. Bar-Ad, *Opt. Lett.* **33**, 2734 (2008).
- [12] L. Cywiński and L. J. Sham, *Phys. Rev. B* **76**, 045205 (2007).
- [13] N. Kazantseva, D. Hinzke, U. Nowak, R. W. Chantrell, U. Atxitia, and O. Chubykalo-Fesenko, *Phys. Rev. B* **77**, 184428 (2008).
- [14] G. Lefkidis, G. P. Zhang, and W. Hübner, *Phys. Rev. Lett.* **103**, 217401 (2009).
- [15] B. Koopmans, G. Malinowski, F. Dalla Longa, D. Steiauf, M. Fahnle, T. Roth, M. Cinchetti, and M. Aeschlimann, *Nature Materials* **9**, 259 (2010).
- [16] A. V. Kimel, A. Kirilyuk, P. A. Usachev, R. V. Pisarev, A. M. Balbashov, and T. Rasing, *Nature* **435**, 655 (2005).
- [17] F. Hansteen, A. Kimel, A. Kirilyuk, and T. Rasing, *Phys. Rev. Lett.* **95**, 047402 (2005).

-
- [18] A. V. Kimel, B. A. Ivanov, R. V. Pisarev, P. A. Usachev, A. Kirilyuk, and T. Rasing, *Nature Physics* **5**, 727 (2009).
- [19] A. M. Kalashnikova, A. V. Kimel, R. V. Pisarev, V. N. Gridnev, A. Kirilyuk, and T. Rasing, *Phys. Rev. Lett.* **99**, 167205 (2007).
- [20] A. H. M. Reid, A. V. Kimel, A. Kirilyuk, J. F. Gregg, and T. Rasing, *Phys. Rev. B* **81**, 104404 (2010).
- [21] C. D. Stanciu, F. Hansteen, A. V. Kimel, A. Kirilyuk, A. Tsukamoto, A. Itoh, and T. Rasing, *Phys. Rev. Lett.* **99**, 047601 (2007).
- [22] K. Vahaplar, A. M. Kalashnikova, A. V. Kimel, D. Hinzke, U. Nowak, R. Chantrell, A. Tsukamoto, A. Itoh, A. Kirilyuk, and T. Rasing, *Phys. Rev. Lett.* **103**, 117201 (2009).
- [23] C. H. Back, R. Allenspach, W. Weber, S. S. P. Parkin, D. Weller, E. L. Garwin, and H. C. Siegmann, *Science* **285**, 864 (1999).
- [24] I. Tudosa, C. Stamm, A. B. Kashuba, F. King, H. C. Siegmann, J. Stöhr, G. Ju, B. Lu, and D. Weller, *Nature* **428**, 831 (2004).
- [25] T. Devolder, A. Tulapurkar, Y. Suzuki, C. Chappert, P. Crozat, and K. Yagami, *J. Appl. Phys.* **98**, 053904 (2005).
- [26] Y. Acremann, J. P. Strachan, V. Chembrolu, S. D. Andrews, T. Tylliszczak, J. A. Katine, M. J. Carey, B. M. Clemens, H. C. Siegmann, and J. Stöhr, *Phys. Rev. Lett.* **96**, 217202 (2006).
- [27] J. C. Slonczewski, *J. of Magn. Magn. Mater.* **159**, L1 (1996).
- [28] M. Aeschlimann, A. Vaterlaus, M. Lutz, M. Stampanoni, and F. Meier, *J. Appl. Phys.* **67**, 4438 (1990).
- [29] M. Aeschlimann, A. Vaterlaus, M. Lutz, M. Stampanoni, F. Meier, H. C. Siegmann, S. Klahn, and P. Hansen, *Appl. Phys. Lett.* **59**, 2189 (1991).
- [30] J. Hohlfeld, T. Gerrits, M. Bilderbeek, T. Rasing, H. Awano, and N. Ohta, *Phys. Rev. B* **65**, 012413 (2001).
- [31] C. D. Stanciu, A. Tsukamoto, A. V. Kimel, F. Hansteen, A. Kirilyuk, A. Itoh, and T. Rasing, *Phys. Rev. Lett.* **99**, 217204 (2007).
- [32] A. Tsukamoto, T. Sato, S. Toriumi, and A. Itoh, *J. Appl. Phys.* **109**, 07D302 (pages 3) (2011).
- [33] P. Weiss, *J. Phys. (Paris)* **6**, 661 (1907).

- [34] P. Neel, Ann. Phys. (Paris) **17**, 5 (1932).
- [35] L. Neel, Science **174**, 985 (1971).
- [36] J. Daval and B. Bechevet, J. of Magn. Magn. Mater. **129**, 98 (1994).
- [37] E. Beaurepaire, M. Maret, V. Halté, J.-C. Merle, A. Daunois, and J.-Y. Bigot, Phys. Rev. B **58**, 12134 (1998).
- [38] M. Vomir, L. H. F. Andrade, L. Guidoni, E. Beaurepaire, and J.-Y. Bigot, Phys. Rev. Lett. **94**, 237601 (2005).
- [39] Z. Chen, R. Gao, Z. Wang, C. Xu, D. Chen, and T. Lai, J. Appl. Phys. **108**, 023902 (2010).
- [40] C. Xu, Z. Chen, D. Chen, S. Zhou, and T. Lai, Appl. Phys. Lett. **96**, 092514 (2010).
- [41] M. Binder, A. Weber, O. Mosendz, G. Woltersdorf, M. Izquierdo, I. Neudecker, J. R. Dahn, T. D. Hatchard, J.-U. Thiele, C. H. Back, et al., Phys. Rev. B **74**, 134404 (2006).
- [42] A. F. Bartelt, A. Comin, J. Feng, J. R. Nasiatka, T. Eimuller, B. Ludescher, G. Schutz, H. A. Padmore, A. T. Young, and A. Scholl, Appl. Phys. Lett. **90**, 162503 (2007).
- [43] M. Wietstruk, A. Melnikov, C. Stamm, T. Kachel, N. Pontius, M. Sultan, C. Gahl, M. Weinelt, H. A. Dürr, and U. Bovensiepen, Phys. Rev. Lett. **106**, 127401 (2011).
- [44] C. Stamm, N. Pontius, T. Kachel, M. Wietstruk, and H. A. Dürr, Phys. Rev. B **81**, 104425 (2010).
- [45] A. G. Gurevich and G. A. Melkov, *Magnetization Oscillations and Waves* (CRC Press, Boca Raton, FL, 1997).
- [46] C. D. Stanciu, Ph.D. thesis, Radboud University Nijmegen (2008).
- [47] R. K. Wangsness, Phys. Rev. **91**, 1085 (1953).
- [48] J. L. Erskine and E. A. Stern, Phys. Rev. B **12**, 5016 (1975).
- [49] B. T. Thole, G. van der Laan, and G. A. Sawatzky, Phys. Rev. Lett. **55**, 2086 (1985).
- [50] G. van der Laan, B. T. Thole, G. A. Sawatzky, J. B. Goedkoop, J. C. Fuggle, J.-M. Esteve, R. Karnatak, J. P. Remeika, and H. A. Dabkowska, Phys. Rev. B **34**, 6529 (1986).

-
- [51] G. Schütz, W. Wagner, W. Wilhelm, P. Kienle, R. Zeller, R. Frahm, and G. Materlik, *Phys. Rev. Lett.* **58**, 737 (1987).
- [52] C. T. Chen, F. Sette, Y. Ma, and S. Modesti, *Phys. Rev. B* **42**, 7262 (1990).
- [53] F. Sette, C. T. Chen, Y. Ma, S. Modesti, and N. V. Smith, *AIP Conf. Proc.* **215**, 787 (1990).
- [54] J. Stöhr and R. Nakajima, *IBM J. Res. Develop.* **42**, 73 (1998).
- [55] J. Stöhr and H. C. Siegmann, *Magnetism: From Fundamentals to Nanoscale Dynamics* (Springer-Verlag, Berlin, 2006).
- [56] A. Rogalev, F. Wilhelm, N. Jaouen, J. Goulon, and J.-P. Kappler, *X-ray Magnetic Circular Dichroism: Historical Perspective and Recent Highlights*, vol. 697 of *Lect. Notes Phys.* (Springer-Verlag, Berlin Heidelberg, 2006).
- [57] J. Stöhr, *J. of Magn. Magn. Mater.* **200**, 470 (1999).
- [58] J. Stöhr and S. Anders, *IBM J. Res. Develop.* **44**, 535 (2000).
- [59] S. Pizzini, J. Vogel, M. Bonfim, and A. Fontaine, *Spin Dynamics in Confined Magnetic Structures II* (Springer-Verlag, Berlin, Germany, 2003).
- [60] A. Scherz, Ph.D. thesis, Freie Universität Berlin (2003).
- [61] E. Beaupaire, H. Bulou, F. Scheurer, and K. Jean-Paul, *Magnetism and Synchrotron Radiation*, vol. 133 of *Springer Proceedings in Physics* (Springer, 2010).
- [62] P. Fischer, *Materials Science and Engineering: R: Reports* **72**, 81 (2011).
- [63] B. T. Thole, P. Carra, F. Sette, and G. van der Laan, *Phys. Rev. Lett.* **68**, 1943 (1992).
- [64] P. Carra, B. T. Thole, M. Altarelli, and X. Wang, *Phys. Rev. Lett.* **70**, 694 (1993).
- [65] M. Bonfim, G. Ghiringhelli, F. Montaigne, S. Pizzini, N. B. Brookes, F. Petroff, J. Vogel, J. Camarero, and A. Fontaine, *Phys. Rev. Lett.* **86**, 3646 (2001).
- [66] C. D. Stanciu, A. V. Kimel, F. Hansteen, A. Tsukamoto, A. Itoh, A. Kirilyuk, and T. Rasing, *Phys. Rev. B* **73**, 220402 (2006).
- [67] I. Radu, K. Vahaplar, C. Stamm, T. Kachel, N. Pontius, H. A. Durr, T. A. Ostler, J. Barker, R. F. L. Evans, R. W. Chantrell, et al., *Nature* **472**, 205 (2011).
- [68] S. Khan, K. Holldack, T. Kachel, R. Mitzner, and T. Quast, *Phys. Rev. Lett.* **97**, 074801 (2006).

- [69] C. Stamm, N. Pontius, T. Kachel, K. Holldack, T. Quast, R. Mitzner, S. Khan, M. Wietstruk, H. A. Dürr, and W. Eberhardt, in *Ultrafast Phenomena XVI* (Springer Berlin Heidelberg, 2009), vol. 92 of *Springer Series in Chemical Physics*, pp. 194–196.
- [70] N. Pontius, C. Stamm, T. Kachel, R. Mitzner, T. Quast, K. Holldack, S. Khan, H. A. Dürr, and W. Eberhardt, in *Ultrafast Phenomena XVI* (Springer Berlin Heidelberg, 2009), vol. 92 of *Springer Series in Chemical Physics*, pp. 119–121.
- [71] BESSY II (Berliner Elektronenspeicherring-Gesellschaft für Synchrotronstrahlung m. b. H.): <http://www.helmholtz-berlin.de/>.
- [72] N. Kazantseva, U. Nowak, R. W. Chantrell, J. Hohlfeld, and A. Rebei, *Europhys. Lett.* **81**, 27004 (2008).
- [73] S. Anisimov, B. Kapeliovich, and T. Perelman, *Sov. Phys. JETP* **39**, 375 (1974).
- [74] N. Kazantseva, D. Hinzke, R. W. Chantrell, and U. Nowak, *Europhys. Lett.* **86**, 27006 (2009).

Summary and outlook

In the last fifty years the study of the dynamics of magnetization processes in magnetic materials has been the focus of intensive research. Today's modern magnetic storage devices are able to write more than a few hundred of gigabits per square inch at a rate of one bit per two nanoseconds. The miniaturization of these devices and the enhancement of their capabilities, like higher data storage densities, faster access and recording times, and lower power consumption, are challenging tasks for further development.

Due to the demand for faster magnetic data storage, it is crucial to investigate the ultimate speed for magnetization reversal. Femtosecond lasers are particularly suited for this purpose. The strong and fast external perturbation by a femtosecond laser pulse brings a magnetic medium into a strongly nonequilibrium state, by causing a rapid demagnetization at subpicosecond time scales. Thus, the field of *laser-induced ultrafast magnetization dynamics* triggered many experimental and theoretical investigations which were also fueled by potential industrial applications.

Exploring the ultimate limits of laser-induced magnetization dynamics has been a subject of scientific curiosity in the past 15 years. In view of this, novel magnetization switching schemes and recent progress in magnetization dynamics were described in Chapter 1. In particular, it was shown that a single 40 fs circularly polarized laser pulse can controllably reverse the magnetization. Although these experiments showed the feasibility of magnetization reversal with a femtosecond stimulus in GdFeCo alloys, the actual time scales and the mechanism of such a reversal had been unknown. The latter became the topic of the research described in this thesis. In order to address these issues, we performed extensive experimental studies of this *all-optical helicity-dependent magnetization reversal* by subpico- and picosecond laser pulses in

ferrimagnetic rare earth – transition metal (RE–TM) amorphous alloys (GdFeCo).

The magnetic and magneto-optical properties of these RE–TM metallic alloys studied in this thesis are explained in Chapter 2. In Chapter 3, we described the main experimental techniques used to investigate the dynamics of magnetization reversal on femtosecond time scales.

The main results presented in this thesis can be divided into two parts. The first part, Chapter 4, focuses on the study of the *route* of the all-optical magnetization reversal. Here we used the method of single-shot time-resolved magneto-optical imaging microscopy. This experimental technique allowed us to reveal the speed of magnetization reversal and showed that the reversal follows an unconventional *linear* path that does not involve precession but occurs via a strongly nonequilibrium state with no net magnetization. These results could be interpreted using atomistic and multiscale simulations. We have also achieved a write-read time of 30 ps which is the fastest write-read event demonstrated for magnetic recording so far. The optimal conditions for all-optical switching as a function of the laser pulse duration, polarization, and alloy composition were studied. The observations showed that these parameters dramatically influence the features of the linear reversal and the speed of it. The latter can be reduced by a convenient tuning of the magnetic properties of the recording medium.

In Chapter 5, we studied the details of the *mechanism* of the ultrafast spin reversal in GdFeCo excited by a subpicosecond stimulus, which was used to heat the sample rapidly above its compensation temperature and initiate the spin reversal in an external magnetic field. Taking advantage of the element-specificity of the X-ray magnetic circular dichroism (XMCD) effect, we were able to follow the dynamic changes of each magnetic sublattice with femtosecond resolution. For this, we used a special technique, so-called “femtosecond slicing” (femtosing), and obtained 100 fs X-ray probe pulses. We have found that the Gd and Fe spins reverse their directions on substantially different time scales, leading to an unexpected occurrence of a transient ferromagnetic-like state with parallel alignment of the net magnetic moments of the Gd and Fe sublattices.

The results presented in this thesis provide new insights into the fundamental limits on the speed of magnetic recording and information processing. Future work in this direction could be made by exploiting the newly developed X-ray sources, using new techniques and instrumentation to explore ultrafast magnetization processes together with further developments in multiscale modeling. In particular, the transient states emerging during laser-induced magnetization reversal can be studied with femtosecond temporal and nanometer spatial resolution by combining the coherent X-ray imaging technique with the ultrashort pulse and high brightness of femtosecond free electron lasers in the soft X-ray regime, like the LCLS facility in Stanford or the new XFEL in Groningen. Some preliminary experiments have been already carried out by our group.

Samenvatting en vooruitblik

Gedurende de laatste 50 jaar is de studie van de dynamica van magnetische processen in magnetische materialen een onderwerp geweest van intensief onderzoek. Moderne apparaten voor magnetische opslag zijn vandaag de dag in staat om meer dan enkele honderden gigabits per vierkante inch informatie weg te schrijven met een snelheid van één bit per twee nanoseconde. Het verder verkleinen van deze apparaten en de verbetering van hun capaciteit, zoals hogere data-opslagdichtheid, snellere lees- en schrijfsnelheid en lager energieverbruik, zijn uitdagende opdrachten voor verdere ontwikkeling.

Door de vraag naar als maar, snellere magnetische data-opslag is het cruciaal om de ultieme omkeersnelheid van magnetisatie te onderzoeken. Femtoseconde lasers zijn bij uitstek geschikt voor dit doel. De sterke en korte externe verstoring door middel van een femtoseconde laserpuls brengt een magnetische materiaal in een sterke niet-evenwicht toestand, veroorzaakt door een snelle demagnetisatie op de subpicoseconde tijdschaal. Daardoor heeft het onderzoeksveld van *laser-geïnduceerde magnetisatie dynamica* vele theoretische en experimentele onderzoeken teweeggebracht die mede zijn gevoed door mogelijke industriële toepassingen.

Het verkennen van de ultieme limiet van laser-geïnduceerde magnetisatie dynamica is de laatste 15 jaar het onderwerp van wetenschappelijke nieuwsgierigheid geweest. Met het oog hierop worden in hoofdstuk 1 nieuwe methodes voor het schakelen van magnetisatie en recente vooruitgang op het gebied van de magnetisatie dynamica beschreven. In het bijzonder is aangetoond dat een enkele 40 fs circulair gepolariseerde laser puls de magnetisatie controleerbaar kan omkeren. Hoewel met deze experimenten de mogelijkheid van magnetisatie omkering met een femtoseconde stimulus in GdFeCo legeringen was aangetoond, was de daadwerkelijke tijdschaal en het mecha-

nisme van het omkeren onbekend. Deze twee aspecten werden onderwerp van het onderzoek dat wordt beschreven in dit proefschrift. Om al deze kwesties te behandelen hebben we uitgebreide experimentele studies verricht naar dit *volledig-optisch heliceit-afhankelijke magnetisatie-omkeren* met subpico- en picoseconde laserpulsen in ferrimagnetische amorfe zeldzame-aarde – overgangsmetaal (ZA-OM) legeringen, zoals GdFeCo.

De magnetische en magneto-optische eigenschappen van de metallische ZA-OM legeringen bestudeerd in dit proefschrift zijn uitgelegd in hoofdstuk 2. In hoofdstuk 3 hebben we de belangrijkste experimentele technieken beschreven die gebruikt zijn om de dynamica van het omkeren van de magnetisatie op de femtoseconde tijdschaal te onderzoeken.

De belangrijkste resultaten die worden gepresenteerd in dit proefschrift kunnen worden verdeeld in twee delen. Het eerste deel, beschreven in hoofdstuk 4, richt zich op de studie van de *route* waarlangs het volledig-optisch magnetisatie-omkeren gebeurt. Hiervoor hebben we de methode van enkele-puls tijdopgeloste magneto-optische microscopie gebruikt. Deze techniek stelde ons in staat om de snelheid van omkeren van de magnetisatie bloot te leggen en toonde aan dat het omkeren een onconventioneel *lineair* pad volgt, waarbij geen precessie optreedt maar die verloopt via een sterke niet-evenwicht toestand zonder netto magnetisatie. Deze resultaten konden worden geïnterpreteerd met behulp van een atomair model en multi-schaal simulaties. Tevens hebben we een schrijf- lees snelheid bereikt van 30 ps, dat tot nu toe de korste waargenomen schrijf- lees actie is voor magnetische opslag. De optimale condities voor volledig-optisch schakelen als functie van laserpulsduur, laserpolarisatie en compositie van de legering zijn eveneens bestudeerd. De observaties toonden aan dat deze parameters de karakteristieken en de snelheid van het lineaire omkeren aangrijpend beïnvloeden. De snelheid kan worden geoptimaliseerd door passend afstemmen van de magnetische eigenschappen van het opslagmedium.

In hoofdstuk 5 hebben we de details van het *mechanisme* van de ultrasnelle spin draaiing in een GdFeCo legering bestudeerd, door excitatie met een subpicoseconde stimulus welke werd gebruikt om het materiaal snel op te warmen boven de compensatietemperatuur en zo spindraaiing te initiëren in een extern magneetveld. Gebruik makend van de element-specificiteit van het magnetisch-circulair dubbelbrekingseffect van zachte Röntgenstraling, waren we in staat om de dynamische veranderingen van ieder magnetisch subrooster te volgen met femtoseconde tijdsresolutie. Hiervoor hebben we een speciale techniek gebruikt, het zogenaamde “femtoseconde slicing” (femtosing), waarmee 100 fs Röntgenstraling pulsen verkregen worden. We hebben gevonden dat de Gd en Fe spins hun oriëntatie op substantieel verschillende tijdschalen omkeren, welke aanleiding geeft tot het onverwacht optreden van een tijdelijk ferromagnetisch-achtige toestand met parallelle ophijning van de netto magnetische momenten in de Gd en Fe subroosters.

De resultaten gepresenteerd in dit proefschrift bieden nieuwe inzichten in de fun-

damentele limieten van de snelheid van magnetische opslag en informatie verwerking. Toekomstig werk in deze richting kan worden verricht door gebruik te maken van de ontwikkeling in Röntgenstraling bronnen, nieuwe technieken en instrumentatie om ultrasnelle magnetische processen te verkennen en verdere ontwikkelingen op het gebied van multi-schaal simulaties en theorie. In het bijzonder, kunnen the tijdelijke toestanden die zich voordoen gedurende the laser-geïnduceerde magnetisatie omkering worden bestudeerd met femtoseconde tijd resolutie en nanometer ruimtelijke resolutie door het combineren van holografisch afbeelden met coherente Röntgenstraling, gebruik makend van de ultrakorte pulsen en de hoge helderheid van de nieuwe generatie vrije electronen lasers in het zachte Röntgen gebied zoals de LCLS faciliteit in Stanford en de geplande ZFEL in Groningen. Enkele inleidende experimenten zijn reeds uitgevoerd door onze groep.

List of Publications

- [1] I. Radu, **K. Vahaplar**, C. Stamm, T. Kachel, N. Pontius, H. A. Dürr, T. A. Ostler, J. Barker, R. F. L. Evans, R. W. Chantrell, A. Tsukamoto, A. Itoh, A. Kirilyuk, T. Rasing, and A. V. Kimel, “Transient ferromagnetic-like state mediating ultrafast reversal of antiferromagnetically coupled spins,” *Nature* **472**, 205 (2011).
- [2] **K. Vahaplar**, A. M. Kalashnikova, A. V. Kimel, D. Hinzke, U. Nowak, R. W. Chantrell, A. Tsukamoto, A. Itoh, A. Kirilyuk, and T. Rasing, “Ultrafast path for optical magnetization reversal via a strongly nonequilibrium state,” *Physical Review Letters* **103**, 117201 (2009).
- This article has been selected as “Editors’ suggestions” and for a “Viewpoint” in *Physics*.
- [3] **K. Vahaplar**, S. Tari, H. Tokuc, and S. Okur, “Effect of Ta buffer layer and thickness on the structural and magnetic properties of Co thin films,” *Journal of Vacuum Science & Technology B* **27**, 2112 (2009).
- [4] **K. Vahaplar**, A. M. Kalashnikova, A. V. Kimel, S. Gerlach, D. Hinzke, U. Nowak, R. W. Chantrell, A. Tsukamoto, A. Itoh, A. Kirilyuk, and T. Rasing, “All-optical magnetization reversal triggered by circularly-polarized laser pulses: experiment and multiscale modeling,” (submitted to *Physical Review B*).

- [5] T. Ostler, R. W. Chantrell, S. E. Moussaoui, L. le Guyader, F. Nolting, A. Tsukamoto, A. Itoh, D. Afanasiev, B. A. Ivanov, A. M. Kalashnikova, **K. Vahaplar**, J. Mentink, A. Kirilyuk, T. Rasing, and A. V. Kimel, “Ultrafast heating as a sufficient stimulus for magnetization reversal in a ferrimagnet,” (submitted).

- [6] I. Radu, C. Stamm, A. Eschenlohr, **K. Vahaplar**, T. Kachel, N. Pontius, F. Radu, T. A. Ostler, R. W. Chantrell, J. Mentink, A. Kirilyuk, T. Rasing, and A. V. Kimel, “Ultrafast decoupling of elemental magnetic moments in ferromagnetic and ferrimagnetic alloys,” (submitted).

- [7] S. E. Kaneko, **K. Vahaplar**, A. M. Kalashnikova, A. V. Kimel, A. Kirilyuk, A. Tsukamoto, A. Itoh, and T. Rasing, “Stochastic single-pulse all-optical magnetization switching in GdFeCo,” (in preparation).



Curriculum Vitae

Name:
Kadir Vahaplar
Date of birth:
28 July 1981
Place of birth:
Izmir, Turkey

- 1995–1999 Highschool, Izmir Atatürk Lisesi, Izmir, Turkey.
- 1999–2003 Bachelor studies at Department of Physics, Pamukkale University, Denizli, Turkey.
- 2004–2007 M.Sc. studies at Department of Physics, Izmir Institute of Technology, Izmir, Turkey.
- 2007–2011 Ph.D. studies at Radboud University Nijmegen, The Netherlands, in the group of Prof. Th. Rasing.